

# Development of Soluble DNTT Derivatives and Application to Organic Devices

(可溶性 DNTT 誘導体の開発と有機デバイスへの応用)

March, 2017

Masanori Sawamoto

GRADUATE SCHOOL OF SCIENCE AND ENGINEERING  
SAITAMA UNIVERSITY

## *Table of contents*

### **Chapter 1 General introduction**

- 1-1 Organic electronics
- 1-2 Organic thin-film transistor (OTFT)
- 1-3 Dinaphtho[2,3-b:2',3'-f]thieno[3,2-b]thiophene (DNTT)
- 1-4 This thesis
- 1-5 References

### **Chapter 2 Synthesis of solution-processable DNTT derivatives**

- 2-1 Introduction
- 2-2 Results and discussion
  - 2-2-1 Molecular design and synthesis
  - 2-2-2 Molecular and thin film properties
  - 2-2-3 TFT fabrication and characterization
  - 2-2-4 Detailed analysis of thin films
- 2-3 Conclusion of chapter 2
- 2-4 Experimental section, supporting data and references

### **Chapter 3 Improvement of solution-processed OTFT using 2-EO-DNTT**

- 3-1 Introduction
- 3-2 Results and discussion
  - 3-2-1 Search for optimal spin-coat conditions
  - 3-2-2 Investigation of device stability
  - 3-2-3 Low voltage operation of OTFTs
- 3-3 Conclusion of chapter 3
- 3-4 Experimental section, supporting data and references

### **Chapter 4 Di-substituted branched-alkyl DNTT as p-type semiconductor for OPV**

- 4-1 Introduction
- 4-2 Results and discussion
- 4-3 Conclusion of chapter 4
- 4-4 Experimental section, supporting data and references

### **Chapter 5 Concluding remarks**

#### **List of publications**

#### **Acknowledgements**

# Chapter 1

## General introduction

### 1-1 Organic electronics

#### Features of organic electronics<sup>1-3</sup>

Organic electronics have fascinating features hardly found in the conventional electronics. That is organic electronics have been promising in terms of their low-cost, low-temperature and fast manufacturability in addition to their compatibility with various kinds of substrates that are thin, large in area, transparent or mechanically flexible. To achieve them, wet processes such as roll-to-roll solution printing is very effective (Figure 1). If such processes are established, the devices such as flexible displays, sensors and solar cell etc. could be manufactured like newspapers. Then, organic electronics will create a big market and contribute to the development of industry and society.

However, the research and development of organic electronics is not fast compared with conventional inorganic electronics. One of the reasons is that organic electronics is an interdisciplinary area that incorporates chemistry (material), physics (device), engineering (process), etc. Nevertheless, researches tend to keep themselves in their own research fields. Therefore, in order to accelerate the research on organic electronics, it is important to simultaneously study materials, devices and processes as much as possible. Based on this idea, I have been engaged in the research on materials, devices and processes and set the theme of doctor thesis aiming at practical application of organic electronics.

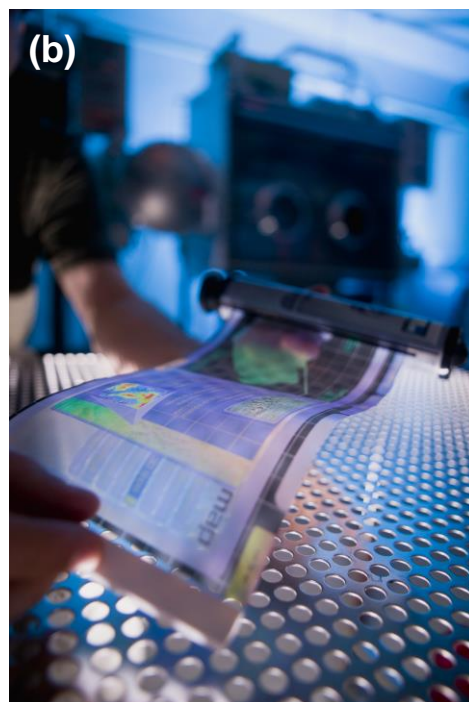


**Figure 1.** OPV module (a), OTFT-based flexible display (b).

### Representative three applications of organic semiconductors<sup>4</sup>

There are three typical device applications in organic electronics: organic light emitting diode (OLED), organic thin film transistor (OTFT) and organic photovoltaic cell (OPV), and their schematic device architectures are shown in Figure 2. The basic working mechanism of each device is as follows. In OLED, electrons and holes are injected by applying a voltage between the electrodes, and photons are generated by excitons created by recombining electrons and holes in light emitting layer. In OTFT, the carriers are injected to the channel by applying a voltage to the gate electrode, and the flow of current between the source and drain electrodes is controlled. In OPV, excitons are generated by light absorption, and then the excitons are separated at the interfaces between p- and n-type materials into holes and electrons, which flow to the electrodes to generate electricity. Among them, research on OLED has progressed to the stage of commercialization.

On the other hand, from the viewpoint of molecular design, the design principal of the active materials in different devices are also largely different as the function of materials and device architectures are largely different. For example, in OLED and OPV, the mobility of the material is not critically important, since the direction of carrier flow is the film-thickness direction (typically, several hundreds nm). Thus, for example, the materials for OLEDs should be nonplanar shape, which gives amorphous film enabling uniform light emission in the entire thin film. On the other hand, in OTFT, the mobility of the material is very important, since the direction of carrier flow is the horizontal in the film with typical channel length of several tens of  $\mu\text{m}$ , so the material is required to have planar molecular structures realizing good crystallinity.

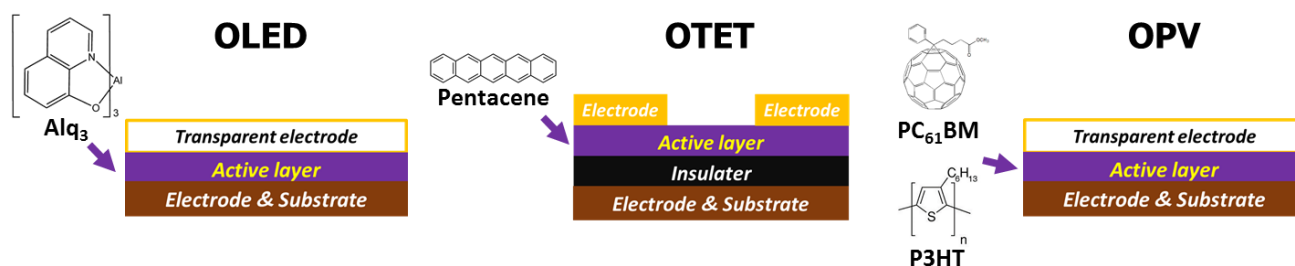


**Figure 2.** Schematic device architectures of OLED, OTFT and OPV.

### Classification of the materials<sup>4</sup>

Various materials with different functions have been developed, and diverse molecular designs have been proposed. The diversity of molecular design is also a major feature of organic electronics. Organic semiconductors can be classified according to the type of carrier, molecular aggregation state, molecular weight, suitable deposition process as well as the application. Regarding the type of carrier, organic semiconductor are basically intrinsic semiconductors, and thus the carrier type is determined by matching between the work function of the electrode and the HOMO or LUMO energy level of the organic semiconductors. Regarding the molecular aggregation state, it can be roughly divided into amorphous and crystalline material. Amorphous materials are preferred in OLED, where film uniformity is important, whereas crystalline materials are preferred in OTFT specialized for carrier transport. Regarding the molecular weight, there are small-molecule material and polymer material, and the polymer is generally defined as a macromolecule with the molecular weight greater than 10,000 and materials with in-between molecular weights are often called oligomer. Thin-film deposition processes are classified into two; wet processes, where the active layers were deposited from the solution, and dry processes, where the thin-films are formed by vapor deposition. Conventionally, as the wet process materials, polymers with good film forming nature from solution have been investigated, but in recent years, small molecules has also attracted widely, and in fact, many small-molecular materials showing high performances by wet process have been reported.

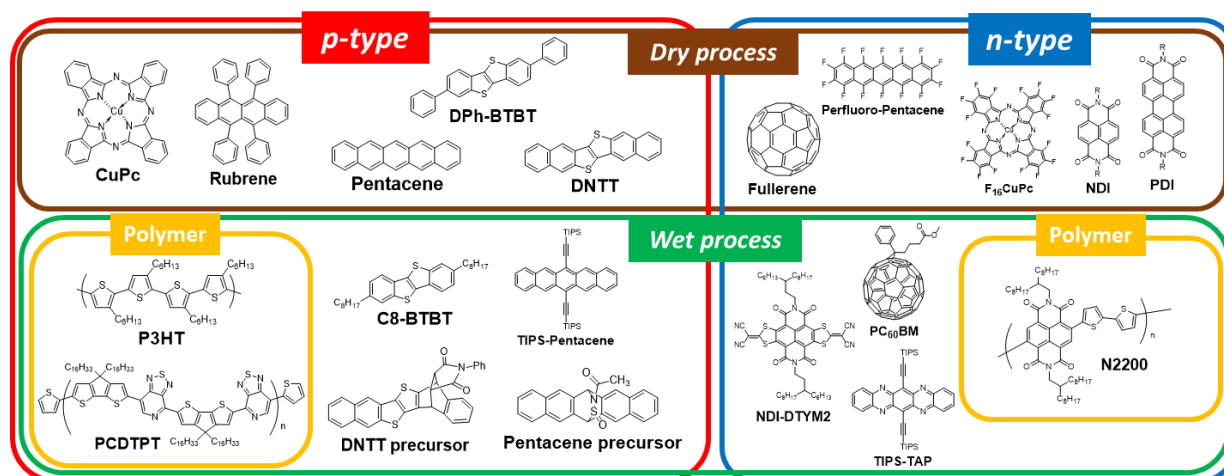


**Figure 3.** Classification of OTFT materials.

### Representative film-forming methods<sup>5</sup>

As mentioned above, the film-forming methods can roughly be classified into “wet process” and “dry process”, but the aforementioned features of organic electronics is realized by “wet process” which can form the film from solution. Compared with vapor deposition (dry process), in wet process, the choice methods and parameters to be optimized in the film formation tend are quite large, and such methods and parameters have a large influence on the device performance. In fact, the importance of a comprehensive understanding of the physical principles of various wet processes is now increasingly realized in the community. An overview of typical wet processes are shown in [Figure 4](#). Of these, particularly important and widely used are “drop-casting” and “spin-coating”. “Drop-casting” is a facile quasi-equilibrium process and involves the casting of an organic semiconductor solution and the subsequent evaporation of the solvent to precipitate and deposit either individual crystals or a thin film. “Spin-coating” is a commonly used wet-process to form organic semiconductor thin films of effectively uniform thickness. The solution is dropped onto a substrate, and the substrate is accelerated to a high angular velocity to simultaneously spread the liquid and evaporate the solvent. The thickness of the wet film is inversely related to the spin speed and also depends on the solution concentration and viscosity. Besides this, there are “inkjet-printing”, “blade-coating”, “spray-coating” and “stamp-printing” etc. and it is important to select an appropriate method and deposition parameters according to the feature of the materials and devices. In this study, I was mainly using “spin-coating”, which is the simplest wet process widely used at lab level.

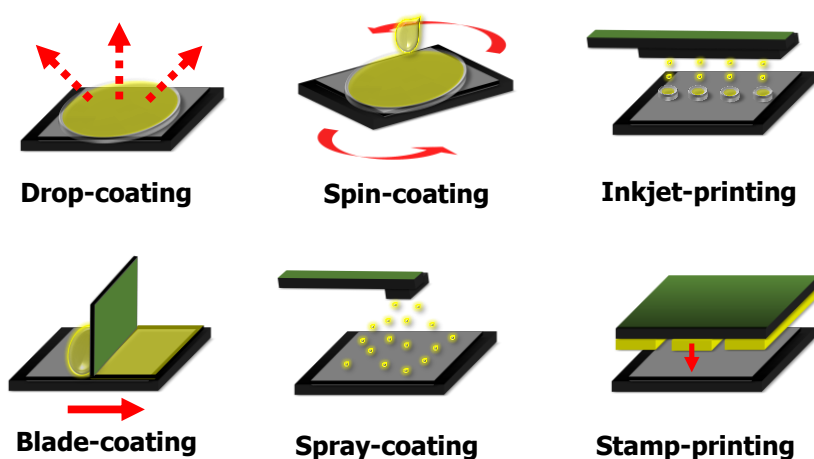


**Figure 4.** A schematic summary of wet process techniques.

## 1-2 Organic thin-film transistor (OTFT)

### Device architecture and operating principle<sup>1-3</sup>

Thin-film transistor (TFT) is a kind of field-effect transistor (FET), and with an organic semiconductor material as an active layer, it is called as organic thin-film transistor (OTFT). As shown in Figure 5a, components necessary for OTFT are a supporting substrate, a gate electrode, a gate insulator, an active layer and source/drain electrodes. The arrangement of each components depends on the device architecture to be applied. There are various architectures for OTFT device, but in evaluating the performance of the material, a bottom-gate/top-contact (BGTC) type is convenient, in which a heavy-doped silicon substrate with a thermal oxide ( $\text{SiO}_2$ ) film is used as the supporting substrate, the gate electrode, and gate insulator ( $\text{SiO}_2$ ). Normally, in the evaluation of OTFTs, the source electrode is connected to the ground, and a voltage is applied to the gate and drain electrode to measure the drain current (the current between the drain and source electrodes). The operating principle is described below.

(1) When gate voltage ( $V_g$ ) is applied, carriers are injected from the source electrode into the organic semiconductor layer to form a channel, and next, when drain voltage ( $V_d$ ) ( $< V_g$ ) is applied, drain current ( $I_d$ ) increase linearly. (**Linear region**) (Figure 5b)

(2) When  $V_d (= V_g)$  is applied, there is no potential difference between the gate and drain electrodes, so that the channel near the drain electrode disappears. (**Pinch-off point**) (Figure 5c)

(3) When  $V_d (> V_g)$  is further applied, the voltages is used to expand the space charge layer in the vicinity of the drain electrode. Therefore,  $I_d$  does not increase. (**Saturation region**) (Figure 5d)

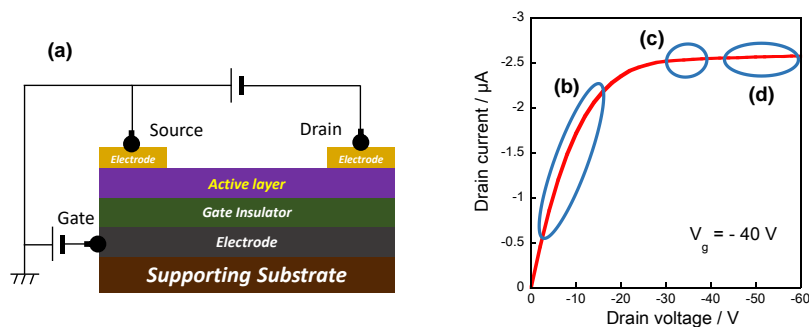


**Figure 5.** Architecture of BGTC-type OTFT (a), Output characteristics in each  $V_d$  region (b) – (d).

Actually, the channel is formed only when  $V_g$  exceeds the threshold voltage ( $V_{th}$ ) due to the influence of trap level existing at the interface, so the effective value of  $V_g$  is  $V_g - V_{th}$ . Overall above situation can be expressed as follows (eq. 1), and the carrier mobility can be estimated.

$$I_d = C_i \mu_{FET} \frac{W}{2L} (V_g - V_{th})^2 \quad \text{eq. 1}$$

This eq. 1 is field-effect mobility evaluation formula in saturation region used in characteristics evaluation of OTFTs.

### Required performances<sup>1-3</sup>

The performances required for materials in the wet processed OTFTs are;

- (1) **High mobility** (At least  $1 \text{ cm}^2/\text{Vs}$  or more)
- (2) **Good coating suitability** (Solubility and film formability, etc.)
- (3) **Good stability** (Environmental [air, light, etc.], electrical, thermal, etc.)
- (4) **Low voltage drivability** (At a few volts)
- (5) **Good circuit design suitability** ( $V_{th}$  is close to 0 V, high on/off ratio, no hysteresis, small variation, etc.).

To produce commercial devices, all these requirements must be achieved simultaneously. There are many reports on materials achieved some of these requirements, but few materials can achieve all at the same time. Although (1), (2) and (3) largely depend on the organic semiconductor of the active layer, it is known that (4) and (5) greatly depend not only on the organic semiconductor but also the interface between the electrode and organic-layer, or insulating- and organic-layer.

### 1-3 Dinaphtho[2,3-b:2',3'-f]thieno[3,2-b]thiophene (DNNT)

#### Concept of DNNT

Pentacene has been used as the standard OTFT material for a long time<sup>6</sup>, but its environmental stability is not good,<sup>7</sup> and thus it is disadvantageous as a practical material. This is due to the benzene rings fused linearly, which increase and decrease the HOMO- and the LUMO- energy level, respectively, simultaneously. As a result, the band gap is greatly reduced inducing decomposition paths through the photo excitation, and the high-lying HOMO energy level can cause air-oxidation, both of which reduce significantly the stability. Because of these instability, the pentacene-based OTFTs show an increase in off-current, a decrease in mobility, and a shift in threshold voltage.

On the other hand, [1]benzothieno[3,2-b][1]benzothiophenes (BTBT) having a thieno[3,2-b]thiophene core in the center of molecule succeeded in keeping low-lying HOMO (Figure 6).<sup>8</sup> It is reasonable to consider that BTBT is an isoelectronic structure with chrysene when compared with tetracene and chrysene having the same number of fused aromatic rings and it is experimentally confirmed that BTBT and chrysene have similar absorption edges and oxidation potentials as well.<sup>9</sup> In such a bent pi-electron system, it is known that even though the number of fused rings increases, the changes in HOMO and LUMO level are small. As a result, the decrease in band gap can be suppressed. Further increase of fused rings enhances the overlap of the HOMO orbitals between molecules in the solid state and also improves thermal stability. This is the design strategy for DNNT.<sup>10</sup>

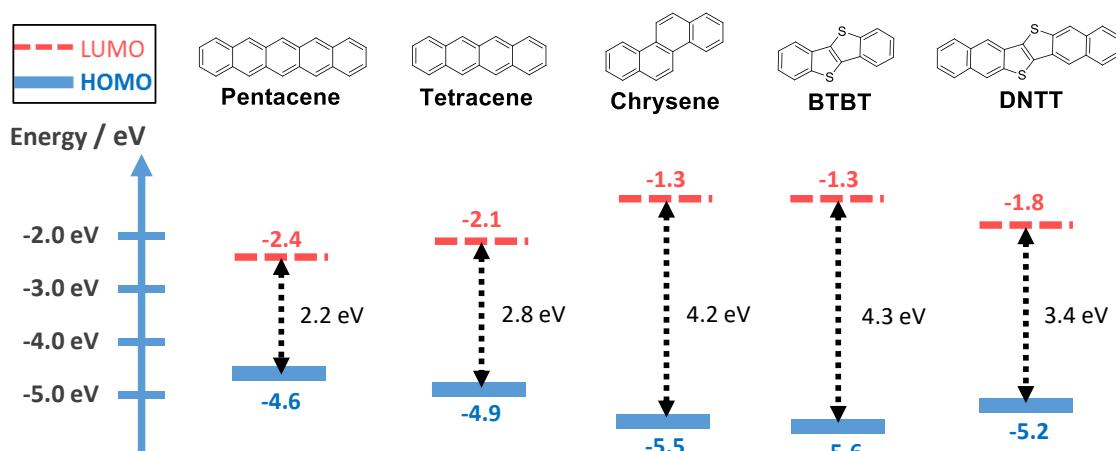


**Figure 6.** Calculated frontier orbitals of pentacene, tetracene, chrysene, BTBT and DNNT.

A typical characteristics of a DNTT-based OTFT fabricated by vapor-deposition is shown in Figure 7b. The mobility is about  $3 \text{ cm}^2/\text{Vs}$  at maximum with clear switching behaviors and low off-current and small hysteresis. Also, because the HOMO energy level of DNTT is low, the OTFT operates without degradation in atmospheric environment. The excellent characteristics of the DNTT-based OTFT devices can be explained by the packing structure elucidated by the single crystal X-ray structural analysis; two-dimensional herringbone structure with the large orbital overlap is the key (Figure 7d, e). Characteristically, the sulfur atoms in DNTT interact effectively between the molecules, and the HOMO coefficient is on the sulfur atoms so that they effectively contribute to increase the overlap of orbitals between the molecules (Figure 7a, e). Furthermore, from the thin film XRD, DNTT molecules form the lamella structure, in which the DNTT molecules stand almost perpendicular to the substrate, and herringbone structure in the in-plane direction (Figure 7f). As a result, a semiconductor channel with a well-balanced two-dimensional electronic structure is formed, which is consistent with the mobility-anisotropy experiments on the single-crystal transistors.<sup>13-15</sup>

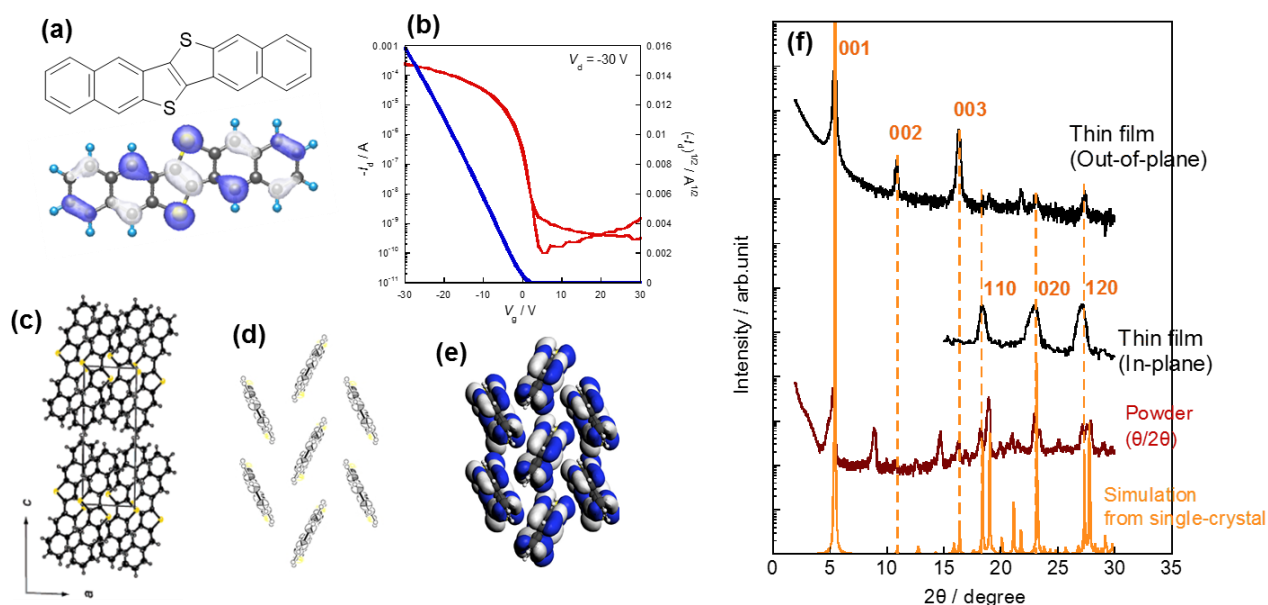


**Figure 7.** Molecular structure and calculated HOMO orbital of DNTT (a), typical transfer characteristics (b), crystal structure of DNTT: b-axis projection (c), herringbone packing (d), intermolecular HOMO overlap (e), XRDs (thin film and powder simulation) of DNTT (f).

### Applications of DNTT to OTFT research

Since DNTT has excellent OTFT characteristics and atmospheric stability as described above, DNTT has been widely applied as a standard OTFT material replacing pentacene for basic study<sup>16-23</sup> and application research.<sup>24, 25</sup> As examples of application of DNTT, Klauk and co-workers reported logic circuits driving at low voltage on the alumina insulator (Figure 8a).<sup>26, 27</sup> Someya and co-workers reported DNTT-based thermally-stable (up to sterilization temperature) OTFTs for medical applications<sup>28</sup> and also ultra-thin organic transistors (ca. 2  $\mu\text{m}$ ) that can be crimped (Figure 8b).<sup>29</sup> In addition, by combining these state-of-the-art technologies based on DNTT, Sakurai and co-workers reported a sheet-like transistor array capable of monitoring the electromyogram just by attaching on the skin, where DNTT is used as active layer material of the transistors (Figure 8c).<sup>30</sup> Although DNTT is an ideal material as a vapor deposition material, DNTT has a critical drawback; namely, DNTT is virtually insoluble in common organic solvents, which prevents application of DNTT into wet-processes.

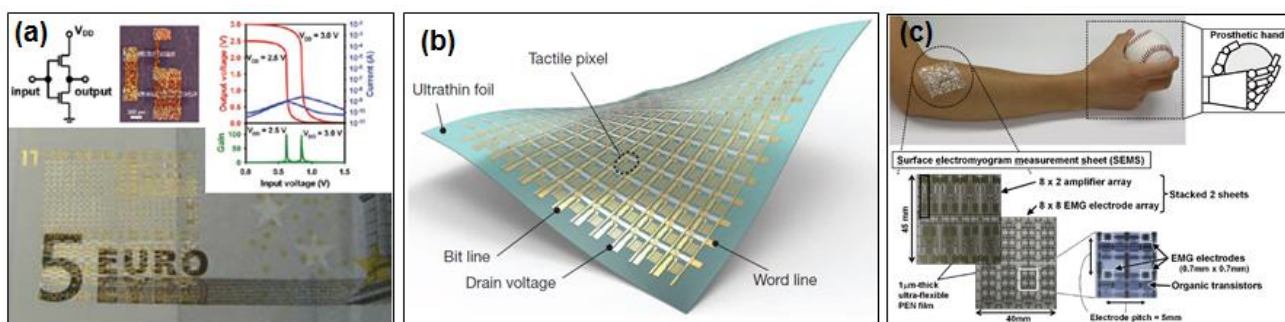


**Figure 8.** Examples of applied research on DNTT. Low-voltage organic circuits on banknote (a), reprinted with permission from ref 27. Copyright 2011 Wiley-VCH. Ultra-lightweight sensor sheet (b), reprinted with permission from ref 29. Copyright 2013 Nature Publishing Group. Electromyogram sensor array (c), reprinted with permission from ref 30. Copyright 2014 IEEE.

## 1-4 This thesis

In this doctoral thesis, I studied solubilization of DNNT, which is very useful as a vapor deposition OTFT material as mentioned above, and attempted to demonstrate high mobility, excellent stability, low voltage drivability, and transistor characteristics suitable for circuit design required for practical application through the wet processes. I also tried to apply the DNNT core to soluble p-type OPV material because solution-processable DNNT derivatives are also attractive for other organic electronics devices.

In Chapter 2, I describe solubilization of DNNT by introducing a branched alkyl group such as 2-ethylhexyl. I further investigate the influence of the number of substituents and the difference in branching position in the branched alkyl group to OTFT characteristics, and selected the most promising DNNT derivative (2-(4-ethyloctyl)-DNNT, 2-EO-DNNT) as a wet-processable material.

In Chapter 3, with 2-EO-DNNT selected in Chapter 2, optimization of spin-coating conditions to achieve further better device performances are discussed. In addition, I tested device stabilities (environmental, electrical, and thermal stabilities), and low-voltage operations, and finally I can demonstrate that all the superior characteristics demonstrated in the vapor-processed DNNT-based OTFTs (high stability, high mobility, low-voltage operation) are realized simultaneously by wet-processed devices with 2-EO-DNNT.

In Chapter 4, as a feasibility study, attempts to apply soluble DNNT derivatives into p-type OPV materials are described. Through this study, I demonstrated the possibilities and issues of future small molecular p-type OPV materials, focusing on the fact that the DNNT core has a deep HOMO level, which can realize high  $V_{oc}$  in OPV devices.

In Chapter 5, I summarize all the experimental work I have carried out, and discuss the future potential of soluble DNNTs as concluding remarks of this doctoral thesis.

## 1-5 References

1. 安達千波矢, 有機半導体のデバイス物性. 講談社: **2012**.
2. 工藤一浩, 有機トランジスタ – 評価と応用技術 -. シーエムシー出版: **2005**.
3. 森健彦; 長谷川達生, 有機トランジスタ材料の評価と応用II. シーエムシー出版: **2008**.
4. Shirota, Y.; Kageyama, H., Charge carrier transporting molecular materials and their applications in devices. *Chemical Reviews* **2007**, *107* (4), 953-1010.
5. Diao, Y.; Shaw, L.; Bao, Z. A.; Mannsfeld, S. C. B., Morphology control strategies for solution-processed organic semiconductor thin films. *Energy & Environmental Science* **2014**, *7* (7), 2145-2159.
6. Kitamura, M.; Arakawa, Y., Pentacene-based organic field-effect transistors. *Journal of Physics-Condensed Matter* **2008**, *20* (18), 16.
7. Maliakal, A.; Raghavachari, K.; Katz, H.; Chandross, E.; Siegrist, T., Photochemical stability of pentacene and a substituted pentacene in solution and in thin films. *Chemistry of Materials* **2004**, *16* (24), 4980-4986.
8. Takimiya, K.; Ebata, H.; Sakamoto, K.; Izawa, T.; Otsubo, T.; Kunugi, Y., 2,7-Diphenyl 1 benzothieno 3,2-b benzothiophene, a new organic semiconductor for air-stable organic field-effect transistors with mobilities up to 2.0 cm<sup>2</sup> V<sup>-1</sup> s<sup>-1</sup>. *Journal of the American Chemical Society* **2006**, *128* (39), 12604-12605.
9. Takimiya, K.; Yamamoto, T.; Ebata, H.; Izawa, T., Design strategy for air-stable organic semiconductors applicable to high-performance field-effect transistors. *Science and Technology of Advanced Materials* **2007**, *8* (4), 273-276.
10. Yamamoto, T.; Takimiya, K., Facile synthesis of highly pi-extended heteroarenes, dinaphtho 2,3-b : 2',3'-f chalcogenopheno 3,2-b chalcogenophenes, and their application to field-effect transistors. *Journal of the American Chemical Society* **2007**, *129* (8), 2224+.
11. Takimiya, K.; Shinamura, S.; Osaka, I.; Miyazaki, E., Thienoacene-Based Organic Semiconductors. *Advanced Materials* **2011**, *23* (38), 4347-4370.
12. Takimiya, K.; Osaka, I.; Mori, T.; Nakano, M., Organic Semiconductors Based on 1 Benzothieno 3,2-b 1 benzothiophene Substructure. *Accounts of Chemical Research* **2014**, *47* (5), 1493-1502.
13. Uno, M.; Tominari, Y.; Yamagishi, M.; Doi, I.; Miyazaki, E.; Takimiya, K.; Takeya, J., Moderately anisotropic field-effect mobility in dinaphtho 2,3-b:2'(3)-f thiopheno 3,2-b thiophenes single-crystal transistors. *Applied Physics Letters* **2009**, *94* (22), 3.
14. Xie, W.; Willa, K.; Wu, Y. F.; Hausermann, R.; Takimiya, K.; Batlogg, B.; Frisbie, C. D., Temperature-Independent Transport in High-Mobility Dinaphtho-Thieno-Thiophene (DNTT) Single Crystal Transistors. *Advanced Materials* **2013**, *25* (25), 3478-3484.
15. Haas, S.; Takahashi, Y.; Takimiya, K.; Hasegawa, T., High-performance dinaphtho-thieno-thiophene single crystal field-effect transistors. *Applied Physics Letters* **2009**, *95* (2).
16. Sanchez-Carrera, R. S.; Atahan, S.; Schrier, J.; Aspuru-Guzik, A., Theoretical Characterization of the Air-Stable, High-Mobility Dinaphtho 2,3-b:2'3'-f thieno 3,2-b -thiophene Organic Semiconductor. *Journal of Physical Chemistry C* **2010**, *114* (5), 2334-2340.

17. Yamagishi, M.; Soeda, J.; Uemura, T.; Okada, Y.; Takatsuki, Y.; Nishikawa, T.; Nakazawa, Y.; Doi, I.; Takimiya, K.; Takeya, J., Free-electron-like Hall effect in high-mobility organic thin-film transistors. *Physical Review B* **2010**, *81* (16), 4.
18. Matsui, H.; Kumaki, D.; Takahashi, E.; Takimiya, K.; Tokito, S.; Hasegawa, T., Correlation between interdomain carrier hopping and apparent mobility in polycrystalline organic transistors as investigated by electron spin resonance. *Physical Review B* **2012**, *85* (3), 9.
19. Yagi, H.; Miyazaki, T.; Tokumoto, Y.; Aoki, Y.; Zenki, M.; Zaima, T.; Okita, S.; Yamamoto, T.; Miyazaki, E.; Takimiya, K.; Hino, S., Ultraviolet photoelectron spectra of 2,7-diphenyl 1 benzothieno 3,2-b 1 benzothiophene and dinaphtho 2,3-b:2 '3 'f thieno 3,2-b thiophene. *Chemical Physics Letters* **2013**, *563*, 55-57.
20. Sakai, K.; Okada, Y.; Kitaoka, S.; Tsurumi, J.; Ohishi, Y.; Fujiwara, A.; Takimiya, K.; Takeya, J., Anomalous Pressure Effect in Heteroacene Organic Field-Effect Transistors. *Physical Review Letters* **2013**, *110* (9), 5.
21. Jung, M. C.; Leyden, M. R.; Nikiforov, G. O.; Lee, M. V.; Lee, H. K.; Shin, T. J.; Takimiya, K.; Qi, Y. B., Flat-Lying Semiconductor-Insulator Interfacial Layer in DNTT Thin Films. *Acs Applied Materials & Interfaces* **2015**, *7* (3), 1833-1840.
22. Aghamohammadi, M.; Rodel, R.; Zschieschang, U.; Ocal, C.; Boschker, H.; Weitz, R. T.; Barrena, E.; Klauk, H., Threshold-Voltage Shifts in Organic Transistors Due to Self-Assembled Monolayers at the Dielectric: Evidence for Electronic Coupling and Dipolar Effects. *Acs Applied Materials & Interfaces* **2015**, *7* (41), 22775-22785.
23. Fujita, T.; Atahan-Evrenk, S.; Sawaya, N. P. D.; Aspuru-Guzik, A., Coherent Dynamics of Mixed Frenkel and Charge-Transfer Excitons in Dinaphtho 2,3-b:2 '3 'f thieno 3,2-b -thiophene Thin Films: The Importance of Hole Delocalization. *Journal of Physical Chemistry Letters* **2016**, *7* (7), 1374-1380.
24. McCarthy, M. A.; Liu, B.; Donoghue, E. P.; Kravchenko, I.; Kim, D. Y.; So, F.; Rinzler, A. G., Low-Voltage, Low-Power, Organic Light-Emitting Transistors for Active Matrix Displays. *Science* **2011**, *332* (6029), 570-573.
25. McCarthy, M. A.; Liu, B.; Rinzler, A. G., High Current, Low Voltage Carbon Nanotube Enabled Vertical Organic Field Effect Transistors. *Nano Letters* **2010**, *10* (9), 3467-3472.
26. Zschieschang, U.; Ante, F.; Yamamoto, T.; Takimiya, K.; Kuwabara, H.; Ikeda, M.; Sekitani, T.; Someya, T.; Kern, K.; Klauk, H., Flexible Low-Voltage Organic Transistors and Circuits Based on a High-Mobility Organic Semiconductor with Good Air Stability. *Advanced Materials* **2010**, *22* (9), 982-+.
27. Zschieschang, U.; Yamamoto, T.; Takimiya, K.; Kuwabara, H.; Ikeda, M.; Sekitani, T.; Someya, T.; Klauk, H., Organic Electronics on Banknotes. *Advanced Materials* **2011**, *23* (5), 654-+.
28. Kuribara, K.; Wang, H.; Uchiyama, N.; Fukuda, K.; Yokota, T.; Zschieschang, U.; Jaye, C.; Fischer, D.; Klauk, H.; Yamamoto, T.; Takimiya, K.; Ikeda, M.; Kuwabara, H.; Sekitani, T.; Loo, Y. L.; Someya, T., Organic transistors with high thermal stability for medical applications. *Nature Communications* **2012**, *3*, 7.
29. Kaltenbrunner, M.; Sekitani, T.; Reeder, J.; Yokota, T.; Kuribara, K.; Tokuhara, T.; Drack, M.; Schwodiauer, R.; Graz, I.; Bauer-Gogonea, S.; Bauer, S.; Someya, T., An Ultra-Lightweight Design for

Imperceptible Plastic Electronics. *Nature* **2013**, *499*, 458.

30. Fuketa, H.; Yoshioka, K.; Shinozuka, Y.; Ishida, K.; Yokota, T.; Matsuhisa, N.; Inoue, Y.; Sekino, M.; Sekitani, T.; Takamiya, M.; Someya, T.; Sakurai, T., 1  $\mu$ m-Thickness Ultra-Flexible and High Electrode-Density Surface Electromyogram Measurement Sheet With 2 V Organic Transistors for Prosthetic Hand Control. *Ieee Transactions on Biomedical Circuits and Systems* **2014**, *8* (6), 824-833.

## Chapter 2

### Synthesis of solution-processable DNTT derivatives

#### 2-1 Introduction

In chapter 2, I have examined a new approach to make DNTT derivatives soluble in organic solvents, in order to apply the superiority of DNTT as the promising core structure for organic semiconducting materials. To achieve this, the primary question is how to solubilize the DNTT core with keeping the semiconducting properties. Several solubilizing modifications preserving the semiconducting characteristics of rigid, insoluble organic semiconducting cores have been reported. For example, to introduce long alkyl groups<sup>1,2</sup> or bulky substituents<sup>3-5</sup> such a way that the substituents do not block, rather inforce, the intermolecular interaction between the semiconducting cores in the condensed phase (Figure 1a, b). Another method could be a so-called “precursor” approach<sup>6-8</sup> where a precursor with a non-planar, deformed structure, being different from the original semiconducting  $\pi$ -conjugated systems, for example, a Diels-Alder cycloaddition adduct, can react thermally or photochemically after solution-deposition at the precursor stage on the substrates to reproduce active semiconducting material (Figure 1c).

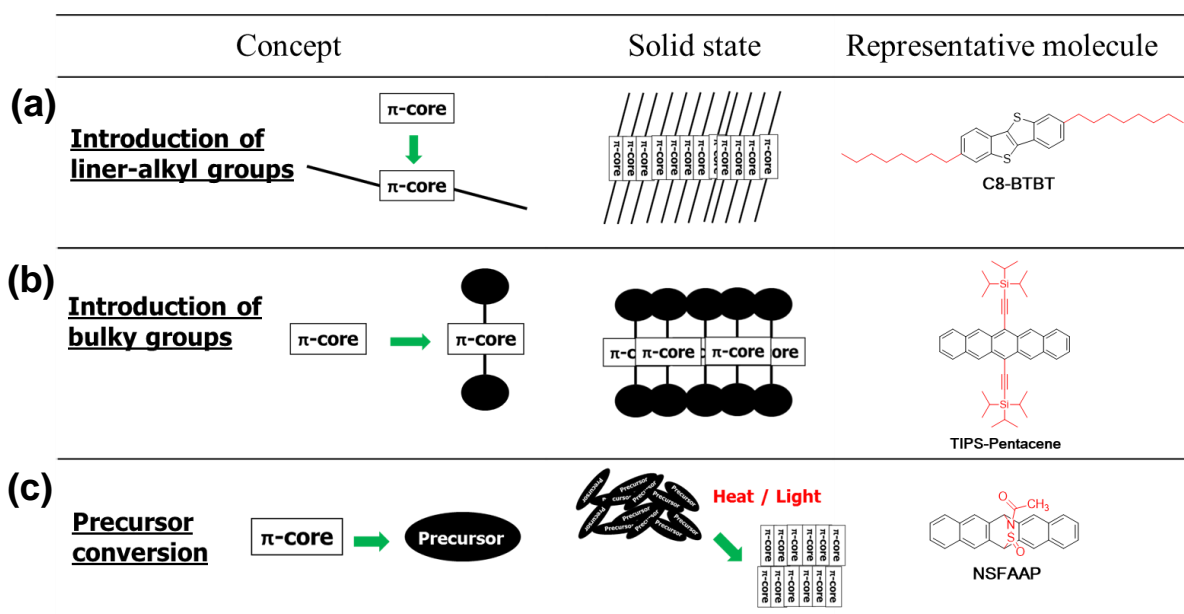


**Figure 1.** Representative three solubilization strategies of aromatic fused polycyclic small molecules

Development of soluble DNTT derivatives via introduction of long alkyl groups was already examined (Figure 2).<sup>9,10</sup> However, the resulting alkylated DNTTs ( $C_n$ -DNTTs) were not very soluble in ordinary organic solvents at room temperature, and thus only a limited solution process technique under specific conditions allows to fabricate solution-processed OTFT<sup>11</sup> which is in sharp contrast to highly soluble dialkylated [1]benzothieno[3,2-*b*][1]benzothiophenes ( $C_n$ -BTBTs),<sup>1</sup> lower homologues of  $C_n$ -DNTTs, which can afford various solution-processed OTFT showing very high mobilities up to  $43 \text{ cm}^2 \text{ V}^{-1} \text{ s}^{-1}$ .<sup>12-15</sup> On the other hand, Kimura and coworkers have successfully developed a new soluble DNTT precursor (5,14-*N*-phenylmaleimide-dinaphtho[2,3-*b*:2',3'-*f*]thieno [3,2-*b*]thiophene) for solution-processed high-performance OTFT with good environmental stability.<sup>16,17</sup> Although the precursor approach to soluble DNTTs was quite successful, the synthesis of the precursor requires less effective Diels-Alder reactions with low yields and the reactions need heating at around  $200 \text{ }^\circ\text{C}$ .

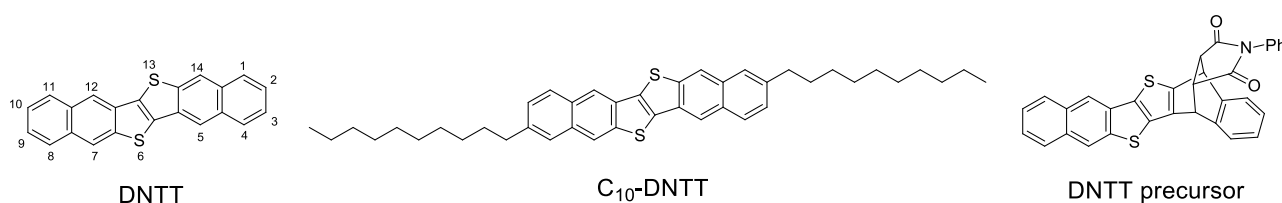


**Figure 2.** Molecular structures of DNTT, alkylated DNTTs ( $C_n$ -DNTTs), and DNTT precursor.

In this chapter, I have reexamined the alkylation approach to soluble DNTTs by employing branched alkyl groups, and found that introduction of branched alkyl group on DNTT can enhance solubility. Furthermore, mono-substituted DNTTs with modest solubilities can afford solution-processed OTFT with mobility higher than  $0.1 \text{ cm}^2 \text{ V}^{-1} \text{ s}^{-1}$ . Here I report their synthesis, electronic properties, thin film structures and OTFT characteristics.

## 2-2 Results and discussion

### 2-2-1 Molecular design and synthesis

It has been widely demonstrated and commonly recognized that branched alkyl groups, such as 2-ethylhexyl, can effectively enhance solubility when they are attached on  $\pi$ -extended organic semiconducting oligomers and polymers. On the other hand, the placement of branched alkyl groups would influence intermolecular interaction between the  $\pi$ -conjugated cores and hence electronic properties of the resulting thin films. For this reason, the number, shape, and size of branched alkyl groups should be carefully tuned.<sup>18,19</sup> With these background, I have designed several DNTT derivatives (Figure 3) in order to know effects from the molecular structures. The first branched alkyl group I have examined is 2-ethylhexyl (EH) group and tried to establish their effective synthetic methods, both for the di-substituted 2,9-bis(2-ethylhexyl)-DNTT (**1a**) and mono-substituted 2-(2-ethylhexyl)-DNTT (**2a**). Then, I modify the structure of branched alkyl group by changing the branching position in the trunk part of the group from the second (EH) to the third (3-ethylheptyl, EHep) or fourth (4-ethyloctyl, EO) carbon atom. As a result, I have synthesized three 2,9-dialkyl- (**1**) and 2-alkyl DNTT derivatives (**2**) as follows.

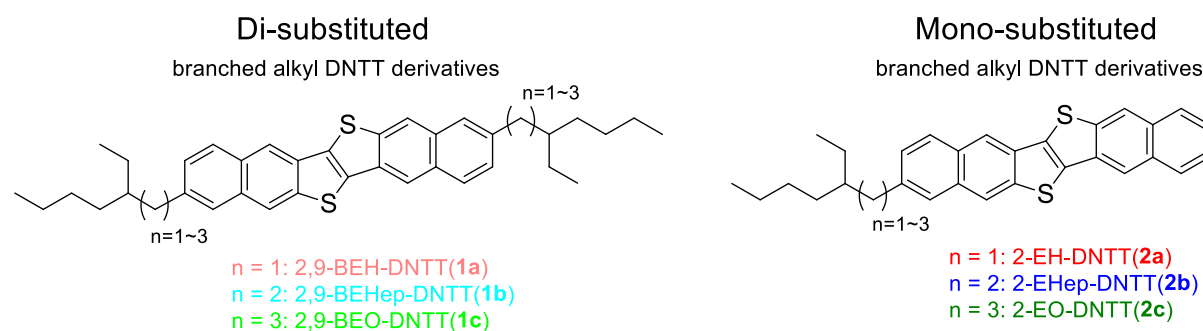
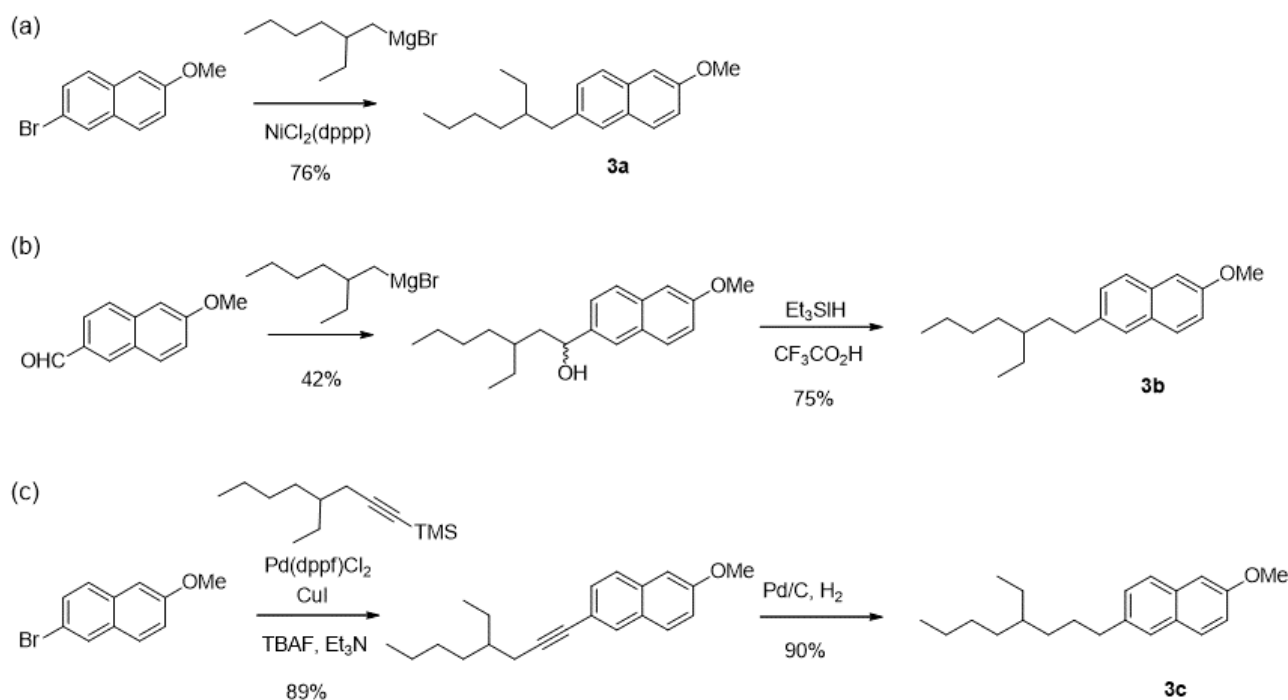


**Figure 3.** Molecular structures of branched alkyl DNTT derivatives.

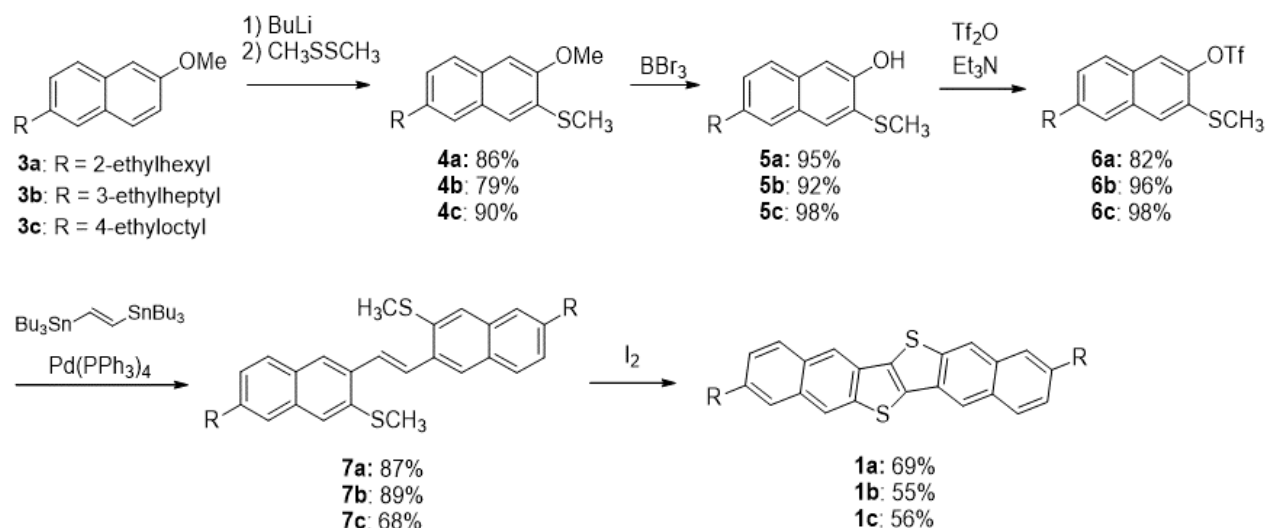
The synthesis of DNTT and its derivatives had been investigated and established a general method starting from 6-substituted 2-methoxynaphthalene derivatives, which can be reliably converted into 2,9-disubstituted DNTT derivatives.<sup>20</sup> For the synthesis of branched-alkylated DNTTs (**1** and **2**), I thus

first synthesized the corresponding 6-alkyl-2-methoxynaphthalenes (**3a–c**, Scheme 1). Depending on the branching position in the alkyl groups, three different approaches were employed. For the synthesis of the 2-ethylhexyl derivative (**3a**), the standard Kumada-Tamao coupling<sup>21</sup> using the corresponding Grignard reagent and 6-bromo-2-methoxynaphthalene can effectively afford the desired 6-ethylhexyl derivative (Scheme 1a). On the other hand, the synthesis of the 3-ethylheptyl derivative (**3b**) was initiated from commercial 6-methoxy-2-naphthaldehyde, which was reacted with 2-ethylhexyl magnesium, in situ generated from 1-bromo-2-ethylhexane, to give the corresponding benzylic alcohol intermediate. The alcoholic functionality was then efficiently removed by ionic deoxygenation with triethylsilane in the presence of trifluoroacetic acid to afford 6-ethylheptyl-2-methoxynaphthalene (**3b**, Scheme 1b).<sup>22,23</sup> Further increase of a carbon atom between the naphthalene core and the branching carbon atom in the alkyl group was achieved by Sonogashira coupling<sup>24</sup> between 6-bromo-2-methoxynaphthalene and 4-ethyloct-1-yne, in situ generated from the corresponding 1-trimethylsilyl derivative,<sup>25,26</sup> followed by hydrogenation (Scheme 1c).



**Scheme 1.** Synthesis of 6-alkyl-2-methoxynaphthalenes (**3a–c**).

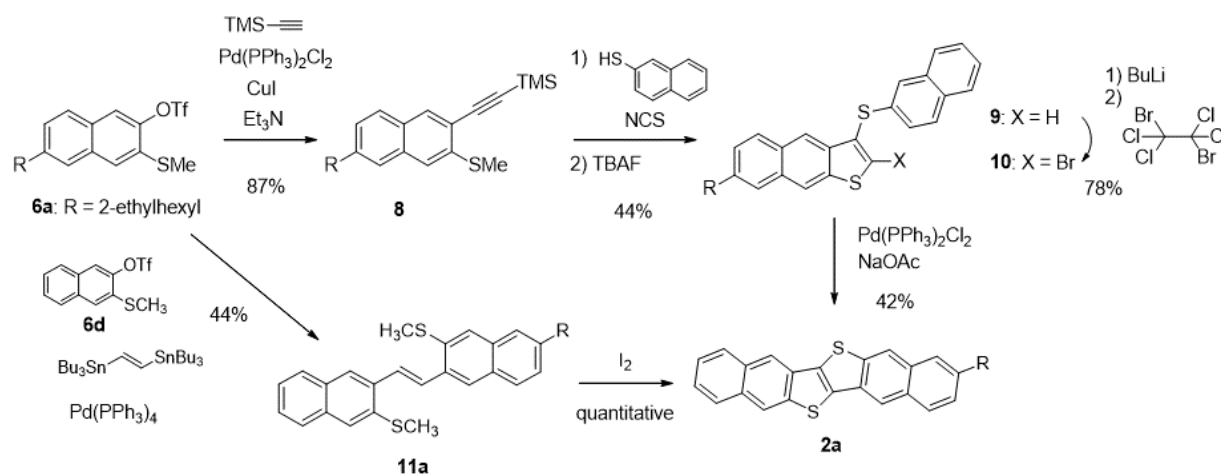
Following the reported procedure,<sup>20</sup> these 6-alkyl-2-methoxynaphthalenes (**3**) were readily converted into 2,9-dialkyl-DNTTs in good yields via the five-step reactions consisting of a methylthiolation at the 3-position to give **4** and a functional conversion of the 2-methoxy group into the corresponding trifluoromethanesulfonyloxy derivative (**6**), followed by a coupling reaction with 1,2-bis(trimethylstannyl)ethene to give the precursor (**7**), which was finally converted into DNTT derivatives (**1**) via the iodine-promoted thieno[3,2-*b*]thiophene formation reaction (Scheme 2). Note that the syntheses of di-substituted DNTT derivatives were quite effective to afford very good yields for all the compounds.



**Scheme 2.** Synthesis of 2,9-dialkyl DNTTs (**1a–c**) from 6-alkyl-2-methoxynaphthalene (**3**).

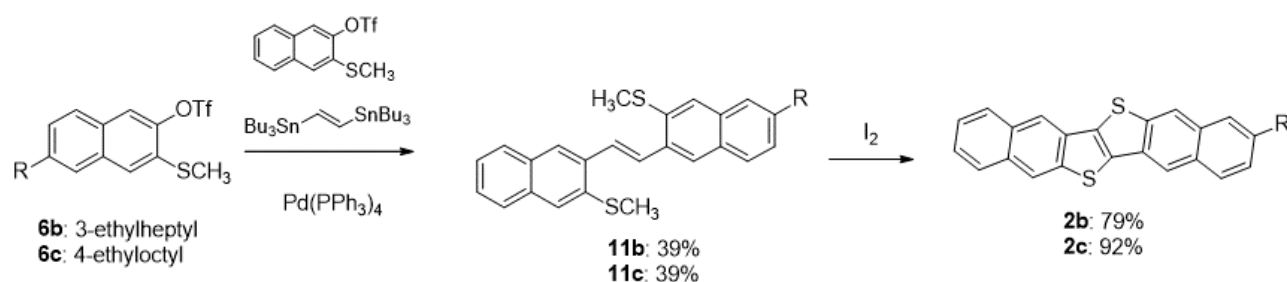
For the synthesis of mono-substituted DNTTs, I examined two different approaches, targeting 2-(2-ethylhexyl)-DNTT (**2a**) as a model case from **6a** (Scheme 3). The first approach was the consecutive thiophene-annulation reaction, which has been demonstrated to be quite effective for the synthesis of unsymmetrical BTBT derivatives and related compounds.<sup>27</sup> Starting from **6a**, a trimethylsilyl (TMS)-protected acetylene moiety was introduced via Stille or Sonogashira coupling reaction, and the resulting acetylene derivative (**8**) was reacted with 2-naphthylsulfenylchloride, in situ generated from 2-naphthalenethiol and *N*-chlorosuccinimide (NCS) followed by the treatment of tetrabutylammonium fluoride (TBAF) to give 7-(2-ethylhexyl)-3-(2-naphthylthio)naphtho [2,3-*b*]thiophene (**9**).<sup>28</sup> After conversion into the bromide (**10**), the intramolecular aryl-aryl coupling catalyzed by bis(triphenylphosphine)palladium(II) dichloride afforded desired **2a** in a 13% total yield via a four-step reaction from **6a**.

The second approach was to use non-selective coupling reaction between two different 3-methylthio-2-(trifluoromethanesulfonyloxy)naphthalenes (**6**) and 1,2-bis(trimethylstannyl)ethene followed by the iodine-promoted thieno[3,2-*b*]thiophene formation reaction (Scheme 3). The first coupling reaction of **6a** and **6d** afforded the unsymmetrical intermediate (**11a**) together with two symmetrical byproducts. Chromatographic purification can effectively isolate desired **11a** in a 44% yield, which was effectively converted into the corresponding DNTT derivative (**2a**) in an almost quantitative yield, resulting in the total yield of 44% via only two steps from **6a**.



**Scheme 3.** Two different approaches to the synthesis of 2-(2-ethylhexyl)-DNTT (**2a**).

In order to effectively use **6a**, which is the most precious intermediate in the syntheses of **2a**, the first selective approach was initially thought to be more desirable than the second, because the second one should go through the non-selective, random coupling, where the maximum yield of the unsymmetrical intermediate is 50%, provided that the reactivity of two substrates are identical. In the actual synthesis, however, it turned out that the fast selective approach has several drawbacks, including low isolated yield in each reaction, particularly the final step (42% isolated yield) and formation of a unexpected byproduct, naphthalene disulfide, which was very difficult to remove from the reaction mixture, in the second step. In contrast, although the yield of the unsymmetrical product in the first non-selective coupling reaction was 44%, the well-established iodine-promoted thienothiophene formation can proceed almost quantitatively, resulting in a quite efficient synthesis of the desired **2a**. From these comparisons, I have concluded that the second non-selective approach is more practical than the first one, and other derivatives with different alkyl groups were accordingly synthesized via the second approach (Scheme 4). Purification of the DNTT derivatives was done by recrystallization and gradient sublimation under reduced pressure to give analytical and device grade samples.



**Scheme 4.** Synthesis of 2-(3-ethylheptyl)- (**2b**) and 2-(4-ethyloctyl)- DNTT (**2c**).

## 2-2-2 Molecular and thin film properties

Molecular properties, such as solubility, melting points, oxidation potentials (Figure 4a), absorption spectra (Figure 4b), and expected HOMO energy levels and HOMO-LUMO energy gaps, of new DNTT derivatives together with parent DNTT and C<sub>10</sub>-DNTT as references are summarized in Table 1. Solubilities of the present DNTT derivatives are, as expected, enhanced significantly, especially for the di-substituted derivatives (**1a–c**). For example, compared to the solubility of C<sub>10</sub>-DNTT in toluene (0.070 g L<sup>-1</sup> at 50 °C in toluene), solubilities of new derivatives are higher by ca. 10-100 times under the identical conditions. The HOMO energy levels ( $E_{\text{HOMOS}}$ ) and energy gaps ( $E_{\text{gs}}$ ) of the derivatives evaluated by the solution electrochemistry and absorption spectra in solution are almost the same with those of the parent DNTT and C<sub>10</sub>-DNTT, indicating no significant electronic perturbation from the branched alkyl groups.

**Table 1. Molecular properties of new DNTT derivatives**

Compound	Solubility/ g L <sup>-1</sup> <sup>a</sup>		M.p. / °C	DSC peaks / °C	$E_{\text{onset/peak}}$ / V <sup>b</sup>	$E_{\text{HOMO}}$ / eV <sup>c</sup>	$\lambda_{\text{peak/edge}}$ / nm <sup>d</sup>	$E_{\text{g}}$ / eV <sup>e</sup>
	CHCl <sub>3</sub>	toluene						
<b>1a</b>	6.2/10	4.6/8.0/16	231	232	1.11/1.32	-5.3	402/416	3.0
<b>1b</b>	1.5/4.6	1.2/2.7/8.0	175	176, 211	1.14/1.32	-5.3	402/416	3.0
<b>1c</b>	6.2/7.8	>15/>15/>15	210	214	1.08/1.32	-5.3	402/417	3.0
<b>2a</b>	1.0/2.4	0.90/1.4/5.3	334	332	1.14/1.34	-5.3	402/417	3.0
<b>2b</b>	0.72/1.3	0.62/1.0/3.1	368	>350	1.12/1.34	-5.3	402/419	3.0
<b>2c</b>	1.1/1.5	0.73/1.1/2.7	345	>350	1.15/1.35	-5.3	402/417	3.0
DNTT <sup>f</sup>	-/< 0.06	-/< 0.06	>400	>350	1.11/1.05	-5.4	402/416	2.9
C <sub>10</sub> -DNTT <sup>g</sup>	-/< 0.06	-/0.070/0.86	310	-	1.08/-	-5.4	402/-	2.9

<sup>a</sup> Solubilities were determined as concentration of saturated solution. Data were obtained at rt and 50 °C in chloroform, and at rt, 50, and 100 °C in toluene.

<sup>b</sup> V vs Ag/AgCl. Pt as working and counter electrodes, PhCN as solvent, Bu<sub>4</sub>NPF<sub>6</sub> (0.1M) as supporting electrolyte, scan rate = 0.1 V s<sup>-1</sup>. All the potentials were calibrated with the Fc/Fc<sup>+</sup> ( $E_{1/2} = +0.60$  V measured under identical conditions). <sup>c</sup> Estimated with a following equation:  $E_{\text{HOMO}} = -(4.20 + E_{\text{onset}})$ . <sup>d</sup> In chloroform solution. <sup>e</sup> Calculated from  $\lambda_{\text{edge}}$ . <sup>f</sup> Data from reference 29. <sup>g</sup> Data from reference 9.

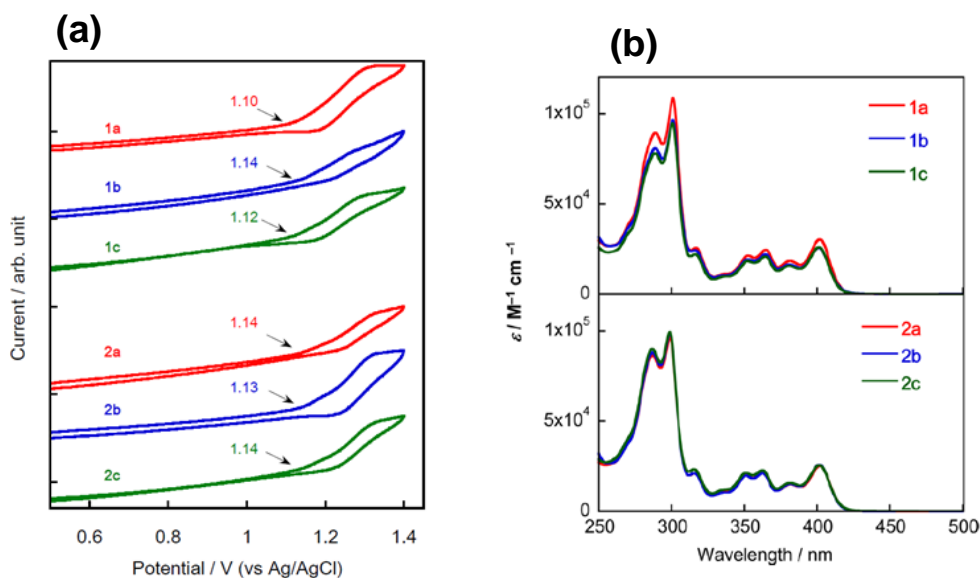


**Figure 4.** Cyclic voltammograms (a), absorption spectra in chloroform solution (b).

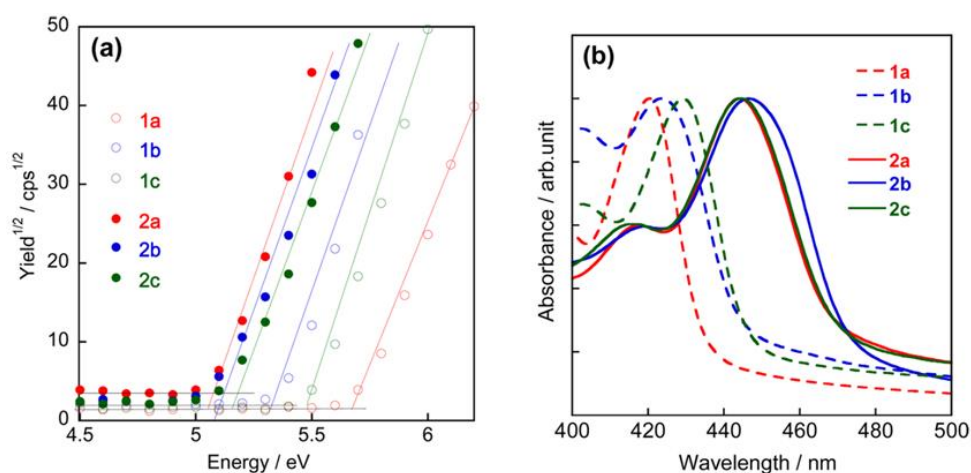
Thin films of the new DNTT derivatives can be deposited by spin-coating from their hot chloroform solution (ca 0.2 wt%). The optical properties of thin films were significantly dependent on the number and shape of branched alkyl group. Figure 5 shows photoelectron yield spectroscopy in air (PESA) and absorption spectra recorded by using the spin-coated thin films. It is noticeable that ionization potentials (IPs) and absorption spectra of the thin films are largely dependent on the number of alkyl groups and also the branching position in the alkyl group (Table 2). In particular, IP of **1a** was determined to be 5.7 eV, which is significantly larger by 0.3 eV than that of DNTT. This can be explained by its reduced intermolecular interaction in the thin film state caused by two 2-ethylhexyl groups at the close proximity to the DNTT core. Such a drastic effect could be mitigated by changing the branching position; IPs of **1b** and **1c** were 5.3 and 5.5 eV, respectively. It is reasonable to consider that the effect caused by the branched-alkyl groups depends on the distance between the branching carbon atom to the DNTT core. In addition, odd-even effect of the branching carbon may exist, which could alter the direction of the branched alkyl groups pointing towards the inside (the DNTT core direction, **1a** and **1c**) or the outside (**1b**). In sharp contrast, all the mono-substituted derivatives (**2a–c**) showed IPs of around 5.1 eV, which is close to that of C<sub>10</sub>-DNTT (4.9 eV).<sup>9</sup>

**Table 2. Thin film properties of DNTT derivatives.**

Compound	IP / eV <sup>a</sup>	$\lambda_{\text{peak/edge}}$ / nm <sup>b</sup>	$E_g$ / eV <sup>c</sup>
<b>1a</b>	5.7	420/435	2.8
<b>1b</b>	5.3	424/447	2.8
<b>1c</b>	5.5	429/446	2.8
<hr/>			
<b>2a</b>	5.1	443/471	2.6
<b>2b</b>	5.1	446/474	2.6
<b>2c</b>	5.1	445/470	2.6
<hr/>			
DNTT <sup>d</sup>	5.4	447/473	2.6
C <sub>10</sub> -DNTT <sup>e</sup>	4.9	470/483	2.6

<sup>a</sup> Determined by photoelectron yield spectroscopy in air (PESA) using the spin-coated thin films on ITO substrates <sup>b</sup> Measured on the spin-coated thin films on the quartz substrates. <sup>c</sup> Calculated from  $\lambda_{\text{edge}}$ . <sup>d</sup> Data from reference 29. <sup>e</sup> Data from reference 9.

The absorption spectra also appeared to reflect the intermolecular interaction in the thin film state. Among the alkylated derivatives, **1a** with the largest IP showed a most blue shifted peak ( $\lambda_{\text{max}}$ : 420 nm), whereas the absorption peaks in the **1b**- and **1c**- thin films were slightly red-shifted (around 424-429 nm). In sharp contrast, much pronounced red shifts were observed for the mono-substituted derivatives (**2a–c**) showing absorption peaks at around 445 nm, regardless of the alkyl groups. By comparing with these thin film absorption spectra with those of DNTT and C<sub>10</sub>-DNTT (Table 2), it can be concluded that, as discussed based on the IP data, **2a–c** with one alkyl group intermolecularly interact in the thin film state to larger extent than **1a–c** with two alkyl groups.

**Figure 5.** PESA (a) and absorption spectra (b) of the spin-coated thin films.

## 2-2-3 TFT fabrication and characterization

### *Thin-film transistor devices based on di-substituted derivatives (1a–c)*

Thin film transistors with a bottom-gate top-contact configuration were fabricated by using spin-coated thin films. Table 3 summarized the device metrics obtained for **1a–c**. Although the performances of TFT are dependent on the alkyl groups, the device performances are generally poor compared with those of the parent DNTT or C<sub>10</sub>-DNTT. In particular, no clear response was observed for the **1a**-based OTFT. On the other hand, the best device characteristics was obtained for **1b**, with hole mobility of 0.011 cm<sup>2</sup> V<sup>-1</sup> s<sup>-1</sup> and *I*<sub>on/off</sub> of 10<sup>5</sup> (Figure 6). The best mobility value is lower than those for DNTT or C<sub>10</sub>-DNTT by more than two orders of magnitude, indicating that the branching in the two attached alkyl groups is not promising approach to soluble DNTT-based organic semiconductors, which is consistent with the physicochemical properties of the thin films state as discussed above.

**Table 3. Characteristics of OTFT based on di-substituted DNTT derivatives.**

Compound	SAM	Spin-coating			Vapor deposition		
		$\mu / \text{cm}^2 \text{V}^{-1} \text{s}^{-1}$ <sup>a</sup>	$V_{\text{th}} / \text{V}$	$I_{\text{on/off}}$	$\mu / \text{cm}^2 \text{V}^{-1} \text{s}^{-1}$ <sup>a</sup>	$V_{\text{th}} / \text{V}$	$I_{\text{on/off}}$
<b>1a</b>	untreated				0.011 (0.0088)	–33	~ 10 <sup>4</sup>
	HMDS				0.026 (0.018)	–34	~ 10 <sup>5</sup>
	OTS	No response			0.010 (0.0060)	–39	~ 10 <sup>6</sup>
	ODTS					-	
<b>1b</b>	untreated	$1.4 (0.59) \times 10^{-3}$	–25	~ 10 <sup>5</sup>	$6.1 (5.0) \times 10^{-4}$	–26	~ 10 <sup>6</sup>
	HMDS	$1.1 (0.57) \times 10^{-2}$	–28	~ 10 <sup>6</sup>	$6.9 (1.4) \times 10^{-4}$	–28	~ 10 <sup>5</sup>
	OTS	$9.8 (5.4) \times 10^{-3}$	–28	~ 10 <sup>7</sup>	$3.4 (2.2) \times 10^{-5}$	–43	~ 10 <sup>4</sup>
	ODTS	$5.5 (2.6) \times 10^{-3}$	–26	~ 10 <sup>6</sup>		-	
<b>1c</b>	untreated	$5.1 (4.0) \times 10^{-5}$	–25	~ 10 <sup>5</sup>	$1.7 (1.7) \times 10^{-3}$	–25	~ 10 <sup>7</sup>
	HMDS	$1.1 (4.4) \times 10^{-5}$	–19	~ 10 <sup>3</sup>	$1.9 (1.4) \times 10^{-3}$	–25	~ 10 <sup>6</sup>
	OTS	$1.6 (0.85) \times 10^{-5}$	–21	~ 10 <sup>4</sup>	$2.2 (1.1) \times 10^{-3}$	–36	~ 10 <sup>7</sup>
	ODTS	$5.7 (2.7) \times 10^{-5}$	–21	~ 10 <sup>6</sup>		-	

<sup>a</sup> Typical values obtained from more than 6 devices. The values in parentheses are average value.

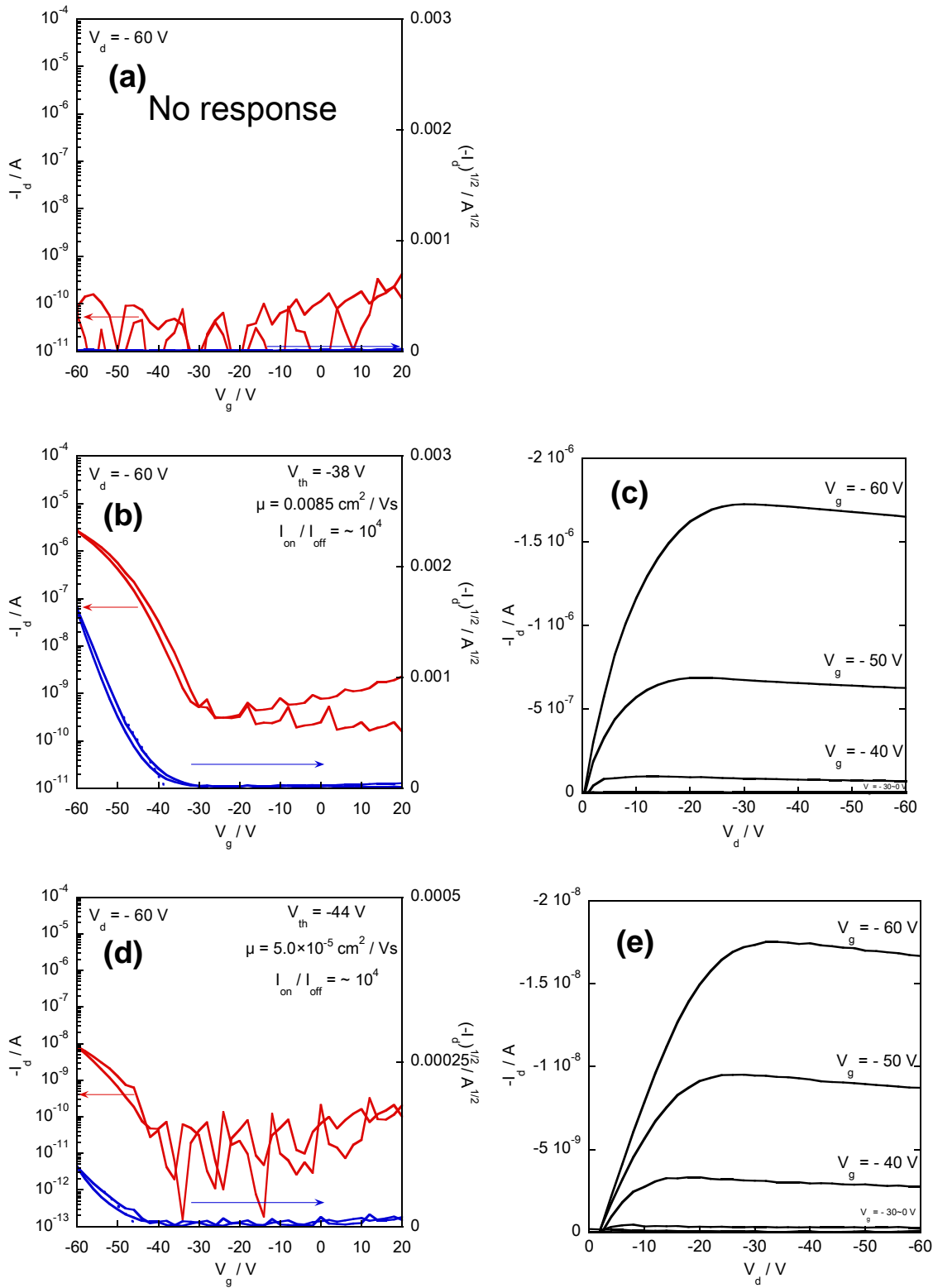


**Figure 6.** Typical transfer and output characteristics of OTFT devices with the spin-coated thin films of **1a** (a) and **1b** (b, c), **1c** (d, e).

### Thin-film transistors based on mono-substituted derivatives (2a–c)

In sharp contrast to the poor semiconducting characteristics of devices based on **1a–c**, mono-substituted ones (**2a–c**) afforded devices with decent transistor characteristics. With spin-coated thin films, **2a–c** gave nicely performed devices with mobility as high as  $0.3 \text{ cm}^2 \text{ V}^{-1} \text{ s}^{-1}$  and  $I_{\text{on/off}}$  of  $\sim 10^7$  (Table 4, Figure 7). Interestingly, **2b**-based devices from several runs of device fabrications showed mobility of up to  $1.6 \text{ cm}^2 \text{ V}^{-1} \text{ s}^{-1}$  with  $I_{\text{on/off}}$  of  $10^5$  (Figure S3), though the reproducibility was not very good. This can be related to the relatively low solubility of the mono-substituted derivatives, which caused lower uniformity of the spin-coated thin films, resulting in larger variation of device characteristics.

**Table 4. Characteristics of solution-processed OTFT based on mono-substituted DNTT derivatives (2a–c).**

Compound	SAM	$\mu / \text{cm}^2 \text{ V}^{-1} \text{ s}^{-1}$ <sup>a</sup>	$V_{\text{th}} / \text{V}$	$I_{\text{on/off}}$
<b>2a</b>	untreated	0.36 (0.27)	-11	$\sim 10^7$
	HMDS	0.11 (0.066)	-6.4	$\sim 10^5$
	OTS	0.12 (0.032)	-11	$\sim 10^5$
	ODTS	0.021 (0.015)	-5.9	$\sim 10^5$
<b>2b</b>	untreated	0.11 (0.064)	-8.3	$\sim 10^5$
	HMDS	0.28 (0.11)	-4.4	$\sim 10^6$
	OTS	0.086 (0.046)	-7.8	$\sim 10^6$
	ODTS	0.19 (0.091)	-9.2	$\sim 10^5$
<b>2c</b>	untreated	0.55 (0.16)	-8.6	$\sim 10^5$
	HMDS	0.28 (0.13)	-15	$\sim 10^5$
	OTS	0.075 (0.029)	0.30	$\sim 10^4$
	ODTS	0.16 (0.056)	-9.0	$\sim 10^4$

<sup>a</sup> Typical values obtained from more than 6 devices. The values in parentheses are average value.

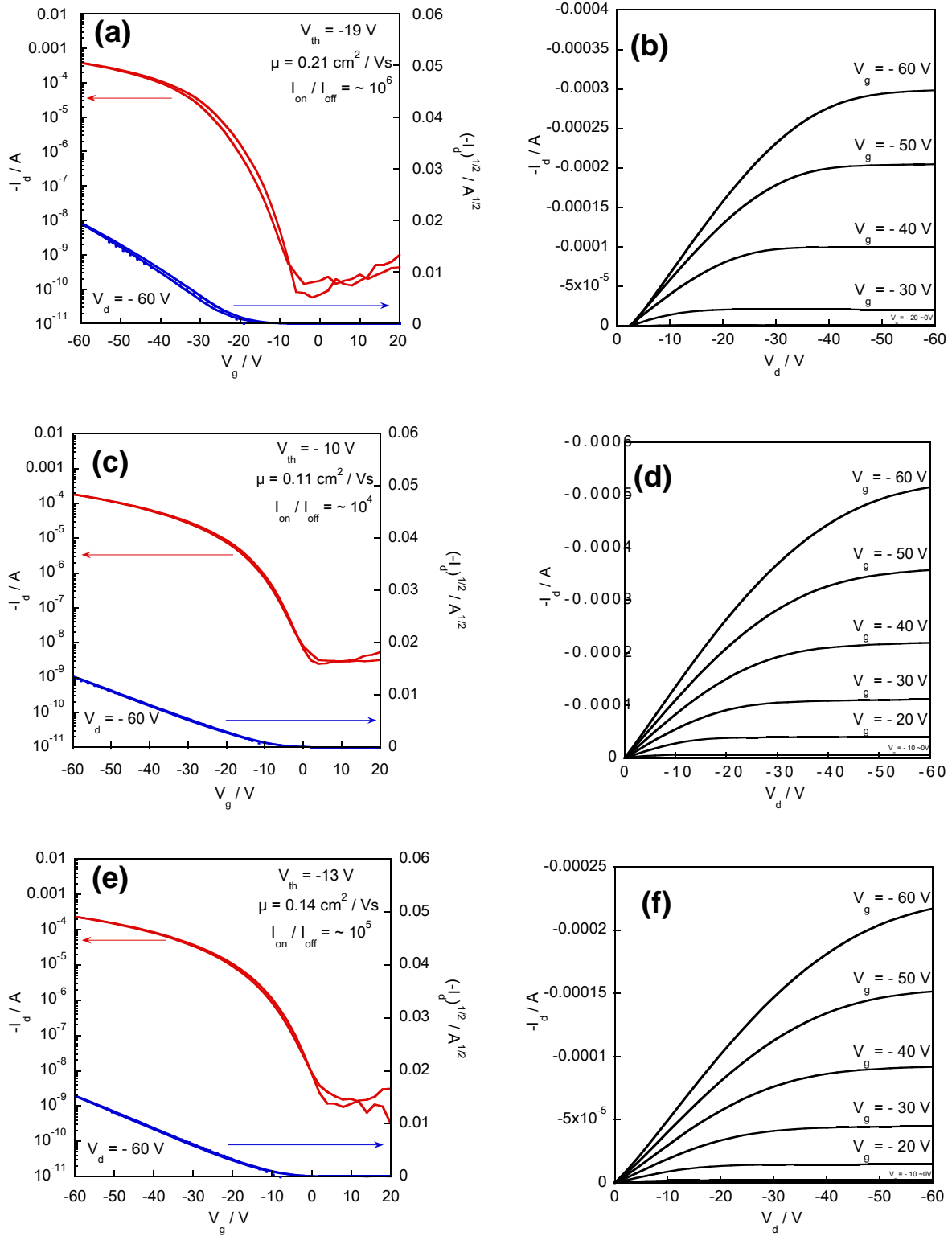


**Figure 7.** Typical transfer and output characteristics of OTFT devices with the spin-coated thin films of **2a** (a, b) and **2b** (c, d), **3c** (e, f).

These promising performances of mono-substituted derivatives impelled us to further confirm their potential as high performance organic semiconductors. I thus fabricated OTFT devices by using the vapor deposited thin films of **2a–c** (Figure 8, Table 5). Vapor deposition in fact afforded thin films with much better uniformity in their appearance, and the device characteristics were rather reproducible. By optimizing the substrate temperature during deposition of thin film and surface treatment of the Si/SiO<sub>2</sub> substrates, the device performances were clearly improved. The extracted mobilities from the saturation regime are higher than those recorded for the solution processed devices; the mobilities for **2b-** and **2c-** based devices reached to 2.5 cm<sup>2</sup> V<sup>-1</sup> s<sup>-1</sup> and  $I_{on/off}$  of  $\sim 10^7$ , which are almost comparable to that of the parent DNNT-based devices.<sup>29</sup> These results indicated that the present mono-substituted DNNT derivatives have high potential as solution-processable organic semiconductors.

**Table 5. Characteristics of vapor-processed OTFTs based 2a–c.**

Compound		2a			2b			2c		
$T_{\text{sub}} /$ °C	SAM	$\mu /$ $\text{cm}^2 \text{V}^{-1} \text{s}^{-1}$ <sup>a</sup>	$V_{\text{th}} /$ V	$I_{\text{on/off}}$	$\mu /$ $\text{cm}^2 \text{V}^{-1} \text{s}^{-1}$ <sup>a</sup>	$V_{\text{th}} /$ V	$I_{\text{on/off}}$	$\mu /$ $\text{cm}^2 \text{V}^{-1} \text{s}^{-1}$ <sup>a</sup>	$V_{\text{th}} /$ V	$I_{\text{on/off}}$
rt	untreated	0.33 (0.26)	−13	$\sim 10^8$	0.90 (0.45)	−6.1	$\sim 10^6$	0.19 (0.10)	−17	$\sim 10^5$
	HMDS	0.70 (0.41)	−15	$\sim 10^7$	0.67 (0.56)	−3.9	$\sim 10^7$	0.17 (0.17)	−13	$\sim 10^6$
	OTS	0.72 (0.55)	−12	$\sim 10^7$	1.4 (0.92)	−3.3	$\sim 10^7$	0.38 (0.18)	−12	$\sim 10^5$
	ODTS	0.48 (0.33)	−13	$\sim 10^6$	0.95 (0.59)	−3.1	$\sim 10^6$	0.43 (0.32)	−16	$\sim 10^6$
60	untreated	0.38 (0.30)	−6.0	$\sim 10^6$	0.48 (0.41)	−0.92	$\sim 10^6$	0.26 (0.21)	−7.5	$\sim 10^7$
	HMDS	0.78 (0.41)	−7.9	$\sim 10^6$	0.79 (0.64)	−1.5	$\sim 10^6$	0.58 (0.38)	−7.9	$\sim 10^6$
	OTS	0.86 (0.58)	−6.9	$\sim 10^7$	0.85 (0.73)	−0.59	$\sim 10^7$	1.1 (0.66)	−4.1	$\sim 10^7$
	ODTS	0.54 (0.40)	−4.8	$\sim 10^7$	0.73 (0.65)	−1.1	$\sim 10^6$	1.2 (0.86)	−9.1	$\sim 10^7$
100	untreated	0.46 (0.32)	−9.4	$\sim 10^7$	0.68 (0.55)	−7.6	$\sim 10^6$	0.66 (0.51)	−13	$\sim 10^8$
	HMDS	0.60 (0.53)	−12	$\sim 10^7$	0.73 (0.66)	−4.2	$\sim 10^7$	0.82 (0.65)	−13	$\sim 10^8$
	OTS	1.5 (1.1)	−11	$\sim 10^7$	1.4 (1.2)	−4.6	$\sim 10^7$	2.7 (1.8)	−15	$\sim 10^{10}$
	ODTS	1.5 (0.82)	−12	$\sim 10^7$	1.3 (1.2)	−2.7	$\sim 10^7$	2.8 (2.4)	−19	$\sim 10^9$
150	untreated	0.53 (0.46)	−9.2	$\sim 10^6$	0.81 (0.52)	−6.8	$\sim 10^7$	1.2 (1.1)	−7.4	$\sim 10^7$
	HMDS	1.1 (0.57)	−2.4	$\sim 10^6$	1.5 (1.2)	−10	$\sim 10^7$	1.4 (1.0)	−5.1	$\sim 10^6$
	OTS	1.1 (0.84)	1.2	$\sim 10^6$	2.5 (1.9)	−16	$\sim 10^7$	2.9 (2.3)	−11	$\sim 10^8$
	ODTS	1.0 (0.65)	−1.6	$\sim 10^6$	2.3 (1.7)	−15	$\sim 10^6$	2.5 (2.3)	−11	$\sim 10^8$
200	untreated	0.53 (0.39)	−19	$\sim 10^6$	1.6 (0.71)	−17	$\sim 10^6$	1.5 (1.1)	−9.5	$\sim 10^7$
	HMDS	0.75 (0.62)	−21	$\sim 10^6$	2.0 (1.2)	−19	$\sim 10^7$	1.8 (1.2)	−11	$\sim 10^7$
	OTS	1.0 (0.73)	−18	$\sim 10^6$	2.2 (1.4)	−20	$\sim 10^7$	3.4 (1.6)	−11	$\sim 10^7$
	ODTS	1.0 (0.70)	−22	$\sim 10^6$	1.7 (1.1)	−16	$\sim 10^7$	2.5 (2.0)	−1.6	$\sim 10^8$

<sup>a</sup> Typical values obtained from more than 6 devices. The values in parentheses are average value.

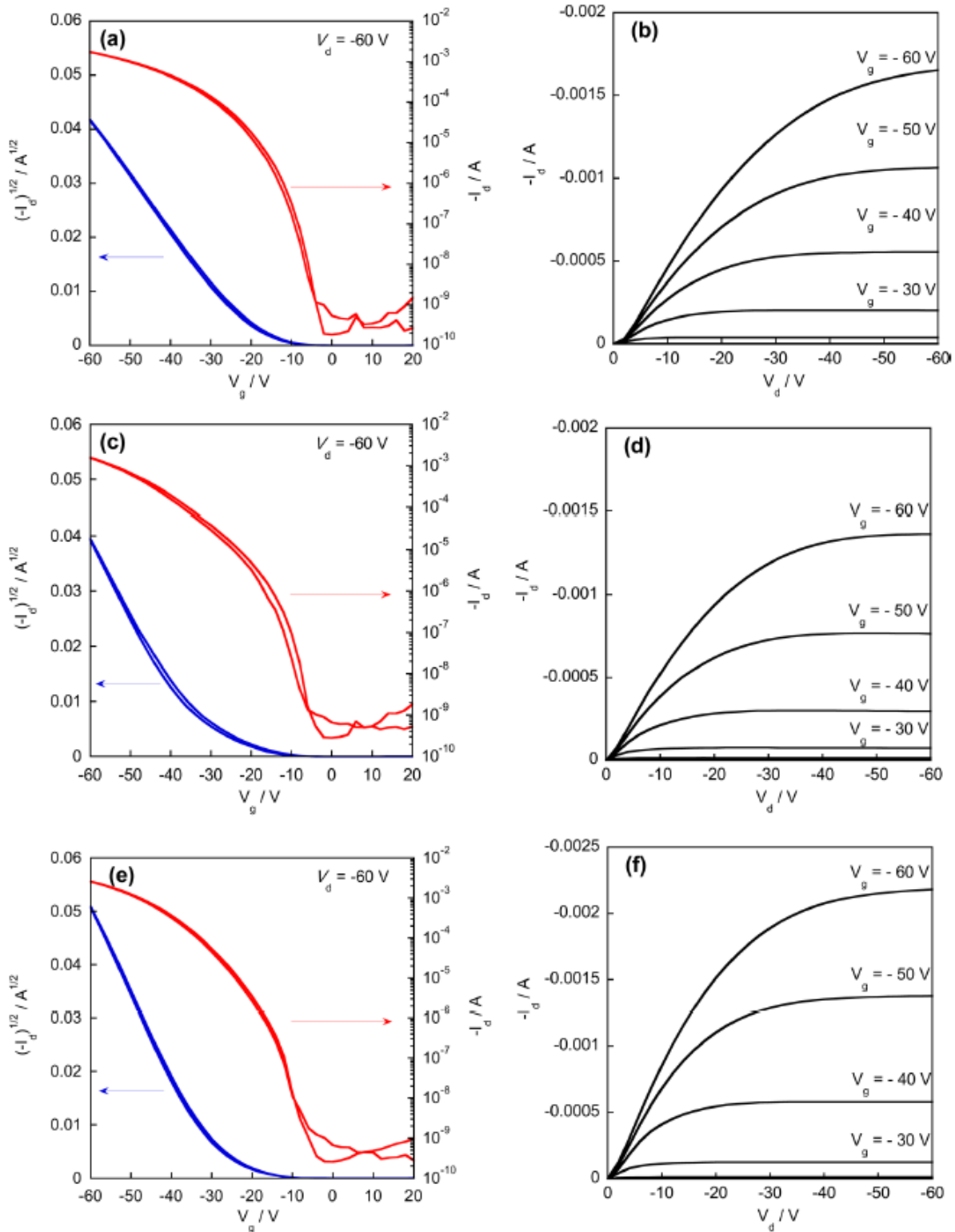


**Figure 8.** Typical transfer and output characteristics of OTFT devices with the vapor-deposited thin films of **2a** (a, b) and **2b** (c, d), **3c** (e, f).

#### 2-2-4 Detailed analysis of thin films

The poor device characteristics of di-substituted DNTT derivatives can be rationalized by their ordering nature in the thin film state elucidated by thin film XRD measurements (Figure 9a, b). In the out-of-plane XRDs, although the thin films showed peaks up to the second- (**1a**), third- (**1b**), or third- (**1c**) order, respectively, the extracted  $d$ -spacings, ca 16 Å (**1a**), 23 Å (**1b**), and 25 Å (**1c**) are definitely shorter than the calculated molecular lengths, ca. 28-29, 31-32, 33-34 Å for **1a**, **1b**, and **1c**, respectively (Figure 9c).

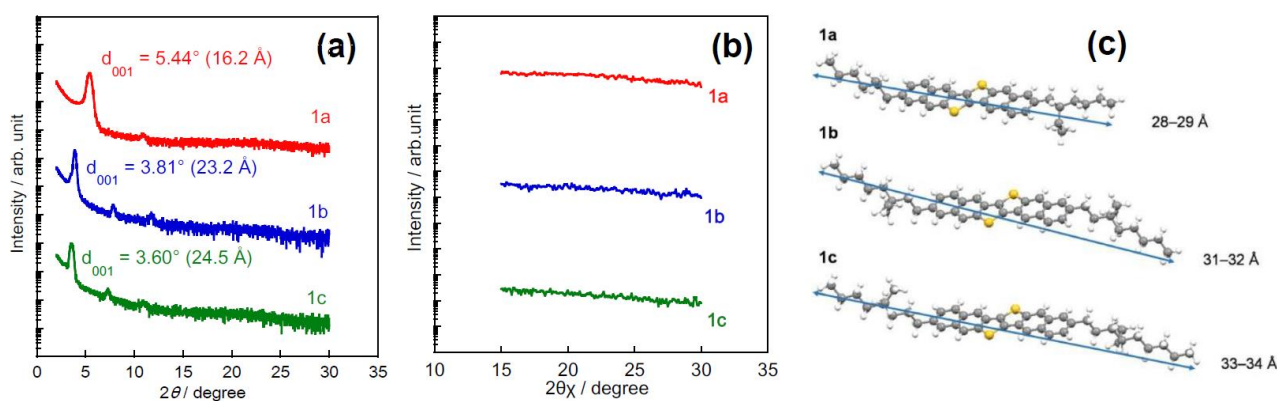


**Figure 9.** Out-of-plane (a) and in-plane (b) XRD of **1a–c**-thin films on the Si/SiO<sub>2</sub> substrate and estimated molecular lengths of **1a–c** (c) with the branched alkyl groups.

These results on the out-of-plane XRDs clearly mean that the molecules in the thin film do not stand perpendicular against the substrate surface, i.e., not the edge-on molecular orientation, which is a common feature for high performance organic semiconductors such as pentacene and DNTT. Besides the different molecular orientation from the edge-on, their in-plane XRDs showed no clear peaks, indicating that the ordering nature of the molecules in the transverse direction on the substrate surface is also poor. The poor ordering nature in the thin film state is qualitatively consistent with the optical properties of their thin films (Figure 5). From these experimental results, I conclude that introduction of two branched alkyl groups at the both end of DNTT core is not promising strategy to develop high-performance soluble organic semiconductors.

By contrast, the promising device characteristics of mono-substituted DNNT derivatives should be related to the packing structure in the thin film state. I attempted to prepare single crystals of **2a–c**, but crystals with sufficient quality for X-ray single crystal analysis could not be obtained. Alternatively, I measured thin film XRDs of spin-coated thin films (Figure 10). Being sharply contrast to those of **1a–c** (Figure 9), all the thin films of **2a–c** showed a series of peaks assignable to lamella structures in the out-of-plane XRDs, which is typical for the thin films of parent DNNT or C<sub>10</sub>-DNNT acting as the decent semiconducting layer. The interlayer spacings (*d*-spacings) are 25.8, 27.1, and 28.3 Å for **2a**, **2b**, and **2c**, respectively (Figure 10a). These *d*-spacings are slightly longer than estimated molecular lengths of the derivatives (22.6, 23.5, and 24.9 Å, respectively), and thus it is speculated that there exists the molecules pointing in the opposite directions, i.e. “anti-parallel” or “staggered” orientation, with the edge-on manner in each lamella layer.

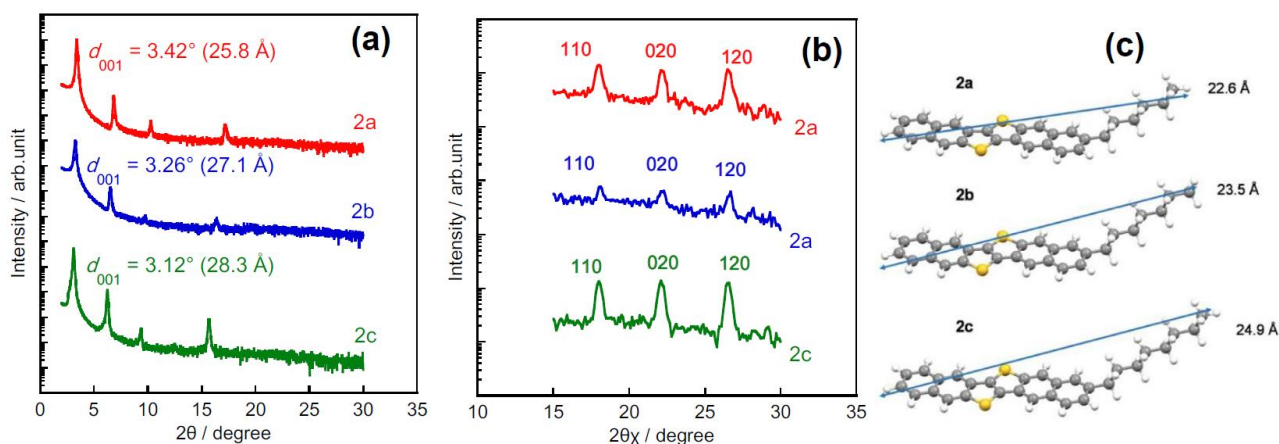


**Figure 10.** Out-of-plane (a) and in-plane (b) XRD of **2a–c**-thin films on the Si/SiO<sub>2</sub> substrate and estimated molecular lengths of **2a–c** (c) with the liner alkyl groups.

In the in-plane XRDs of the three compounds, on the other hand, clear three peaks in  $2\theta_{\chi} = 15$  to  $30^{\circ}$  regime are observed (Figure 10b), which are typical for in-plane XRDs of thin films of organic semiconductors with the herringbone arrangement in each lamella layer. This feature in the in-plane XRD is quite similar to parent DNNT and other related materials.<sup>30</sup> Provided that the crystallites in the thin film belong to *monoclinic* space groups or ones with higher symmetry and have the preferred

orientation along the normal to the substrate as the crystallographic  $c$ -axis as in the case of DNTT, the three peaks can be indexed as 110, 020, and 120, respectively.<sup>31, 32</sup> This assignment then provides the  $ab$  unit cell of each compound as depicted in Figure 11. Speculated sizes of the  $ab$  cells,  $a = \text{ca. } 6.2$ ,  $b = 8.0 \text{ \AA}$  (Table 6), are almost identical for three compounds with in the experimental errors and slightly larger in the  $b$ -axis direction than those of DNTT ( $a = 6.187$ ,  $b = 7.662 \text{ \AA}$ ), implying that the large branched alkyl groups may slightly push the DNTT cores away apart from the adjacent molecules. Nevertheless, it is interesting to point out that even with such large alkyl groups, the molecules crystallize into the herringbone packing, indicating fairly strong cohesive nature of the DNTT core. As a result, the high performance thin film transistors based on **2a–c** can be explained by the structural point of view.

**Table 6. Structural parameters of  $ab$ -cell extracted from XRDs.**

compound	$d$ -spacing <sup>a</sup> / $\text{\AA}$	Molecular length ( $l$ ) / $\text{\AA}$ <sup>b</sup>	$a$ / $\text{\AA}$ <sup>c</sup>	$b$ / $\text{\AA}$ <sup>d</sup>
<b>2a</b>	25.8	21.4	6.2	8.0
<b>2b</b>	27.3	22.4	6.2	8.0
<b>2c</b>	28.3	23.6	6.2	8.0
DNTT	16.3 (16.21(1)) <sup>e</sup>	15.3 (15.35) <sup>e</sup>	6.1 (6.187(4)) <sup>e</sup>	7.7 (7.662(6)) <sup>e</sup>

Calculated interlayer spacing from the 001 reflection. <sup>b</sup> Obtained from molecular geometries optimized by the DFT calculations (B3LYP/6-31G\*). Value in parentheses for DNTT is obtained from single crystal X-ray analysis. <sup>c</sup> Length of the crystallographic axis in the stacking direction estimated from the in-plane XRD data. Value in parentheses for DNTT is obtained from single crystal X-ray analysis. <sup>d</sup> Length of crystallographic  $b$ -axis (the side-by-side direction) estimated from the in-plane XRD data. Value in parentheses for DNTT is obtained from single crystal X-ray analysis. <sup>e</sup> See reference 29.

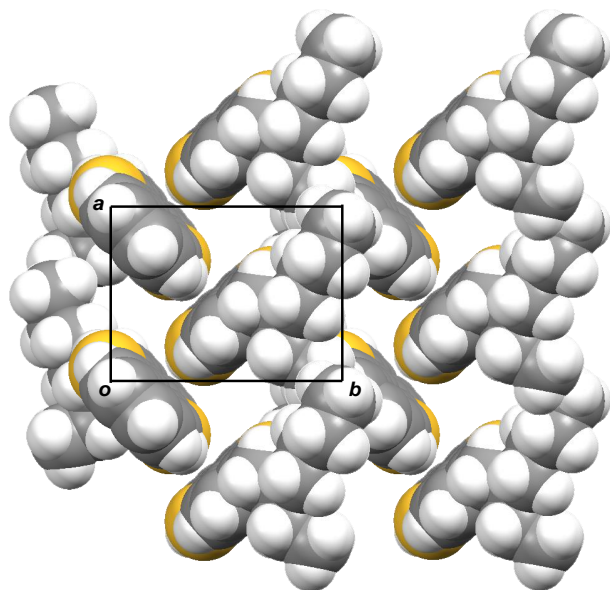


**Figure 11.** Predicted packing structure of **2a**: Schematic picture of the crystallographic  $ab$ -cell with herringbone molecular packing.

### 2-3 Conclusion of chapter 2

Aiming to develop DNNT-based solution-processable organic semiconductors, I have examined introduction of branched alkyl groups, such as 2-ethylhexyl, 3-ethylheptyl, and 4-ethyloctyl group. As expected, solubility of newly developed DNNT derivatives were markedly improved, and particularly the di-substituted DNNT derivatives (**1a–c**) showed solubility as high as 16 g L<sup>-1</sup> in hot toluene. However, judging from the very poor transistor characteristics with lower mobility by more than two orders of magnitude than that of parent DNNT, **1a–c** were proved useless as an active semiconducting material in solution-processed OTFT. Structural evaluation based on their thin-film XRD revealed that they afforded thin films with poor crystalline order compared with that of parent DNNT. This means that the intermolecular ordering in the thin film state was weakened by two branched alkyl groups, resulting in poor intermolecular orbital overlap in the thin film state.

In sharp contrast, the introduction of one branched alkyl group on the DNNT core did not lower solubility considerably and yielded good semiconducting characteristics: OTFT devices fabricated with the spin-coated thin films can work properly showing mobilities of up to 0.5 cm<sup>2</sup> V<sup>-1</sup> s<sup>-1</sup>, and ones fabricated with vapor deposition afforded mobility as high as 2.5 cm<sup>2</sup> V<sup>-1</sup> s<sup>-1</sup>, indicating their potential as solution processable high-performance organic semiconductors. It is quite intriguing that the mono-substitution keeps the structural characteristics of parent DNNT and other related high performance DNNT derivatives in the thin film state; the lamella structure with the herringbone packing motif on the substrate confirmed by thin-film XRDs, which strongly support the high mobility of their thin-film OTFTs. As a result, introduction of one branched alkyl group at the 2-position of DNNT can enhance the solubility with keeping decent semiconducting characteristics.

Among the derivatives with different branching positions of the alkyl groups, 2-ethylhexyl derivative (**2a**) having the branching position closest to the DNNT core afforded slightly inferior device characteristics compared with 3-ethylheptyl (**2b**) and 4-ethyloctyl derivatives (**2c**) in the vapor-processed OTFT, indicating that the close proximity of the branching position can decrease the intermolecular orbital overlap in the solid state. Although there may be slight differences in the device

characteristics depending on the branched alkyl groups, the most important knowledge I obtained from the present study is that such a simple modification as the introduction of one branched alkyl group on a largely  $\pi$ -extended thienoacene core, which can be accomplished by synthesis, is a promising strategy for the development of solution-processable organic semiconductors. This design strategy cannot be synthetically a big task, and thus it would be applicable to many other organic semiconductors based on the naked thienoacenes and related compounds for solution-processable organic semiconductor.

## 2-4 Experimental section and References

### Synthesis

**General:** All chemicals and solvents are reagent grade unless otherwise indicated. Tetrahydrofuran (THF), *N, N*-dimethylformamide (DMF) and toluene were purified with standard procedures prior to use. All reactions were carried out under nitrogen atmosphere unless otherwise mentioned. Melting points were uncorrected.  $^1\text{H}$  and  $^{13}\text{C}$  NMR spectra operated at 400 and 100 MHz, respectively, were obtained in deuterated chloroform ( $\text{CDCl}_3$ ) with TMS as the internal reference; chemical shifts ( $\delta$ ) are reported in parts per million (ppm). EI-MS spectra were obtained using an electron impact ionization procedure (70 eV).

### ***6-(2-Ethylhexyl)-2-methoxynaphthalene (3a).***

To a solution of 6-bromo-2-methoxynaphthalene (10 g, 42 mmol),  $\text{Ni}(\text{dppp})\text{Cl}_2$  (2.3 g, 4.2 mmol) in THF (100 mL) was added at 0 °C 2-ethylhexylmagnesiumbromide solution in diethyl ether, prepared from 2-ethylhexyl bromide (36 g, 168 mmol) and Mg (4.1 g, 172 mmol) in diethyl ether (170 mL), and the resulting mixture was stirred at rt for 6h. The mixture was diluted with water and filtered to remove unreacted Mg and other solid precipitates. The filtrate was extracted with diethyl ether and the combined extracts were washed with brine, dried ( $\text{MgSO}_4$ ), and concentrated in vacuo. The concentrate was purified by column chromatography on silica gel eluted with hexane/dichloromethane to give 6-(2-ethylhexyl)-2-methoxynaphthalene (**3a**) as a pale yellow oil (7.6 g, 69%).  $^1\text{H}$  NMR  $\delta$  0.85–0.91 (m, 6H), 1.23–1.36 (m, 8H), 1.64 (spt,  $J = 6.0$  Hz, 1H), 2.59–2.71 (m, 2H), 3.91 (s, 3H), 7.09–7.14 (m, 2H), 7.27 (dd,  $J = 8.5, 1.8$  Hz, 1H), 7.50 (br. s, 1H), 7.65 (d,  $J = 7.1$  Hz, 1H), 7.67 (d,  $J = 8.2$  Hz, 1H);  $^{13}\text{C}$  NMR  $\delta$  11.0, 14.3, 23.2, 25.6, 29.0, 32.5, 40.3, 41.2, 55.5, 105.8, 118.7, 126.6, 127.3, 128.7, 129.0, 129.2, 133.0, 137.3, 157.2; EI-MS  $m/z = 270$  [ $\text{M}^+$ ]; HR-MS (EI) Calcd for  $\text{C}_{19}\text{H}_{26}\text{O}$  [ $\text{M}^+$ ]: 270.1984, found: 270.1978.

**6-(3-Ethylheptyl)-2-methoxynaphthalene (3b).**

To a solution of 6-methoxyl-2-naphthaldehyde (1.0 g, 5.4 mmol) in THF (20 mL) was slowly added at 0 °C 2-ethylhexylmagnesiumbromide solution in diethyl ether, prepared from 2-ethylhexyl bromide (3.1 g, 16 mmol) and Mg (410 mg, 17 mmol) in diethyl ether (20 mL), and the resulting mixture was stirred at rt for 5 h. The mixture was diluted with water and filtered to remove unreacted Mg and other solid precipitates. The filtrate was extracted with diethyl ether and the combined extracts were washed with brine, dried (MgSO<sub>4</sub>), and concentrated in vacuo. The concentrate was purified by column chromatography on silica gel eluted with hexane/dichloromethane to give 6-(3-ethyl-2-hydroxyheptyl)-2-methoxynaphthalene (0.67 g, 42%) as a pale yellow oil, which was used to the next reaction without further purification. <sup>1</sup>H NMR δ 0.80–0.93 (m, 6H), 1.15–1.50 (m, 9H), 1.61–1.88 (m, 2H), 1.82 (d, J = 3.2 Hz, 1H), 3.92 (s, 3H), 4.83–4.95 (m, 1H), 7.10–7.18 (m, 2H), 7.46 (dd, J = 8.5, 1.6 Hz, 1H), 7.71 (s, 1H), 7.72 (d, J = 3.7 Hz, 1H), 7.74 (d, J = 3.2 Hz, 1H); <sup>13</sup>C NMR δ (10.5, 10.7), 14.3, 23.3, (25.6, 26.3), (28.7, 28.8), (32.6, 33.1), (35.5, 35.6), 43.3, 55.5, (73.0, 73.0), 105.8, 119.1, (124.6, 124.7), 124.8, 127.3, 128.9, 129.5, 134.2, (140.5, 140.6), 157.8; EI-MS m/z = 300 [M<sup>+</sup>]; HR-MS (APCI) Calcd for C<sub>20</sub>H<sub>28</sub>O<sub>2</sub> [M<sup>+</sup>]: 300.20838, found: 300.20816.

Trifluoroacetic acid (11 g, 100 mmol) was added into a solution of 6-(3-ethyl-1-hydroxyheptyl)-2-methoxynaphthalene (3.0 g, 10 mmol) in dichloromethane (50 mL). After the mixture was cooled to 0 °C, triethylsilane (1.6 mL, 10 mmol) was added, and the reaction mixture was stirred at the same temperature for 30 min. The resulting mixture was diluted with water and extracted with dichloromethane. The combined organic layer was washed with brine, dried (MgSO<sub>4</sub>), and concentrated in vacuo. The concentrate was purified by column chromatography on silica gel eluted with hexane to give **3b** (2.3 g, 82%) as a pale yellow oil. <sup>1</sup>H NMR δ 0.84–0.95 (m, 6H), 1.21–1.43 (m, 9H), 1.58–1.68 (m, 2H), 2.66–2.74 (m, 2H), 3.91 (s, 3H), 7.09–7.14 (m, 2H), 7.30 (dd, J = 8.5, 1.6 Hz, 1H), 7.54 (s, 1H), 7.65 (d, J = 3.2 Hz, 1H), 7.67 (d, J = 4.6 Hz, 1H); <sup>13</sup>C NMR δ 11.0, 14.3, 23.3, 25.9, 29.1, 32.9, 33.3, 35.4, 38.7, 55.4, 105.8, 118.7, 126.2, 126.8, 128.1, 129.0, 129.3, 133.0, 138.7, 157.2; EI-MS m/z = 284 [M<sup>+</sup>]; HR-MS (APCI) Calcd for C<sub>20</sub>H<sub>29</sub>O [M + H]<sup>+</sup>: 285.22159, found: 285.22129.

**6-(4-Ethyl-octyl)-2-methoxynaphthalene (3c).**

Tetrabutylammonium fluoride (1 M in THF, 84 mL, 84 mmol) was added to a solution of 2-bromo-6-methoxynaphthalene (5.0 g, 21 mmol), 4-ethyl-1-trimethylsilyloct-1-yne (13.3 g, 64 mmol), Pd(dppf)Cl<sub>2</sub>·CH<sub>2</sub>Cl<sub>2</sub> (3.4 g, 4.2 mmol), and CuI (800 mg, 4.2 mmol) in toluene (100 mL) at rt. After the mixture was stirred at rt for 1 h, triethylamine (100 mL) was added, and the resulting mixture was stirred at 70 °C for 18 h. After cooling to rt, the mixture was diluted with water and extracted with hexane. The combined extracts were washed with brine, dried (MgSO<sub>4</sub>), and concentrated in vacuo to give 6-(4-ethyloctyn-1-yl)-2-methoxynaphthalene (15.3 g, 89%) as a colorless oil, which was directly utilized in the next hydrogenation reaction without further purification. <sup>1</sup>H NMR δ 0.86–1.00 (m, 6H), 1.24–1.39 (m, 4H), 1.42–1.55 (m, 5H), 2.43 (d, J = 5.5 Hz, 2H), 3.91 (s, 3H), 7.08 (d, J = 2.3 Hz, 1H), 7.13 (dd, J = 9.1, 2.3 Hz, 1H), 7.42 (dd, J = 8.4, 1.3 Hz, 1H), 7.63 (d, J = 8.4 Hz, 1H), 7.66 (d, J = 9.1 Hz, 1H), 7.82 (br s, 1H); <sup>13</sup>C NMR δ 11.4, 14.3, 23.1, 23.5, 26.3, 29.2, 33.0, 39.1, 55.5, 81.9, 88.9, 105.9, 119.3 (×2), 126.7, 128.7, 129.2, 129.5, 130.9, 133.8, 158.1; EI-MS m/z = 294 [M<sup>+</sup>]; HR-MS (EI) Calcd for C<sub>21</sub>H<sub>26</sub>O [M<sup>+</sup>]: 294.1984, found: 294.1985.

A solution of 6-(4-ethyloctyn-1-yl)-2-methoxynaphthalene (15.3 g, crude product) and 10 wt % Pd/C (2.8 g, 2.6 mmol) in THF (150 mL) was purged with hydrogen gas, and the mixture was stirred at rt, and the progress of hydrogenation was traced by GC-MS analysis. The catalyst was then filtered off and the filtrate was concentrated in vacuo. Column chromatography of the residue on silica gel eluted with hexane gave **3c** as a colorless oil (12.5 g, 90%). <sup>1</sup>H NMR δ 0.77–0.93 (m, 6H), 1.12–1.41 (m, 11H), 1.60–1.73 (m, 2H), 2.66–2.77 (m, 2H), 3.91 (s, 3H), 7.08–7.14 (m, 2H), 7.30 (dd, J = 8.5, 1.6 Hz, 1H), 7.54 (s, 1H), 7.65 (d, J = 4.1 Hz, 1H), 7.68 (d, J = 4.6 Hz, 1H); <sup>13</sup>C NMR δ 11.0, 14.3, 23.3, 26.0, 28.8, 29.1, 33.0, 33.1, 36.5, 38.9, 55.4, 105.8, 118.7, 126.3, 126.7, 128.0, 129.0, 129.3, 133.0, 138.3, 157.2; EI-MS m/z = 298 [M<sup>+</sup>]; HR-MS (EI) Calcd for C<sub>21</sub>H<sub>30</sub>O [M<sup>+</sup>]: 298.2297, found: 298.2303.

**6-(2-Ethylhexyl)-3-methylthio-2-methoxynaphthalene (4a).**

To a solution of 6-(2-ethylhexyl)-2-methoxynaphthalene (**3a**, 7.0 g, 26 mmol) in THF (40 mL) was added a 1.6 M hexane solution of *n*-BuLi (33 mL, 53 mmol) at 0 °C. After the mixture was stirred for 1 h at rt, dimethyldisulfide (4.6 mL, 51 mmol) was added to the solution at 0 °C and the resulting mixture was stirred for 1 h at rt. The mixture was poured into a saturated aqueous ammonium chloride solution and was extracted with hexane. The combined extracts were washed with brine, dried (MgSO<sub>4</sub>) and concentrated in vacuo to give crude 6-(2-ethylhexyl)-3-methylthio-2-methoxynaphthalene (**4a**) contaminated with the 1-methylthio isomer (<10%, based on <sup>1</sup>H NMR spectra), which was purified by column chromatography on silica gel eluted with hexane to give practically pure **4a** as a colorless oil (46%). <sup>1</sup>H NMR δ 0.82–0.93 (m, 6H), 1.20–1.39 (m, 8H), 1.58–1.69 (m, 1H), 2.54 (s, 3H), 2.58–2.70 (m, 2H), 3.99 (s, 3H), 7.06 (s, 1H), 7.21 (dd, J = 8.5, 1.6 Hz, 1H), 7.41 (s, 1H), 7.45 (s, 1H), 7.62 (d, J = 8.2 Hz, 1H); <sup>13</sup>C NMR δ 11.0, 14.3, 14.7, 23.2, 25.6, 29.1, 32.6, 40.3, 41.2, 56.0, 104.8, 123.0, 126.1, 126.3, 127.7, 129.5(×2), 130.5, 137.8, 154.2; EI-MS m/z = 316 [M<sup>+</sup>]; HR-MS (EI) Calcd for C<sub>20</sub>H<sub>28</sub>OS [M<sup>+</sup>]: 316.1861, found: 316.1864.

**6-(3-Ethylheptyl)-3-methylthio-2-methoxynaphthalene (4b).**

The title compound was prepared in the same manner as **4a**. Colorless oil. 74% isolated yield. <sup>1</sup>H NMR δ 0.83–0.96 (m, 6H), 1.21–1.44 (m, 9H), 1.57–1.70 (m, 2H), 2.53 (s, 3H), 2.63–2.77 (m, 2H), 3.99 (s, 3H), 7.05 (s, 1H), 7.24 (dd, J = 8.5, 1.6 Hz, 1H), 7.41 (s, 1H), 7.49 (s, H), 7.62 (d, J = 8.2 Hz, 1H); <sup>13</sup>C NMR δ 11.0, 14.3, 14.7, 23.3, 25.9, 29.0, 32.9, 33.3, 35.3, 38.7, 56.0, 104.8, 123.0, 125.0, 126.5, 127.1, 129.5, 129.6, 130.5, 139.2, 154.2; EI-MS m/z = 330 [M<sup>+</sup>]; HR-MS (APCI) Calcd for C<sub>21</sub>H<sub>31</sub>OS [M + H]<sup>+</sup>: 331.20901, found: 331.20905.

**6-(4-Ethyl-octyl)-3-methylthio-2-methoxynaphthalene (4c).**

The title compound was prepared in the same manner as **4a**. Colorless oil. 65% isolated yield. <sup>1</sup>H NMR δ 0.77–0.93 (m, 6H), 1.15–1.39 (m, 11H), 1.59–1.73 (m, 2H), 2.53 (s, 3H), 2.71 (t, J = 7.8 Hz, 2H),

3.99 (s, 3H), 7.05 (s, 1H), 7.24 (dd, J = 8.2, 1.8 Hz, 1H), 7.41 (s, 1H), 7.49 (s, 1H), 7.62 (d, J = 8.2 Hz, 1H);  $^{13}\text{C}$  NMR  $\delta$  11.0, 14.3, 14.7, 23.3, 26.0, 28.8, 29.1, 33.0, 33.1, 36.6, 38.9, 56.0, 104.8, 123.0, 125.1, 126.4, 127.1, 129.5, 129.6, 130.6, 138.9, 154.2; EI-MS  $m/z$  = 344 [ $\text{M}^+$ ]; HR-MS (EI) Calcd for  $\text{C}_{22}\text{H}_{32}\text{OS}$  [ $\text{M}^+$ ]: 344.2174, found: 344.2166.

***6-(2-Ethylhexyl)-3-methylthio-2-hydroxynaphthalene (5a).***

To a solution of 6-(2-ethylhexyl)-3-methylthio-2-methoxynaphthalene (**4a**, 17 g, 54 mmol) in dichloromethane (150 mL) was added dropwise a dichloromethane solution of  $\text{BBr}_3$  (ca. 4 M, 2.7 mL, 110 mmol) at  $-78$  °C. After the stirring was maintained for 5 h at room temperature, the mixture was poured onto crushed ice. The resulting mixture was extracted with dichloromethane. The combined organic layers were washed with brine, dried ( $\text{MgSO}_4$ ), and concentrated in vacuo. The concentrate was purified by column chromatography on silica gel to give 6-(2-ethylhexyl)-3-methylthio-2-hydroxynaphthalene (**5a**, 15 g, 95%) as a colorless oil.  $^1\text{H}$  NMR  $\delta$  0.85–0.91 (m, 6H), 1.20–1.38 (m, 8H), 1.58–1.70 (m, 1H), 2.42 (s, 3H), 2.57–2.70 (m, 2H), 6.56 (s, 1H), 7.25 (dd, J = 8.2, 1.8 Hz, 1H), 7.28 (s, 1H), 7.45 (s, 1H), 7.60 (d, J = 8.2 Hz, 1H), 7.93 (s, 1H);  $^{13}\text{C}$  NMR  $\delta$  10.9, 14.3, 20.0, 23.2, 25.6, 29.0, 32.5, 40.2, 41.1, 109.1, 124.2, 126.3, 126.8, 129.2, 129.4, 133.6, 133.7, 137.5, 152.2; EI-MS  $m/z$  = 302 [ $\text{M}^+$ ]; HR-MS (EI) Calcd for  $\text{C}_{19}\text{H}_{26}\text{OS}$  [ $\text{M}^+$ ]: 302.1704, found: 302.1701.

***6-(3-Ethylheptyl)-3-methylthio-2-hydroxynaphthalene (5b).***

The title compound was prepared in the same manner as **5a**. Pale yellow oil. 92% isolated yield.  $^1\text{H}$  NMR  $\delta$  0.83–0.95 (m, 6H), 1.19–1.44 (m, 9 H), 1.58–1.68 (m, 2 H), 2.41 (s, 3H), 2.64–2.75 (m, 2 H), 6.55 (s, 1H), 7.27–7.32 (m, 2 H), 7.49 (s, 1H), 7.61 (d, J = 8.2 Hz, 1H), 7.94 (s, 1H);  $^{13}\text{C}$  NMR  $\delta$  11.0, 14.3, 20.1, 23.3, 25.9, 29.0, 32.9, 33.2, 35.2, 38.7, 109.2, 124.2, 125.7, 126.5, 128.9, 129.3, 133.6, 133.7, 139.0, 152.2; EI-MS  $m/z$  = 316 [ $\text{M}^+$ ]; HR-MS (APCI) Calcd for  $\text{C}_{20}\text{H}_{29}\text{OS}$  [ $\text{M} + \text{H}$ ] $^+$ : 317.19336, found 317.19296.

**6-(4-Ethylloctyl)-3-methylthio-2-hydroxynaphthalene (5c).**

The title compound was prepared in the same manner as **5a**. Pale yellow oil. 98% isolated yield.  $^1\text{H}$  NMR  $\delta$  0.77–0.93 (m, 6H), 1.15–1.37 (m, 11H), 1.59–1.71 (m, 2 H), 2.41 (s, 3H), 2.70 (t,  $J = 7.6$  Hz, 2H), 6.56 (s, 1H), 7.27–7.32 (m, 2H), 7.49 (s, 1H), 7.61 (d,  $J = 8.7$  Hz, 1H), 7.94 (s, 1H);  $^{13}\text{C}$  NMR  $\delta$  11.0, 14.3, 20.0, 23.3, 26.0, 28.7, 29.1, 33.0, 33.0, 36.5, 38.9, 109.2, 124.2, 125.8, 126.4, 128.8, 129.3, 133.6, 133.7, 138.6, 152.2; EI-MS  $m/z = 330$  [ $\text{M}^+$ ]; HR-MS (EI) Calcd for  $\text{C}_{21}\text{H}_{30}\text{OS}$  [ $\text{M}^+$ ]: 330.2017, found: 330.2023.

**6-(2-Ethylhexyl)-3-methylthio-2-(trifluoromethanesulfonyloxy)-naphthalene (6a).**

To a solution of 3-methylthio-6-(2-ethylhexyl)-2-hydroxynaphthalene (**5a**, 15 g, 50 mmol) and triethylamine (21 mL, 149 mmol) in dichloromethane (100 mL) was added trifluoromethanesulfonic anhydride (13 mL, 74 mmol) at 0 °C. After stirring for 3 h at room temperature, the mixture was diluted with water, and the resulting mixture was extracted with dichloromethane. The combined organic layers were washed with brine, dried ( $\text{MgSO}_4$ ), and concentrated in vacuo to give practically pure 6-(2-ethylhexyl)-3-methylthio-2-(trifluoromethanesulfonyloxy)naphthalene (**6a**, 20 g, 92%) as a colorless oil.  $^1\text{H}$  NMR  $\delta$  0.84–0.94 (m, 6H), 1.23–1.36 (m, 8 H), 1.59–1.72 (m, 1H), 2.59 (s, 3H), 2.63–2.75 (m, 2H), 7.33 (dd,  $J = 8.5, 1.6$  Hz, 1H), 7.54 (s, 1H), 7.63 (s, 1H), 7.68 (s, 1H), 7.71 (d,  $J = 8.7$  Hz, 1H);  $^{13}\text{C}$  NMR  $\delta$  10.9, 14.2, 15.8, 23.1, 25.5, 29.0, 32.5, 40.4, 41.1, 118.8 (q,  $J_{\text{CF}} = 321$  Hz), 119.3, 126.3, 126.4, 127.6, 129.0, 129.6, 130.8, 133.0, 141.9, 144.9; EI-MS  $m/z = 434$  [ $\text{M}^+$ ]; HR-MS (EI) Calcd for  $\text{C}_{20}\text{H}_{25}\text{F}_3\text{O}_3\text{S}_2$  [ $\text{M}^+$ ]: 434.1197, found: 434.1197.

**6-(3-Ethylheptyl)-3-methylthio-2-(trifluoromethanesulfonyloxy)-naphthalene (6b).**

The title compound was prepared in the same manner as **6a**. Colorless oil. 96% isolated yield.  $^1\text{H}$  NMR  $\delta$  0.84–0.95 (m, 6H), 1.20–1.44 (m, 9 H), 1.59–1.69 (m, 2H), 2.59 (s, 3H), 2.69–2.80 (m, 2H), 7.36 (dd,  $J = 8.5, 1.6$  Hz, 1H), 7.57 (s, 1H), 7.63 (s, 1H), 7.68 (s, 1H), 7.72 (d,  $J = 8.2$  Hz, 1H);  $^{13}\text{C}$  NMR  $\delta$  10.9, 14.3, 15.9, 23.3, 25.9, 29.0, 32.8, 33.5, 35.1, 38.7, 118.8 (q,  $J_{\text{CF}} = 321$  Hz), 119.3, 125.2, 126.4,

127.8, 128.5, 130.0, 130.8, 133.1, 143.2, 144.9; EIMS  $m/z = 448 [M^+]$ ; HR-MS (APCI) Calcd for  $C_{21}H_{27}F_3O_3S_2 [M + H]^+$ : 448.13482, found: 448.13486.

***6-(4-Ethylloctyl)-3-methylthio-2-(trifluoromethanesulfonyloxy)-naphthalene (6c).***

The title compound was prepared in the same manner as **6a**. Colorless oil. 98% isolated yield.  $^1H$  NMR  $\delta$  0.77–0.94 (m, 6H), 1.12–1.40 (m, 11H), 1.60–1.74 (m, 2H), 2.59 (s, 3H), 2.75 (t,  $J = 7.6$  Hz, 2H), 7.36 (dd,  $J = 8.5, 1.6$  Hz, 1H), 7.57 (s, 1H), 7.63 (s, 1H), 7.68 (s, 1H), 7.72 (d,  $J = 8.7$  Hz, 1H);  $^{13}C$  NMR  $\delta$  11.0, 14.3, 15.9, 23.3, 26.0, 28.5, 29.1, 32.9, 33.0, 36.6, 38.9, 118.8 (q,  $J_{CF} = 321$  Hz), 119.3, 125.4, 126.5, 127.8, 128.5, 129.6, 130.8, 133.1, 142.8, 145.0; EI-MS  $m/z = 462 [M^+]$ ; HR-MS (EI) Calcd for  $C_{22}H_{29}F_3O_3S_2 [M^+]$ : 462.1510, found: 462.1509.

***trans-1,2-Bis(6-(2-ethylhexyl)-3-methylthionaphthalen-2-yl)-ethene (7a).***

To a deaerated solution of 6-(2-ethylhexyl)-3-methylthio-2-(trifluoromethanesulfonyloxy) naphthalene (**6a**, 1.5 g, 3.4 mmol) and trans-1,2-bis(tributylstannyl)ethene (1.0 g, 1.7 mmol) in DMF (27 mL) were added  $Pd(PPh_3)_4$  (160 mg, 0.13 mmol) and lithium chloride (140 mg, 3.4 mmol). The mixture was heated at 90 °C for 24h in the dark and then diluted with water. The mixture was extracted with chloroform. The combined extracts were washed with brine, dried ( $MgSO_4$ ), and concentrated in vacuo. The concentrate was passed through a silica gel pad eluted with hexane to give trans-1,2-bis(6-(2-ethylhexyl)-3-methylthionaphthalen-2-yl)-ethene (**7a**, 880 mg, 87%) as a yellow oil.  $^1H$  NMR  $\delta$  0.80–0.97 (m, 12H), 1.19–1.41 (m, 16 H), 1.60–1.74 (m, 2H), 2.58 (s, 6H), 2.61–2.74 (m, 4H), 7.26 (dd,  $J = 8.6, 1.5$  Hz, 2H), 7.49 (s, 2H), 7.59 (s, 2H), 7.64 (s, 2H), 7.75 (d,  $J = 8.2$  Hz, 2H), 8.06 (s, 2H);  $^{13}C$  NMR  $\delta$  11.0, 14.3, 16.6, 23.2, 25.6, 29.1, 32.6, 40.6, 41.2, 124.1, 125.0, 126.2, 127.7, 128.0, 128.4, 130.2, 133.6, 134.4, 135.8, 140.4; EI-MS  $m/z = 596 [M^+]$ ; HR-MS (EI) Calcd for  $C_{40}H_{52}S_2 [M^+]$ : 596.3510, found: 596.3500.

***trans-1,2-Bis(6-(3-ethylheptyl)-3-methylthionaphthalen-2-yl)-ethene (7b).***

The title compound was prepared in the same manner as **7a**. Yellow oil. 89% isolated yield. <sup>1</sup>H NMR δ 0.86–0.95 (m, 12H), 1.21–1.44 (m, 18H), 1.60–1.71 (m, 4H), 2.58 (s, 6H), 2.68–2.77 (m, 4H), 7.28 (dd, J = 8.5, 1.6 Hz, 2H), 7.52 (s, 2H), 7.58 (s, 2H), 7.64 (s, 2H), 7.76 (d, J = 8.7 Hz, 2H), 8.05 (s, 2H); <sup>13</sup>C NMR δ 11.0, 14.4, 16.6, 23.3, 25.9, 29.1, 32.9, 33.5, 35.1, 38.7, 124.1, 125.0, 125.0, 127.4, 127.9, 128.3, 130.2, 133.7, 134.4, 135.8, 141.8; EI-MS m/z = 624 [M<sup>+</sup>]; HR-MS (APCI) Calcd for C<sub>42</sub>H<sub>57</sub>S<sub>2</sub> [M + H]<sup>+</sup>: 625.38962, found: 625.39008.

***trans-1,2-Bis(6-(4-ethyloctyl)-3-methylthionaphthalen-2-yl)-ethene (7c).***

The title compound was prepared in the same manner as **7a**. Yellow oil. 83% isolated. <sup>1</sup>H NMR δ 0.76–0.95 (m, 12H), 1.15–1.40 (m, 22H), 1.59–1.77 (m, 4H), 2.58 (s, 6H), 2.74 (t, J = 7.6 Hz, 4H), 7.28 (dd, J = 8.7, 1.4 Hz, 2H), 7.52 (s, 2H), 7.59 (s, 2H), 7.64 (s, 2H), 7.76 (d, J = 8.2 Hz, 2H), 8.05 (s, 2H); <sup>13</sup>C NMR δ 11.0, 14.3, 16.6, 23.2, 26.0, 28.6, 29.1, 33.0, 33.1, 36.8, 38.9, 124.1, 125.0, 125.2, 127.4, 127.9, 128.4, 130.2, 133.7, 134.4, 135.8, 141.4; EI-MS m/z = 652 [M<sup>+</sup>]; HR-MS (EI) Calcd for C<sub>44</sub>H<sub>60</sub>S<sub>2</sub> [M<sup>+</sup>]: 652.4136, found: 652.4147.

***2,9-Bis(2-ethylhexyl)dinaphtho[2,3-b:2',3'-f]thieno[3,2-b]-thiophene (1a).***

A mixture of **7a** (400 mg, 0.67 mmol) and iodine (5.3 g, 21 mmol) in chloroform (20 mL) was refluxed for 14 h and then was poured into aqueous sodium hydrogen sulfite (20 mL). The mixture was extracted with chloroform (30 mL) and the combined extracts were washed with brine, dried (MgSO<sub>4</sub>), and concentrated in vacuo. The residue was washed with hexane to give the title compound (260 mg, 69%) as a yellow solid. Analytical and device grade samples were obtained by twice vacuum gradient sublimation. M.p. 231 °C; <sup>1</sup>H NMR δ 0.83–0.98 (m, 12H), 1.22–1.44 (m, 16H), 1.64–1.79 (m, 2H), 2.67–2.81 (m, 4H), 7.36 (dd, J = 8.5, 1.6 Hz, 2H), 7.66 (s, 2H), 7.94 (d, J = 8.7 Hz, 2H), 8.31 (s, 2H), 8.33 (s, 2H); <sup>13</sup>C NMR δ 11.0, 14.3, 23.2, 25.7, 29.0, 32.6, 40.6, 41.1, 119.9, 121.9, 126.6, 128.1, 128.1, 130.0, 131.7, 131.9, 133.5, 139.8, 140.9; EI-MS m/z = 564 [M<sup>+</sup>]; HR-MS (EI) Calcd for C<sub>38</sub>H<sub>44</sub>S<sub>2</sub>

[M<sup>+</sup>]: 564.2884, found: 564.2877.

***2,9-Bis(3-ethylheptyl)dinaphtho[2,3-b:2',3'-f]thieno[3,2-b]-thiophene (1b).***

The title compound was prepared in the same manner as **1a**. Yellow solid. 92% isolated yield. M.p. 185 °C; <sup>1</sup>H NMR δ 0.87–0.95 (m, 12H), 1.26–1.45 (m, 18H), 1.63–1.78 (m, 4H), 2.73–2.86 (m, 4H), 7.39 (dd, J = 8.5, 1.6 Hz, 2H), 7.70 (s, 2H), 7.95 (d, J = 8.7 Hz, 2H), 8.31 (s, 2H), 8.33 (s, 2H); <sup>13</sup>C NMR δ 11.0, 14.3, 23.3, 26.0, 29.1, 32.9, 33.6, 35.1, 38.8, 119.9, 121.9, 125.5, 127.6, 128.3, 130.0, 131.8, 131.9, 133.5, 141.0, 141.2; EI-MS m/z = 592 [M<sup>+</sup>]; HR-MS (APCI) Calcd for C<sub>40</sub>H<sub>49</sub>S<sub>2</sub> [M + H]<sup>+</sup>: 593.32702, found: 593.32721.

***2,9-Bis(4-ethyloctyl)dinaphtho[2,3-b:2',3'-f]thieno[3,2-b]-thiophene (1c).***

The title compound was prepared in the same manner as **1a**. Yellow solid. 69% isolated. M.p. 210 °C; <sup>1</sup>H NMR δ 0.81–0.92 (m, 12H), 1.20–1.42 (m, 22H), 1.65–1.78 (m, 4H), 2.80 (t, J = 7.6 Hz, 4H), 7.39 (dd, J = 8.5, 1.6 Hz, 2H), 7.70 (s, 2H), 7.95 (d, J = 8.7 Hz, 2H), 8.31 (s, 2H), 8.33 (s, 2H); <sup>13</sup>C NMR δ 11.0, 14.3, 23.3, 26.0, 28.6, 29.1, 33.0, 33.1, 36.8, 38.9, 119.9, 121.9, 125.6, 127.6, 128.2, 130.0, 131.8, 131.9, 133.5, 140.8, 140.9; EI-MS m/z = 620 [M<sup>+</sup>]; HR-MS (EI) Calcd for C<sub>42</sub>H<sub>52</sub>S<sub>2</sub> [M<sup>+</sup>]: 620.3510, found: 620.3497.

***6-(2-Ethylhexyl)-3-methylthio-2-(2-(trimethylsilyl)ethyn-1-yl)-naphthalene (8).***

A mixture of **6a** (280 mg, 0.64 mmol), trimethylsilylacetylene (190 mg, 1.9 mmol), CuI (12 mg, 0.064 mmol), PPh<sub>3</sub> (17 mg, 0.064 mmol), and Pd(PPh<sub>3</sub>)<sub>2</sub>Cl<sub>2</sub> (23 mg, 0.032 mmol) in toluene (3 mL) and Et<sub>3</sub>N (3 mL) was heated at 70 °C for 20 h. After cooling, the mixture was diluted with water and extracted with toluene. The combined organic layers were washed with brine, dried (MgSO<sub>4</sub>), and concentrated in vacuo. The residue was purified by column chromatography on silica gel with hexane, to give **8** (210 mg, 87%) as a pale yellow oil. <sup>1</sup>H NMR δ 0.31 (s, 9 H), 0.79–0.94 (m, 6H), 1.18–1.38 (m, 8H), 1.57–1.71 (m, 1H), 2.54 (s, 3H), 2.57–2.69 (m, 2H), 7.19 (dd, J = 8.5, 1.6 Hz, 1H), 7.37 (s, 1H), 7.43

(s, 1H), 7.59 (d, J = 8.2 Hz, 1H), 7.90 (s, 1H);  $^{13}\text{C}$  NMR  $\delta$  0.1, 10.9, 14.3, 15.3, 23.1, 25.6, 29.0, 32.5, 40.5, 41.1, 100.4, 102.6, 118.9, 121.4, 126.2, 127.3, 127.7, 129.0, 132.6, 133.7, 138.2, 141.4; EI-MS  $m/z = 382$  [ $\text{M}^+$ ]; HR-MS (EI) Calcd for  $\text{C}_{24}\text{H}_{34}\text{SSi}$  [ $\text{M}^+$ ]: 382.2150, found: 382.2156.

***7-(2-Ethylhexyl)-3-(2'-naphthylthio)naphtho[2,3-b]thiophene (9).***

To a solution of 2-naphthalenethiol (88 mg, 0.55 mmol) in dichloromethane (5 mL) was added N-chlorosuccinimide (74 mg, 0.55 mmol) at 0 °C, and the resulting mixture was stirred at rt for 20 min to in situ prepare 2-naphthylsulfenyl chloride in dichloromethane. The 2-naphthylsulfenyl chloride solution was then added to a solution of **8** (150 mg, 0.39 mmol) in dichloromethane (5 mL) at 0 °C, and the resulting mixture was further stirred for 1.5 h at rt. The mixture was poured into water and extracted with dichloromethane. The combined organic layers were washed with brine, dried ( $\text{MgSO}_4$ ), and concentrated in vacuo. The concentrate was dissolved in THF (5 mL) and to the solution was added a solution of tetrabutylammonium fluoride (1 M in THF solution, 0.26 mL, 0.26 mmol). The mixture was stirred for 1 h, diluted with water, and extracted with hexane. The combined extracts were dried ( $\text{MgSO}_4$ ) and concentrated in vacuo. The concentrate was purified by column chromatography on silica gel eluted with hexane to give **9** (110 mg, 44%) as a yellow oil.  $^1\text{H}$  NMR  $\delta$  0.82–0.93 (m, 6H), 1.17–1.39 (m, 8H), 1.60–1.75 (m, 1H), 2.62–2.78 (m, 2H), 7.26 (dd, J = 8.5, 1.6 Hz, 1H), 7.32 (dd, J = 8.6, 1.9 Hz, 1H), 7.35–7.46 (m, 2H), 7.59–7.66 (m, 3H), 7.68 (d, J = 8.7 Hz, 1H), 7.71–7.77 (m, 1H), 7.79 (d, J = 8.5 Hz, 1H), 7.80 (s, 1H), 8.28 (s, 1H), 8.32 (s, 1H);  $^{13}\text{C}$  NMR  $\delta$  11.0, 14.3, 23.2, 25.6, 29.0, 32.6, 40.6, 41.0, 120.9, 121.5, 123.7, 125.8, 125.9, 125.9, 126.3, 126.7, 127.3, 127.9( $\times 2$ ), 128.5, 128.8, 129.8, 131.6, 131.9, 133.8, 133.9, 134.0, 137.1, 138.2, 139.8; EI-MS  $m/z = 454$  [ $\text{M}^+$ ]; HR-MS (EI) Calcd for  $\text{C}_{30}\text{H}_{30}\text{S}_2$  [ $\text{M}^+$ ]: 454.1789, found: 454.1797.

***2-Bromo-7-(2-ethylhexyl)-3-(2'-naphthylthio)naphtho[2,3-b]thiophene (10).***

**9** (170 mg, 0.37 mmol) was dissolved in THF (5 mL) and to the solution was added *n*-BuLi (1.6 M hexane solution, 0.58 mL, 0.93 mmol) at  $-78$  °C. The mixture was stirred at room temperature for 1 h and then cooled to  $-78$  °C. 1,2-dibromotetrachloroethane (240 mg, 0.74 mmol) was added, and the

resulting mixture was stirred at room temperature for 19 h. Then, the reaction mixture was diluted with water and extracted with hexane. The combined organic layers were washed with brine, dried (MgSO<sub>4</sub>) and concentrated in vacuo. The concentrate was purified by column chromatography on silica gel with hexane to give **10** (150 mg, 78%) as a yellow oil. <sup>1</sup>H NMR δ 0.83–0.91 (m, 6H), 1.21–1.36 (m, 8H), 1.61–1.72 (m, 1H), 2.61–2.77 (m, 2H), 7.23–7.31 (m, 2H), 7.34–7.46 (m, 2H), 7.57–7.76 (m, 3H), 7.67 (d, J = 8.7 Hz, 1H), 7.79 (d, J = 8.7 Hz, 1H), 8.19 (s, 1H), 8.27 (s, 1H); <sup>13</sup>C NMR δ 10.9, 14.3, 23.2, 25.6, 29.0, 32.5, 40.6, 41.0, 119.9, 122.0, 124.9, 125.5, 125.5, 125.8, 126.4, 126.7, 127.3, 127.9, 128.2, 128.4, 129.0, 130.0, 131.8, 131.9, 133.0, 133.9, 137.1, 137.5, 140.2; EI-MS m/z = 532 [M<sup>+</sup>]; HR-MS (EI) Calcd for C<sub>30</sub>H<sub>29</sub>BrS<sub>2</sub> [M<sup>+</sup>]: 532.0894, found: 532.0875.

**2-(2-Ethylhexyl)dinaphtho[2,3-b:2',3'-f]thieno[3,2-b]thiophene (2a).**

To a deaerated solution of **10** (87 mg, 0.16 mmol) and sodium acetate (27 mg, 0.32 mmol), in *N,N*-dimethylacetamide (10 mL) was added Pd(PPh<sub>3</sub>)<sub>2</sub>Cl<sub>2</sub> (12 mg, 0.016 mmol). The mixture was stirred for 12 h at 140 °C and diluted with water. The resulting precipitate was collected by filtration, and the crude product was washed with methanol and dried. The residue was purified by column chromatography on silica gel eluted with chloroform to give 2-(2-ethylhexyl)dinaphtho [2,3-b:2',3'-f]thieno[3,2-b]thiophene (**2a**) as a yellow solid (72 mg, 42%). M.p. 334 °C; <sup>1</sup>H NMR δ 0.84–0.97 (m, 6H), 1.21–1.41 (m, 8H), 1.66–1.80 (m, 1H), 2.75 (d, J = 6.9 Hz, 2H), 7.35 (dd, J = 8.5, 1.6 Hz, 1H), 7.45–7.56 (m, 2H), 7.66 (s, 1H), 7.86–7.96 (m, 2H), 7.97–8.06 (m, 1H), 8.29 (s, 1H), 8.31 (s, 1H), 8.33 (s, 1H), 8.39 (s, 1H); <sup>13</sup>C NMR δ 11.0, 14.2, 23.2, 26.0, 29.2, 32.9, 40.9, 41.3, 120.1, 120.2, 122.0, 122.6, 125.8, 126.0, 126.7, 127.5, 128.2, 128.3, 128.5, 130.2, 131.6, 131.7, 132.0, 132.8, 133.5, 133.9, 134.2, 140.6, 140.6, 141.1; EI-MS m/z = 452 [M<sup>+</sup>]; HR-MS (EI) Calcd for C<sub>30</sub>H<sub>28</sub>S<sub>2</sub> [M<sup>+</sup>]: 452.1632, found: 452.1619.

***trans-1-(6-(2-Ethylhexyl)-3-methylthionaphthalen-2-yl)-2-(3-methylthionaphthalen-2-yl)ethene***  
**(11a).**

To a solution of 6-(2-ethylhexyl)-3-methylthio-2-(trifluoromethanesulfonyloxy)-naphthalene (**6a**, 140 mg, 0.31 mmol), 3-methylthio-2-(trifluoromethanesulfonyloxy)naphthalene (**6d**, 100 mg, 0.31 mmol),<sup>20</sup> and *trans*-1,2-bis(tributylstannyl)ethene (210 mg, 0.34 mmol) in DMF (10 mL) was added Pd(PPh<sub>3</sub>)<sub>4</sub> (19 mg, 0.016 mmol) and lithium chloride (26 mg, 0.62 mmol). The mixture was heated at 100 °C for 20 h in the dark and then diluted with water. The mixture was extracted with toluene, and the combined extracts were washed with brine, dried (MgSO<sub>4</sub>) and concentrated in vacuo. The residue was passed through a silica gel pad eluted with hexane to give **11a** (66 mg, 44%) as a yellow oil. <sup>1</sup>H NMR δ 0.85–0.92 (m, 6H), 1.19–1.42 (m, 8H), 1.60–1.76 (m, 1H), 2.59 (s, 3H), 2.59 (s, 3H), 2.64–2.75 (m, 2H), 7.26 (dd, J = 8.0, 1.8 Hz, 1H), 7.37–7.48 (m, 2H), 7.50 (s, 1H), 7.60 (s, 1H), 7.61–7.71 (m, 3H), 7.72–7.90 (m, 3H), 8.06 (s, 1H), 8.09 (s, 1H); <sup>13</sup>C NMR δ 11.0, 14.3, 16.5, 16.6, 23.2, 25.6, 29.1, 32.6, 40.6, 41.2, 124.2, 124.4, 125.1, 125.3, 125.8, 126.2, 126.6, 126.7, 127.8, 128.0, 128.1, 128.2, 128.9, 130.2, 131.7, 133.5, 133.7, 134.3, 135.2, 135.8, 136.1, 140.5; EI-MS m/z = 484 [M<sup>+</sup>]; HR-MS (EI) Calcd for C<sub>32</sub>H<sub>36</sub>S<sub>2</sub> [M<sup>+</sup>]: 484.2258, found: 484.2255.

***trans-1-(6-(3-Ethylheptyl)-3-methylthionaphthalen-2-yl)-2-(3-methylthionaphthalen-2-yl)ethene***  
**(11b).**

The title compound was prepared in the same manner as **11a**. Yellow oil. 39% isolated yield. <sup>1</sup>H NMR δ 0.83–0.97 (m, 6H), 1.20–1.46 (m, 9 H), 1.58–1.72 (m, 2H), 2.58 (s, 3H), 2.58 (s, 3H), 2.68–2.77 (m, 2H), 7.28 (dd, J = 8.5, 1.6 Hz, 1H), 7.36–7.48 (m, 2H), 7.52 (s, 1H), 7.58 (s, 1H), 7.60–7.70 (m, 3H), 7.71–7.88 (m, 3H), 8.05 (s, 1H), 8.08 (s, 1H); <sup>13</sup>C NMR δ 11.0, 14.3, 16.5, 16.6, 23.3, 25.9, 29.0, 32.9, 33.5, 35.1, 38.7, 124.1, 124.3, 125.1, 125.1, 125.2, 125.7, 126.5, 126.7, 127.4, 127.9, 128.0, 128.2, 128.9, 130.1, 131.7, 133.5, 133.8, 134.3, 135.2, 135.9, 136.0, 141.8; EI-MS m/z = 498 [M<sup>+</sup>]; HR-MS (EI) Calcd for C<sub>33</sub>H<sub>38</sub>S<sub>2</sub> [M<sup>+</sup>]: 498.2415, found: 498.2424.

***trans-1-(6-(4-Ethylloctyl)-3-methylthionaphthalen-2-yl)-2-(3-methylthionaphthalen-2-yl)ethene (11c).***

The title compound was prepared in the same manner as **11a**. Yellow oil. 39% isolated yield. <sup>1</sup>H NMR δ 0.78–0.95 (m, 6H), 1.15–1.41 (m, 11H), 1.62–1.76 (m, 2H), 2.58 (s, 3H), 2.59 (s, 3H), 2.74 (t, J = 7.6 Hz, 2H), 7.29 (dd, J = 8.2, 1.4 Hz, 1H), 7.38–7.48 (m, 2H), 7.52 (s, 1H), 7.59 (s, 1H), 7.61–7.71 (m, 3H), 7.71–7.89 (m, 3H), 8.06 (s, 1H), 8.08 (s, 1H); <sup>13</sup>C NMR δ 11.0, 14.3, 16.5, 16.6, 23.3, 26.0, 28.6, 29.1, 33.0, 33.1, 36.8, 38.9, 124.2, 124.4, 125.1, 125.2, 125.2, 125.7, 126.5, 126.7, 127.4, 127.9, 128.0, 128.2, 128.9, 130.2, 131.7, 133.5, 133.8, 134.3, 135.2, 135.8, 136.1, 141.5; EI-MS m/z = 512 [M<sup>+</sup>]; HR-MS (EI) Calcd for C<sub>34</sub>H<sub>40</sub>S<sub>2</sub> [M<sup>+</sup>]: 512.2571, found: 512.2570.

***2-(2-Ethylhexyl)dinaphtho[2,3-b:2',3'-f]thieno[3,2-b]thiophene (2a).***

A mixture of **11a** (300 mg, 0.62 mmol) and I<sub>2</sub> (5.3 g, 21 mmol) in chloroform was stirred at 70 °C for 7 h and then poured into aqueous sodium hydrogen sulfite (20 mL). The mixture was extracted with chloroform, and the combined extracts were washed with brine, dried (MgSO<sub>4</sub>), and concentrated in vacuo. The concentrate was washed with hexane to give **2a** (280 mg, quantitative) as a yellow solid. The spectroscopic data of the product obtained by this method were identical with those obtained for the previous method.

***2-(3-Ethylheptyl)dinaphtho[2,3-b:2',3'-f]thieno[3,2-b]thiophene (2b).***

The title compound was prepared in the same manner as **2a**. Yellow solid. 79% isolated yield. M.p. 368 °C; <sup>1</sup>H NMR δ 0.84–0.99 (m, 6H), 1.22–1.42 (m, 9H), 1.62–1.79 (m, 2H), 2.72–2.88 (m, 2H), 7.37 (dd, J = 8.5, 1.6 Hz, 1H), 7.45–7.56 (m, 2H), 7.68 (s, 1H), 7.87–7.96 (m, 2H), 7.98–8.04 (m, 1H), 8.29 (s, 1H), 8.31 (s, 1H), 8.32 (s, 1H), 8.38 (s, 1H); <sup>13</sup>C NMR δ 11.0, 14.2, 23.3, 26.2, 29.2, 33.1, 33.8, 35.2, 39.0, 120.1, 120.2, 122.0, 122.6, 125.6, 125.8, 126.0, 127.5, 127.7, 128.4, 128.5, 130.2, 131.6, 131.7, 132.0, 132.1, 132.7, 133.5, 134.2, 141.1, 141.4; EI-MS m/z = 466 [M<sup>+</sup>]; HR-MS (APCI) Calcd for C<sub>31</sub>H<sub>31</sub>S<sub>2</sub> [M + H]<sup>+</sup>: 467.18617, found: 467.18637.

***2-(4-Ethylloctyl)dinaphtho[2,3-b:2',3'-f]thieno[3,2-b]thiophene (2c).***

The title compound was prepared in the same manner as **2a**. Yellow solid. 92% isolated yield. M.p. 358 °C; <sup>1</sup>H NMR δ 0.81–0.94 (m, 6H), 1.19–1.41 (m, 11H), 1.67–1.82 (m, 2H), 2.81 (t, J = 7.8 Hz, 2H), 7.38 (dd, J = 8.7, 1.8 Hz, 1H), 7.46–7.55 (m, 2H), 7.69 (s, 1H), 7.88–7.97 (m, 2H), 7.98–8.05 (m, 1H), 8.30 (s, 1H), 8.32 (s, 1H), 8.33 (s, 1H), 8.39 (s, 1H); <sup>13</sup>C NMR δ 11.1, 14.2, 23.3, 26.2, 28.6, 29.3, 33.2, 33.3, 36.9, 39.1, 120.1, 120.2, 122.0, 122.6, 125.7, 125.8, 126.0, 127.5, 127.7, 128.3, 128.5, 130.2, 131.6, 131.7, 132.0, 132.1, 132.8, 133.5, 134.2, 141.0, 141.1, 141.1; EI-MS m/z = 480 [M<sup>+</sup>]; HR-MS (EI) Calcd for C<sub>32</sub>H<sub>32</sub>S<sub>2</sub> [M<sup>+</sup>]: 480.1945, found: 480.1953.

### Physicochemical properties

UV–vis absorption spectra were measured in chloroform solution (concentration:  $10^{-5}$  M) on a Shimadzu UV-3600 spectrometer. Cyclic voltammograms (CVs) were recorded on an ALS Electrochemical Analyzer Model 612D in benzonitrile containing tetrabutylammonium hexafluorophosphate ( $\text{Bu}_4\text{NPF}_6$ , 0.1 M) as supporting electrolyte at a scan rate of  $0.1 \text{ Vs}^{-1}$ . Counter and working electrodes were made of Pt, and the reference electrode was Ag/AgCl. All the potentials were calibrated with the standard ferrocene/ferrocenium redox couple ( $\text{Fc}/\text{Fc}^+$ :  $E_{1/2} = +0.60 \text{ V}$  measured under identical conditions). X-ray diffractions of thin films deposited on the Si/SiO<sub>2</sub> substrate were obtained with a Rigaku Ultima IV diffractometer with a Cu K $\alpha$  source ( $\lambda = 1.54187 \text{ \AA}$ ) in the air.

### Fabrication and characterization of OTFTs.

OTFT devices based on **1** and **2** were fabricated in a top-contact-bottom-gate (TCBG) configuration on a heavily doped n<sup>+</sup>-Si (100) wafer with a 200 nm thermally grown SiO<sub>2</sub> (C<sub>i</sub> = 17.3 nF cm<sup>-2</sup>). The substrate surfaces were treated with hexamethyldisilazane (HMDS), octyltrichlorosilane (OTS) or octadecyltrichlorosilane (ODTS) as reported previously.<sup>29</sup> Thin films as the active layer were spin-coated from chloroform solution (0.2–0.8 wt %) under ambient conditions or vacuum-deposited (50 nm thick, monitored by quartz oscillator) on the Si/SiO<sub>2</sub> substrates maintained at various temperatures (T<sub>sub</sub>) at a rate of 1 Ås<sup>-1</sup> under a pressure of ~10<sup>-3</sup> Pa. The thickness of the spin-coated thin films was ca. 40–80 nm evaluated by a surface profiler. On top of the organic thin film, gold films (80 nm) as drain and source electrodes were deposited through a shadow mask. For a typical device, the drain-source channel length (L) and width (W) are 40 μm and 3000 μm, respectively.

Characteristics of the OTFT devices were measured at room temperature under ambient conditions with a Keithley 4200 semiconducting parameter analyzer. Field-effect mobility (μ<sub>FET</sub>) was calculated in the saturation (V<sub>d</sub> = V<sub>g</sub> = -60) of the I<sub>d</sub> using the following equation

$$I_d = C_i \mu_{FET} \frac{W}{2L} (V_g - V_{th})^2$$

where C<sub>i</sub> is the capacitance of the SiO<sub>2</sub> dielectric layer, and V<sub>g</sub> and V<sub>th</sub> are the gate and threshold voltages, respectively. The current on/off ratio (I<sub>on</sub>/I<sub>off</sub>) was determined from the I<sub>d</sub> at V<sub>g</sub> = 0 V (I<sub>off</sub>) and V<sub>g</sub> = -60 V (I<sub>on</sub>). The μ<sub>FET</sub> data were typical values from more than 6 devices.

*Differential scanning calorimetry of 1 and 2*

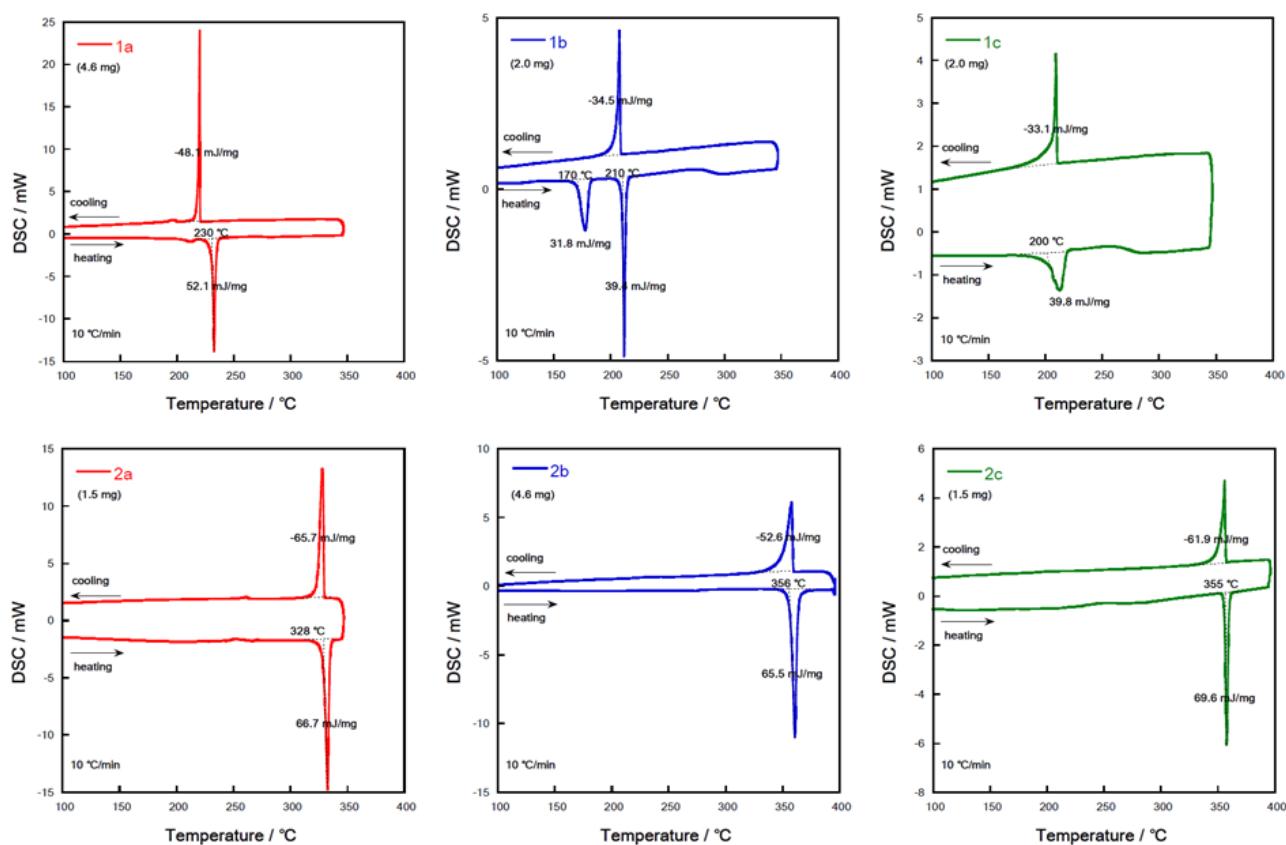


**Figure S1.** Differential scanning calorimetry (DSC) profiles of **1** and **2**.

*Digital microscope images of spin-coated thin films of 2*

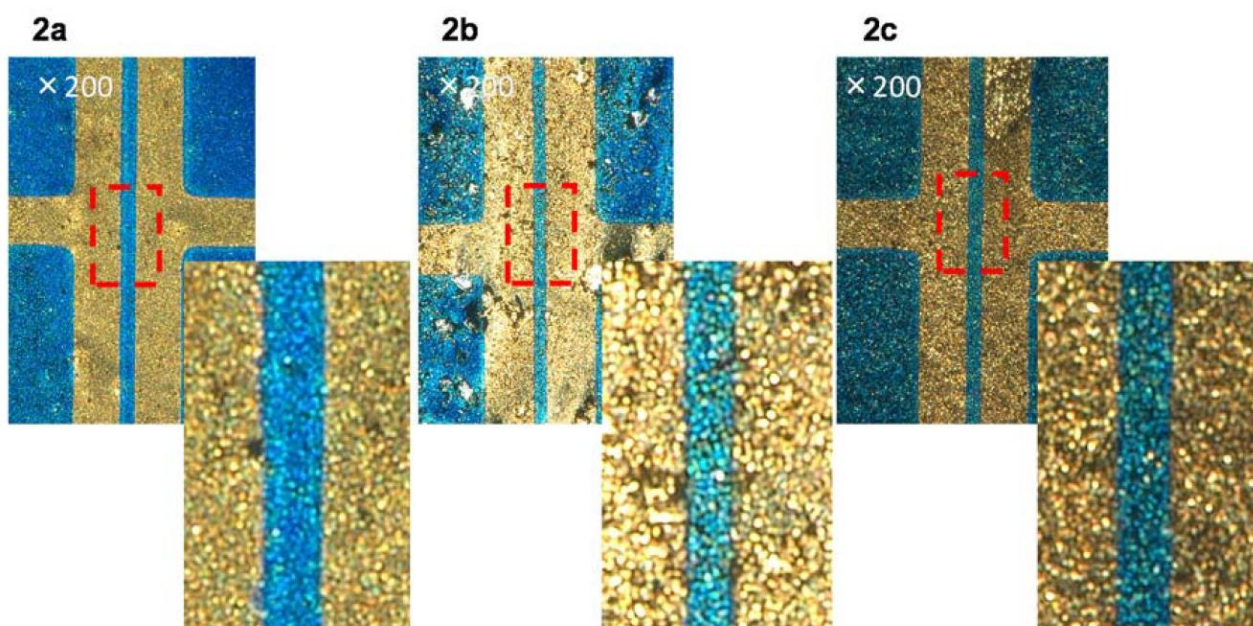


**Figure S2.** Digital microscope images of spin-coated thin films of **2**.

Transfer and output characteristics of **2b**-based solution processed OTFT showing mobility of up to  $1.6 \text{ cm}^2 \text{V}^{-1} \text{s}^{-1}$

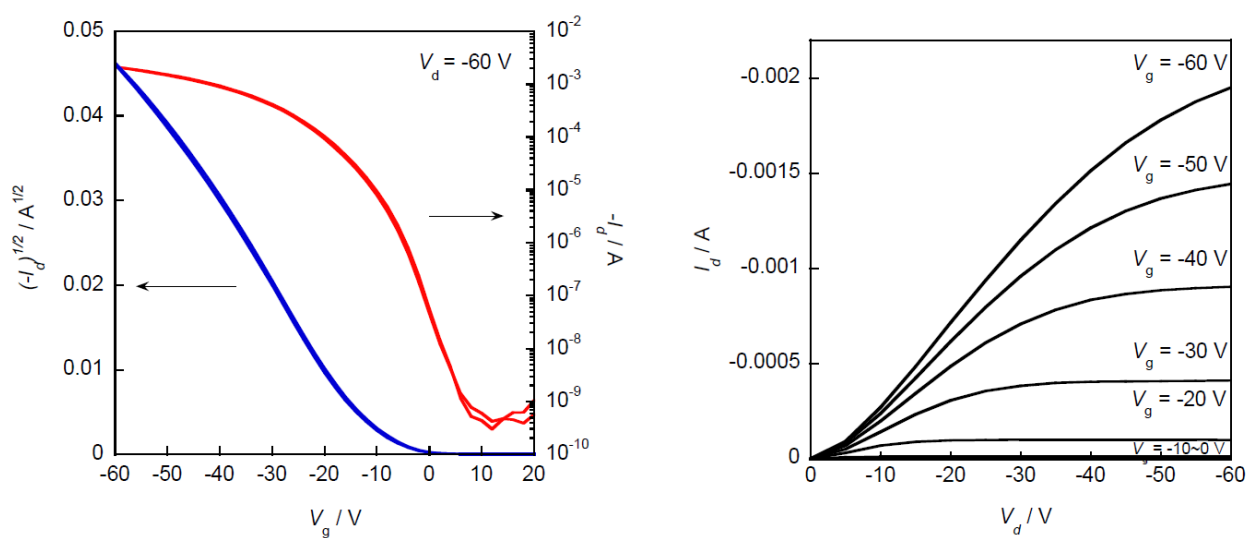


**Figure S3.** Transfer and output characteristics of **2b**-based solution processed OTFT.

## References

1. Ebata, H.; Izawa, T.; Miyazaki, E.; Takimiya, K.; Ikeda, M.; Kuwabara, H.; Yui, T., Highly Soluble [1]Benzothieno[3,2-b]benzothiophene (BTBT) Derivatives for High-Performance, Solution-Processed Organic Field-Effect Transistors. *J. Am. Chem. Soc.* **2007**, *129*, 15732.
2. Izawa, T.; Miyazaki, E.; Takimiya, K., Solution-Processible Organic Semiconductors Based on Selenophene-Containing Heteroarenes, 2,7-Dialkyl[1]benzoselenopheno[3,2-b][1]benzoselenophenes (Cn-BSBSs): Syntheses, Properties, Molecular Arrangements, and Field-Effect Transistor Characteristics. *Chem. Mater.* **2009**, *21*, 903.
3. Sheraw, C. D.; Jackson, T. N.; Eaton, D. L.; Anthony, J. E., Functionalized Pentacene Active Layer Organic Thin-Film Transistors. *Adv. Mater.* **2003**, *15*, 2009.
4. Payne, M. M.; Parkin, S. R.; Anthony, J. E.; Kuo, C. C.; Jackson, T. N., Organic Field-Effect Transistors from Solution-Deposited Functionalized Acenes with Mobilities as High as 1 cm<sup>2</sup>/Vs. *J. Am. Chem. Soc.* **2005**, *127*, 4986.
5. Schweicher, G.; Lemaur, V.; Niebel, C.; Ruzié, C.; Diao, Y.; Goto, O.; Lee, W. Y.; Kim, Y.; Arlin, J. B.; Karpinska, J.; Kennedy, A. R.; Parkin, S. R.; Olivier, Y.; Mannsfeld, S. C. B.; Cornil, J.; Geerts, Y. H.; Bao, Z., Bulky End-Capped [1]Benzothieno[3,2-b]benzothiophenes: Reaching High-Mobility Organic Semiconductors by Fine Tuning of the Crystalline Solid-State Order. *Adv. Mater.* **2015**, *27*, 3066.
6. Herwig, P. T.; Müllen, K., A Soluble Pentacene Precursor: Synthesis, Solid-State Conversion into Pentacene and Application in a Field-Effect Transistor. *Adv. Mater.* **1999**, *11*, 480.
7. Afzali, A.; Dimitrakopoulos, C. D.; Breen, T. L., High-Performance, Solution-Processed Organic Thin Film Transistors from a Novel Pentacene Precursor. *J. Am. Chem. Soc.* **2002**, *124*, 8812.
8. Aramaki, S.; Sakai, Y.; Ono, N., Solution-Processible Organic Semiconductor for Transistor Applications: Tetrabenzoporphyrin. *Appl. Phys. Lett.* **2004**, *84*, 2085.
9. Kang, M. J.; Doi, I.; Mori, H.; Miyazaki, E.; Takimiya, K.; Ikeda, M.; Kuwabara, H., Alkylated Dinaphtho[2,3-b:2',3'-f]Thieno[3,2-b]Thiophenes (Cn-DNTTs): Organic Semiconductors for High-Performance Thin-Film Transistors. *Adv. Mater.* **2011**, *23*, 1222.
10. Kang, M. J.; Miyazaki, E.; Osaka, I.; Takimiya, K., Two Isomeric Didecyl-dinaphtho[2,3-b:2',3'-f]thieno[3,2-b]thiophenes: Impact of Alkylation Positions on Packing Structures and Organic Field Effect Transistor Characteristics. *Jpn. J. Appl. Phys.* **2012**, *51*, 11PD04.
11. Nakayama, K.; Hirose, Y.; Soeda, J.; Yoshizumi, M.; Uemura, T.; Uno, M.; Li, W.; Kang, M. J.; Yamagishi, M.; Okada, Y.; Miyazaki, E.; Nakazawa, Y.; Nakao, A.; Takimiya, K.; Takeya, J., Patternable Solution-Crystallized Organic Transistors with High Charge Carrier Mobility. *Adv. Mater.* **2011**, *23*, 1626.
12. Soeda, J.; Hirose, Y.; Yamagishi, M.; Nakao, A.; Uemura, T.; Nakayama, K.; Uno, M.; Nakazawa, Y.; Takimiya, K.; Takeya, J., Solution-Crystallized Organic Field-Effect Transistors with Charge-Acceptor Layers: High-Mobility and Low-Threshold-Voltage Operation in Air. *Adv. Mater.* **2011**, *23*, 3309.
13. Liu, C.; Minari, T.; Lu, X.; Kumatani, A.; Takimiya, K.; Tsukagoshi, K., Solution-Processable Organic Single Crystals with Bandlike Transport in Field-Effect Transistors. *Adv. Mater.* **2011**, *23*, 523.
14. Minemawari, H.; Yamada, T.; Matsui, H.; Tsutsumi, J. y.; Haas, S.; Chiba, R.; Kumai, R.; Hasegawa,

- T., Inkjet Printing of Single-Crystal Films. *Nature* **2011**, *475*, 364.
15. Yuan, Y.; Giri, G.; Ayzner, A. L.; Zoombelt, A. P.; Mannsfeld, S. C. B.; Chen, J.; Nordlund, D.; Toney, M. F.; Huang, J.; Bao, Z., Ultra-High Mobility Transparent Organic Thin Film Transistors Grown by an Off-Centre Spin-Coating Method. *Nat. Commun.* **2014**, *5*, 4005.
16. Kimura, Y.; Nagase, T.; Kobayashi, T.; Hamaguchi, A.; Ikeda, Y.; Shiro, T.; Takimiya, K.; Naito, H., Soluble Organic Semiconductor Precursor with Specific Phase Separation for High-Performance Printed Organic Transistors. *Adv. Mater.* **2015**, *27*, 727.
17. Hamaguchi, A.; Negishi, T.; Kimura, Y.; Ikeda, Y.; Takimiya, K.; Bisri, S. Z.; Iwasa, Y.; Shiro, T., Single Crystal-Like Organic Thin-film Transistors Fabricated from Dinaphtho[2,3-b:2',3'-f]thieno[3,2-b]thiophene (DNFT) Precursor-Polystyrene Blends. *Adv. Mater.* **2015**, *27*, 6606.
18. Lei, T.; Wang, J. Y.; Pei, J., Roles of Flexible Chains in Organic Semiconducting Materials. *Chem. Mater.* **2014**, *26*, 594.
19. Zhang, F.; Hu, Y.; Schuetfort, T.; Di, C. a.; Gao, X.; McNeill, C. R.; Thomsen, L.; Mannsfeld, S. C. B.; Yuan, W.; Sirringhaus, H.; Zhu, D., Critical Role of Alkyl Chain Branching of Organic Semiconductors in Enabling Solution-Processed N-Channel Organic Thin-Film Transistors with Mobility of up to 3.50 cm<sup>2</sup> V<sup>-1</sup> s<sup>-1</sup>. *J. Am. Chem. Soc.* **2013**, *135*, 2338.
20. Niimi, K.; Kang, M. J.; Miyazaki, E.; Osaka, I.; Takimiya, K., General synthesis of dinaphtho[2,3-b:2',3'-f]thieno[3,2-b]thiophene (DNFT) derivatives. *Org Lett* **2011**, *13* (13), 3430-3.
21. Tamao, K.; Sumitani, K.; Kumada, M., Selective Carbon-Carbon Bond Formation by Cross-Coupling of Grignard Reagents with Organic Halides. Catalysis by Nickel-Phosphine Complexes. *J. Am. Chem. Soc.* **1972**, *94*, 4374.
22. Kursanov, D. N.; Parnes, Z. N.; Loim, N. M., Applications of Ionic Hydrogenation to Organic Synthesis. *Synthesis* **1974**, *1974*, 633.
23. Baer, H. H.; Zamkane, M., Stereospecific Synthesis of (-)-Anisomycin from D-Galactose. *J. Org. Chem.* **1988**, *53*, 4786.
24. Sonogashira, K.; Tohda, Y.; Hagihara, N., A Convenient Synthesis of Acetylenes: Catalytic Substitutions of Acetylenic Hydrogen with Bromoalkenes, Iodoarenes and Bromopyridines. *Tetrahedron Lett.* **1975**, *16*, 4467.
25. Cui, W.; Zhao, Y.; Tian, H.; Xie, Z.; Geng, Y.; Wang, F., Synthesis and Characterizations of Poly(9,10-bisarylethynyl-2,6-anthrylene)s and Poly(9,10-bisalkynyl-2,6-anthrylene). *Macromolecules* **2009**, *42*, 8021.
26. Yuan, M.; Rice, A. H.; Luscombe, C. K., Benzo[2,1-b:3,4-b']dithiophene-Based Low-Bandgap Polymers for Photovoltaic Applications. *J. Polym. Sci., Part A: Polym. Chem.* **2011**, *49*, 701.
27. Mori, T.; Nishimura, T.; Yamamoto, T.; Doi, I.; Miyazaki, E.; Osaka, I.; Takimiya, K., Consecutive Thiophene-Annulation Approach to  $\pi$ -Extended Thienoacene-Based Organic Semiconductors with [1]Benzothieno[3,2-b][1]benzothiophene (BTBT) Substructure. *J. Am. Chem. Soc.* **2013**, *135*, 13900.
28. Yue, D.; Larock, R. C., Synthesis of 2,3-Disubstituted Benzo[b]thiophenes via Palladium-Catalyzed Coupling and Electrophilic Cyclization of Terminal Acetylenes. *J. Org. Chem.* **2002**, *67*, 1905.

29. Yamamoto, T.; Takimiya, K., Facile synthesis of highly pi-extended heteroarenes, dinaphtho[2,3-b:2',3'-f]chalcogenopheno[3,2-b]chalcogenophenes, and their application to field-effect transistors. *J Am Chem Soc* **2007**, *129* (8), 2224-5.
30. Takimiya, K.; Osaka, I.; Mori, T.; Nakano, M., Organic Semiconductors Based on [1]Benzothieno[3,2-b][1]benzothiophene Substructure. *Acc. Chem. Res.* **2014**, *47*, 1493.
31. Yamamoto, T.; Nishimura, T.; Mori, T.; Miyazaki, E.; Osaka, I.; Takimiya, K., Largely  $\pi$ -Extended Thienoacenes with Internal Thieno[3,2-b]thiophene Substructures: Synthesis, Characterization, and Organic Field-Effect Transistor Applications. *Org. Lett.* **2012**, *14*, 4914.
32. Abe, M.; Mori, T.; Osaka, I.; Sugimoto, K.; Takimiya, K., Thermally, Operationally, and Environmentally Stable Organic Thin-Film Transistors Based on Bis[1]benzothieno[2,3-d:2',3'-d']naphtho[2,3-b:6,7-b']dithiophene Derivatives: Effective Synthesis, Electronic Structures, and Structure-Property Relationship. *Chem. Mater.* **2015**, *27*, 5049.

## Chapter 3

### Improvement of solution-processed OTFT using 2-EO-DNTT

#### 3-1 Introduction

Among the mono-substituted branched alkyl DNTT derivatives shown in Chapter 2, 2-EO-DNTT (Figure 1a) which is introduced 4-ethyloctyl group at the 2-position on DNTT core showed mobility of up to ca.  $0.5 \text{ cm}^2 \text{ V}^{-1} \text{ s}^{-1}$  by spin-coating and  $3 \text{ cm}^2 \text{ V}^{-1} \text{ s}^{-1}$  by vapor-deposition. The solubility of this 2-EO-DNTT is ca.  $3 \text{ g L}^{-1}$  to heated chloroform (it's equivalent to 0.2 wt%). In the results of XRD measurements on  $\text{SiO}_2/\text{Si}$  substrate (Figure 1e), the diffraction peaks for out-of-plane direction were observed with series of peaks which are assignable to lamella structures, while, for in-plane direction were observed with three distinct peaks which are typical for small-molecular organic materials forming herringbone arrangement. Judging from these results, 2-EO-DNTT is believed to form packing structure which is similar to parent DNTT on the substrate.<sup>1,2</sup> Therefore, 2-EO-DNTT is considered to have a potential as solution-processable small-molecular high-performance organic semiconductor material if the film is formed under optimal condition.<sup>3,4</sup>

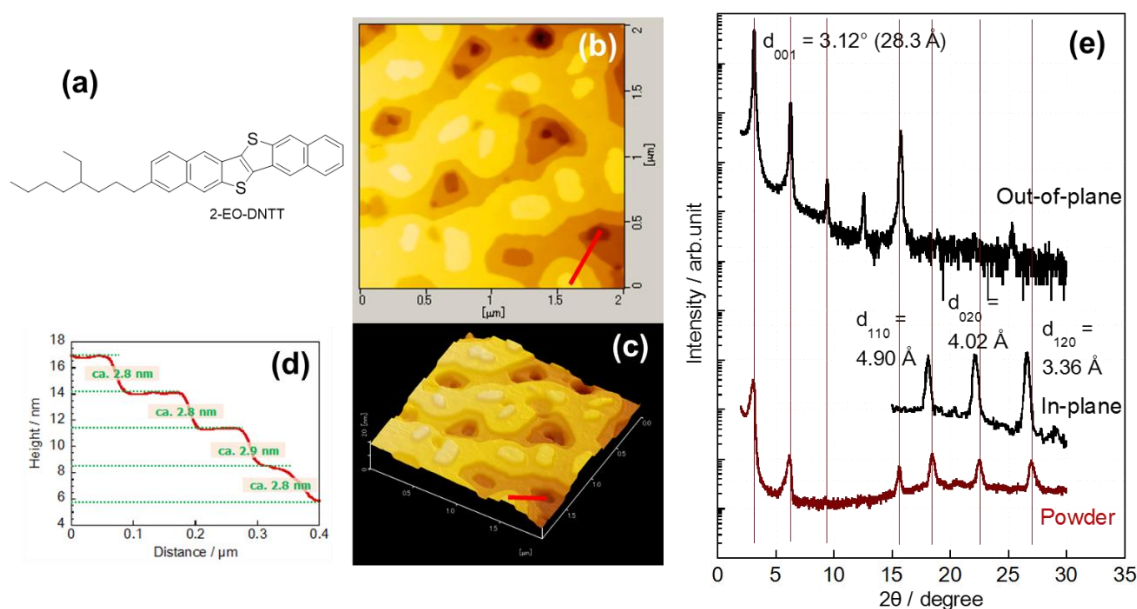


**Figure 1.** Molecular structure of 2-EO-DNTT (a). Top view (b) and bird's-eye view (c) of SPM topography image of vapor-deposited thin film ( $T_{\text{sub}} = 150 \text{ }^\circ\text{C}$ ). Cross-sectional profile of the red line in Figure 1b, c (d). Out-of-plane, In-plane of vapor-deposited thin film and powder XRDs (e).

In Chapter 3, I tried to improve OTFT characteristics using 2-EO-DNTT by spin-coating and succeeded in showing the mobility of up to  $2.6 \text{ cm}^2 \text{ V}^{-1} \text{ s}^{-1}$  by changing the spin-coating manners and solvents. Subsequently, I checked the OTFT stabilities (environmental, electrical, and thermal), and low-voltage operations using gate-insulator with thin  $\text{AlO}_x$  and phosphonic acid SAM. As mentioned in Chapter 1, stabilities and low-voltage drivability of OTFT materials are very important to produce commercial devices. However, OTFT materials that meet all the criteria mentioned above are still limited.<sup>5</sup>

## 3-2 Results and discussion

### 3-2-1 Search for optimal spin-coat conditions

As described in Chapter 2, thin-film deposition of 2-EO-DNTT was carried out by spin-coating, where a hot chloroform solution of 2-EO-DNTT (50  $\mu\text{L}$  of 0.2 wt % solution at the boiling temperature) was dropped onto the octyltrichlorosilane (OTS)-modified Si/SiO<sub>2</sub> substrate, and then the substrate was spun at 3000 rpm for 30 seconds (method 1). The resulting thin film consisted of crystalline grains (Figure 2a) and acted as the active layer in the TFT devices showing mobilities in the order of  $10^{-1} \text{ cm}^2 \text{ V}^{-1} \text{ s}^{-1}$  (Figure 2d, g).

I then examined a different deposition procedure; the identical semiconductor solution was dropped onto the spinning substrate (3000 rpm).<sup>6</sup> When the 50  $\mu\text{L}$  solution was dropped at once (method 2), the resulting films seemed to have smoother surface and lower thickness than the ones obtained by the method 1 (Figure 2b). The mobilities of the OTFTs with the films were lower by one order of magnitude than those obtained from the devices fabricated by the method 1 (Figure 2e, h). In contrast, when the solution was dropped in several portions (50  $\mu\text{L}$ , typically 8 drops, method 3), the films with apparently larger thickness were obtained (Figure 2c). Surprisingly, the TFTs with the films as the active layer showed significantly enhanced mobilities of up to  $2.1 \text{ cm}^2 \text{ V}^{-1} \text{ s}^{-1}$  (Figure 2f, i).

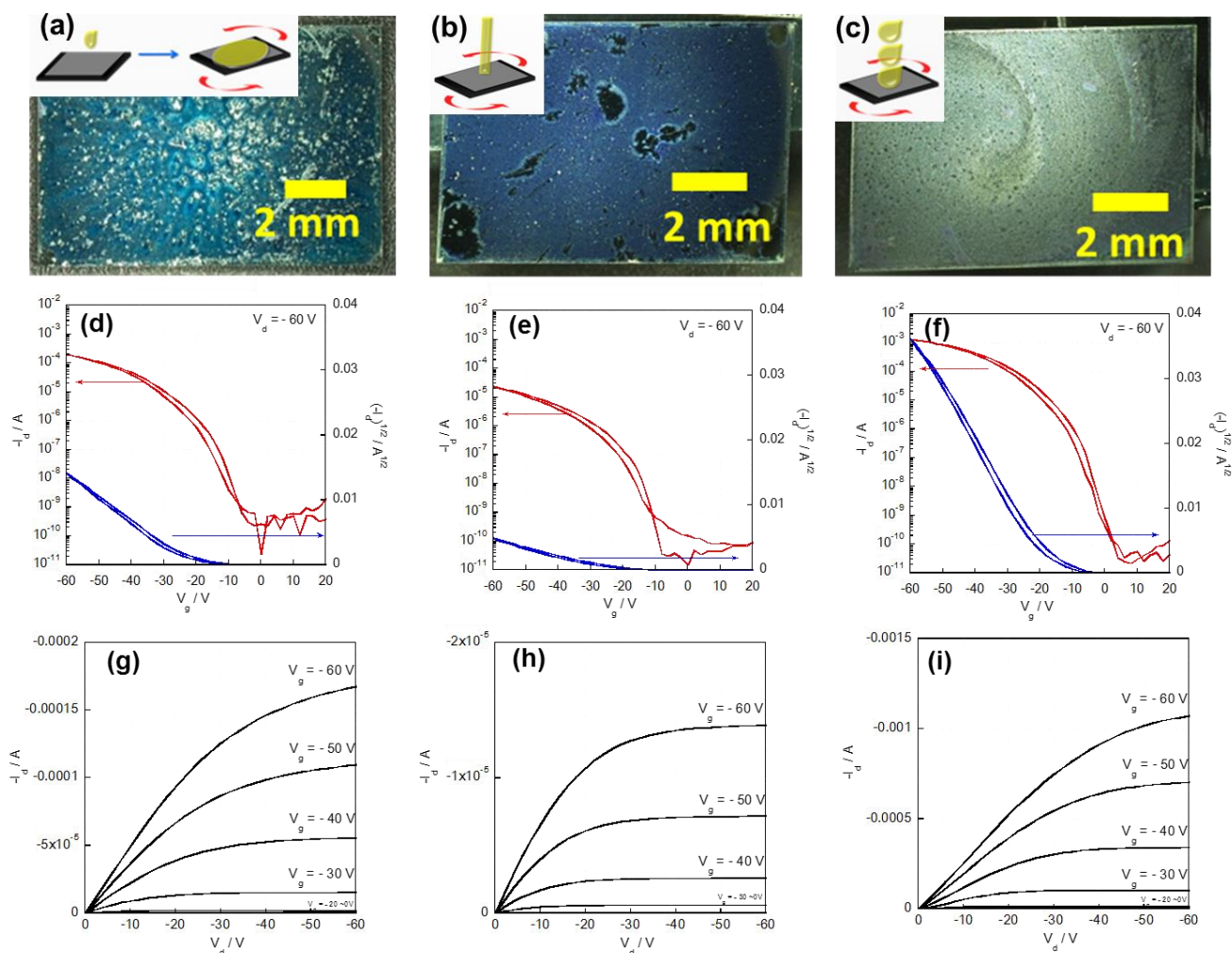


**Figure 2.** Optical microscope images of spin-coated thin films by the method 1-3, respectively (a-c). Transfer (d-f) and output characteristics (g-i) of TFTs consisting of the thin films fabricated by method 1-3, respectively.

In order to understand the cause for the significantly different TFT characteristics depending on the spin-coating methods, I first carried out the X-ray diffraction (XRD) measurements of the thin films (Figure 3). All the films fabricated by the different methods showed almost identical XRD patterns both in the out-of-plane and in-plane measurements, indicating that the molecular orientation and the packing structure are not affected by the methods. I then examined the thin films by scanning probe microscopy (SPM) with the dynamic force mode (DFM): as shown in Figure 4, the step-and-terrace

structure was clearly observed for all the films, and the step heights, ca. 2.8 nm, are virtually the same as the lamella  $d$ -spacing observed in the out-of-plane XRDs (2.84 nm). This also supports the result of the XRD measurements; i.e., no actual differences in the packing structure and molecular orientation in the thin films fabricated by the different spin-coating methods.

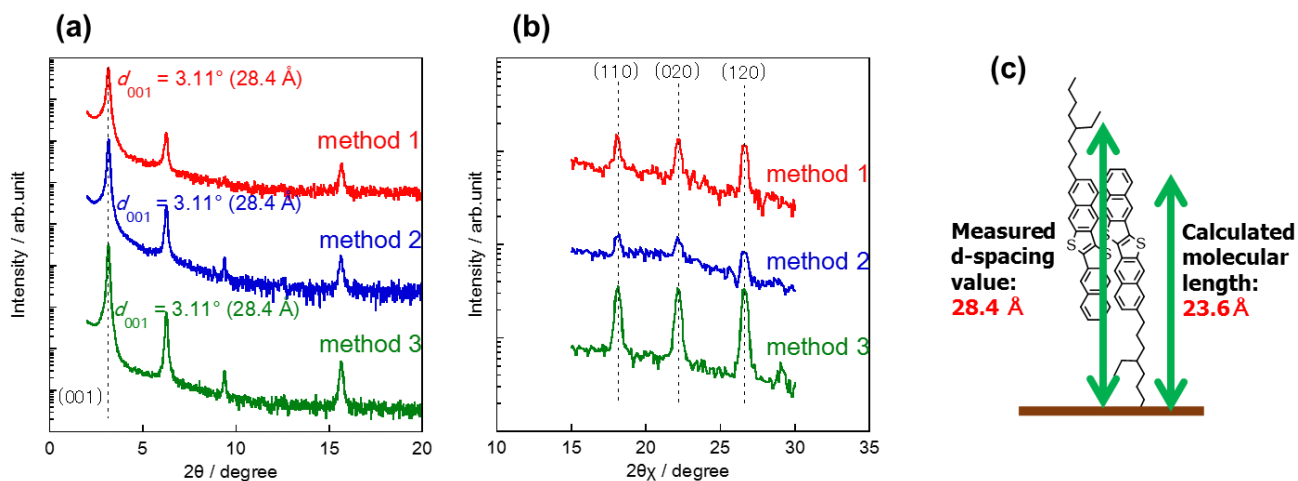


**Figure 3.** Out-of-plane (a) and in-plane (b) XRDs of 2-EO-DNTT spin-coated thin films fabricated by the method 1-3. Schematic picture of molecular orientation on the substrate (c).

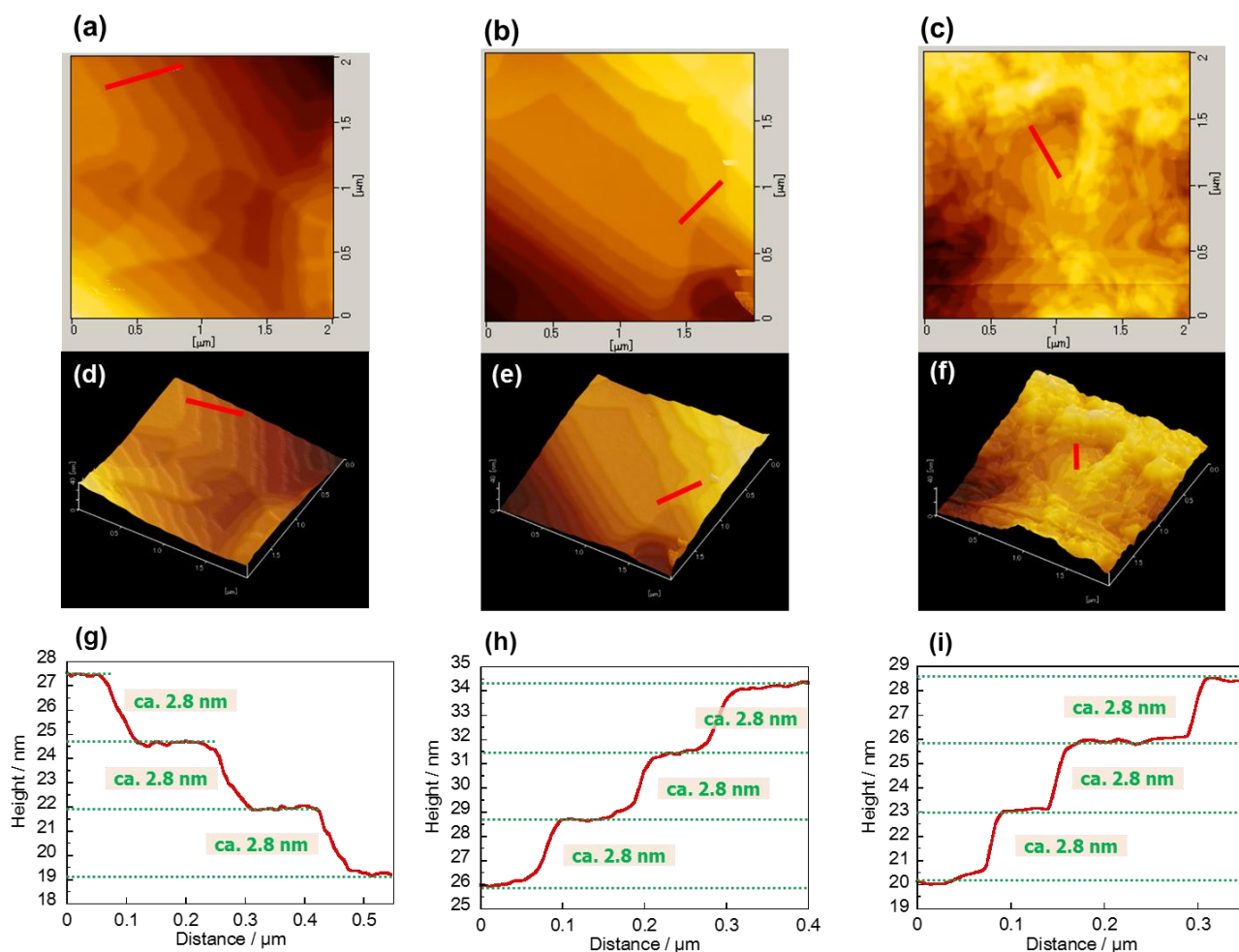


**Figure 4.** Scanning probe microscopy (SPM) images with dynamic force mode (DFM) of thin films fabricated by the method 1 (a,d,g), 2 (b,e,h), and 3 (c,f,i), respectively. Topography images (a-c). Bird's-eye view (d-f). Cross-sectional profiles along the red lines in a-c (g-i).

Although the optical microscope images in low magnification (Figure 2a–c) are not quite helpful to detect the actual difference between the films fabricated by the different methods, characteristic features in each film were observed in the highly magnified optical microscope images ( $\times 850$ , Figure 5a–c); the density of the crystallites in the films are significantly different, and the surface of the substrate does not seem to be covered completely in the films fabricated by the method 1 and 2.

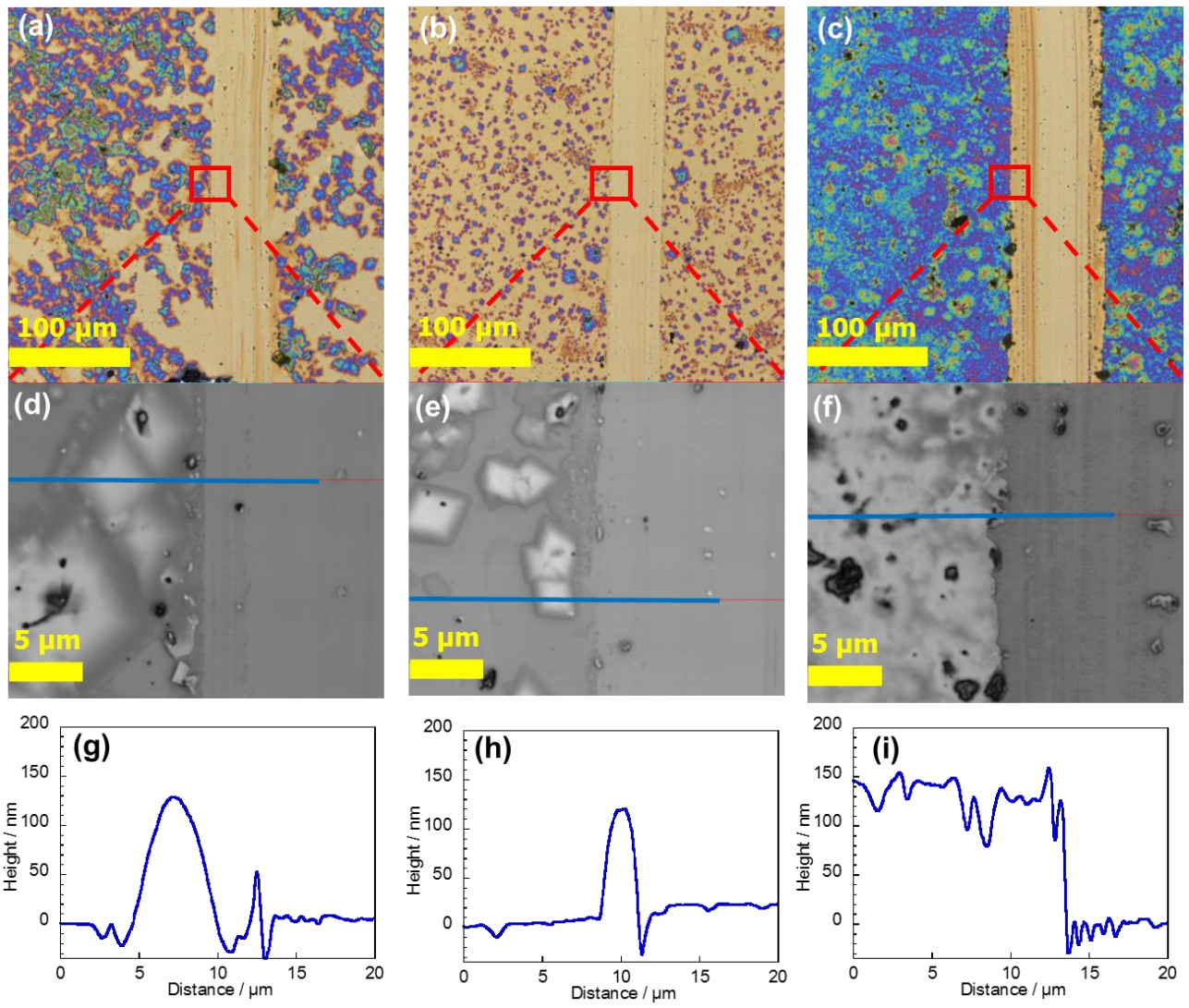


**Figure 5.** High-magnification images of scratched region of the thin films fabricated by the method 1 (a,d,g), 2 (b,e,h), and 3 (c,f,i), respectively. Confocal optical microscope images (a-c). Confocal laser scanning microscope images (d-f). Cross-sectional profiles of the blue lines in d-f (g-i).

Confocal laser microscope images with much higher magnification ( $\times 10625$ , [Figure 5d–f](#)) together with the cross-sectional profile of the scratched area of the thin films ([Figure 5g–i](#)) further confirm the different density of crystallites in the films; the films fabricated by the method 1 and 2 have the “sea-island” structure, where the crystallites (islands) are observed on the substrate surface or very thin layer of the semiconducting material (sea). In contrast, it is clearly observed that the much dense film was formed by the method 3, where the thickness of the film is ca. 150 nm ([Figure 5i](#)). From these results it can be concluded that the coverage of the channel region by the semiconductor, in other words, the connectivity of the crystallites, is the key for the TFT performances.

It is interesting to note that even though all the film fabrications were carried out with the same amount of solution, the quality of the resulting films is largely dependent on the method for the supply of the semiconductor solution. In the present experiments, the surface energy of the substrate seems to be low, as it was modified with the OTS-SAM, which could make the nucleation of the semiconducting crystallites slow on the substrate.<sup>7</sup> This can explain the poor coverage of the substrate by the semiconducting crystallites in the films deposited by the method 1 and 2. On the other hand, the repetitive supply of the semiconducting solution in small portions can allow nucleation in each drop of the solution, and the crystallites formed by the early stage can be the core for crystal growth in the subsequent drops of the solution. These assumptions were further confirmed by observing the films in each additional drop of the semiconductor solution ([Figure 6](#)).

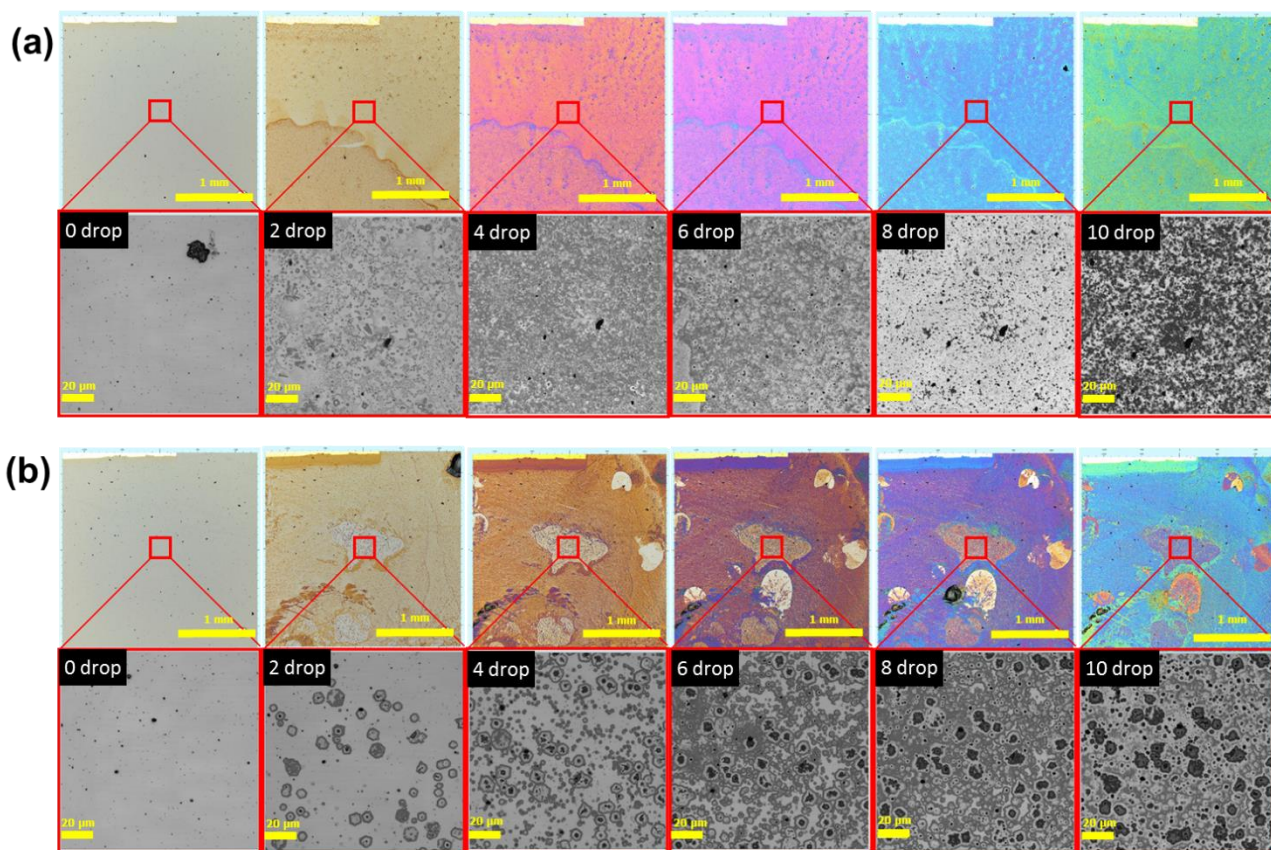


**Figure 6.** Confocal optical and laser microscope images ( $\times 107$  and  $\times 2125$ ) of 2-EO-DNTT films with different amount of solution. Each drop was ca.  $10 \mu\text{L}$ , 0.2 wt% in chloroform (a) and 1,1,2-trichloroethane (b).

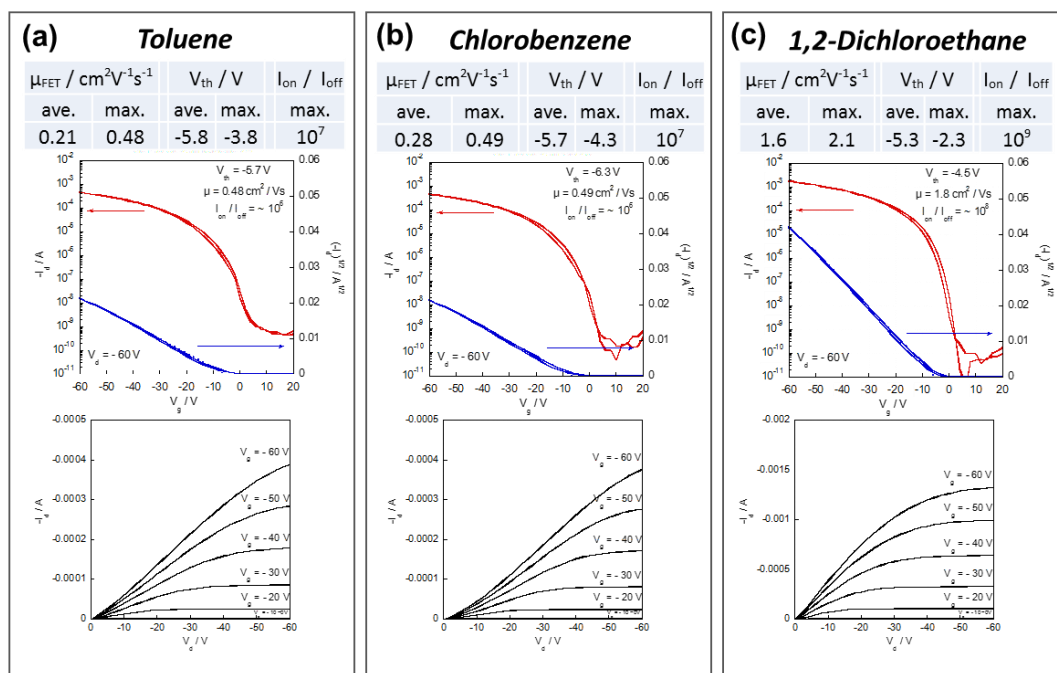


**Figure 7.** Characteristics of OTFTs fabricated with the spin-coated thin films of 2-EO-DNTT from toluene (a), chlorobenzene (b), and 1,2-dichloroethane (c), respectively.

Through the careful inspection of the films, it is concluded that the method 3 is a reliable way to fabricate a thin-film of 2-EO-DNTT for TFTs. Further optimization by the same spin-coating method with toluene, chlorobenzene, 1, 2-dichloroethane, and 1, 1, 2-trichloroethane was also tried (Figure 7). When the film deposition was carried out with 1, 1, 2-trichloroethane as the solvent, the film uniformity was further improved, and the resulting OTFTs showed slightly higher mobility, up to  $2.6 \text{ cm}^2 \text{ V}^{-1} \text{ s}^{-1}$  (average of 12 devices,  $2.4 \text{ cm}^2 \text{ V}^{-1} \text{ s}^{-1}$ , Figure 8), with the optimized amount of solution and spinning rate (Figure 9). The higher boiling point of 1, 1, 2-trichloroethane ( $114 \text{ }^\circ\text{C}$ ) than chloroform ( $61 \text{ }^\circ\text{C}$ ) likely allowed better nucleation and crystal growth on the substrate, which decreases inhomogeneous area that does not contribute to efficient carrier transport.<sup>8,9</sup> Such high mobilities of up to  $2.6 \text{ cm}^2 \text{ V}^{-1} \text{ s}^{-1}$ , large on/off ratios, and small dependence of mobility on the gate voltage (Figure 8b) are almost comparable to those obtained from the vapor-deposited DNTT-based TFTs. This impelled us to test the device stability, to confirm the utility of 2-EO-DNTT as a solution processable organic semiconductor and to evaluate the effect of the branched alkyl groups on the devices stability.

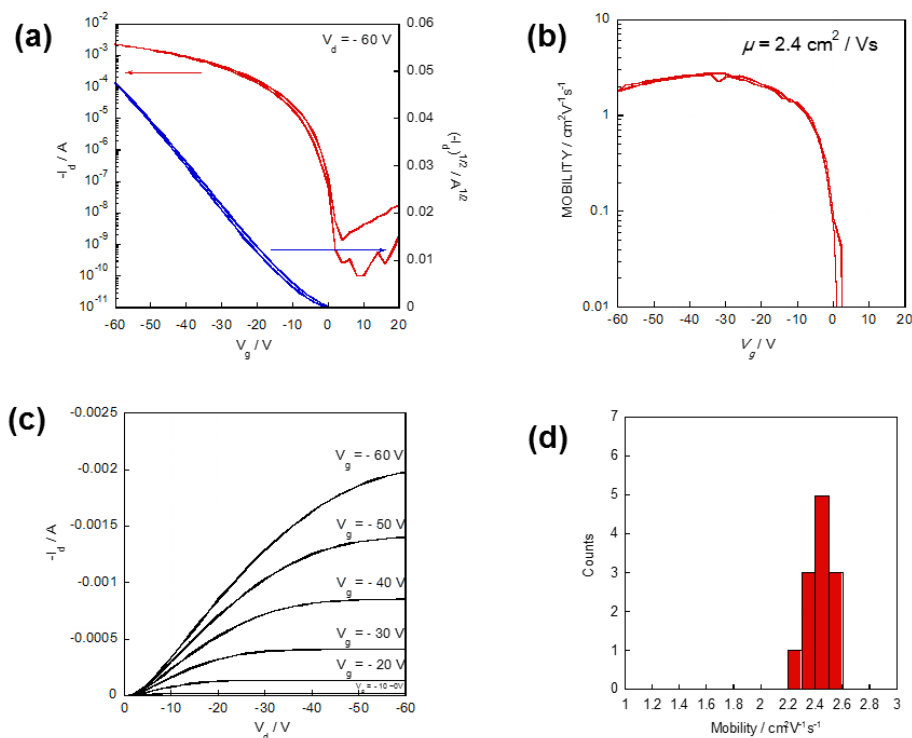


**Figure 8.** Properties of 2-EO-DNTT-TFTs fabricated from the 1,1,2-trichloroethane solution. Transfer characteristics (a). Mobility dependence on  $V_g$  (b). Output characteristic (c). Distribution of mobilities (d).

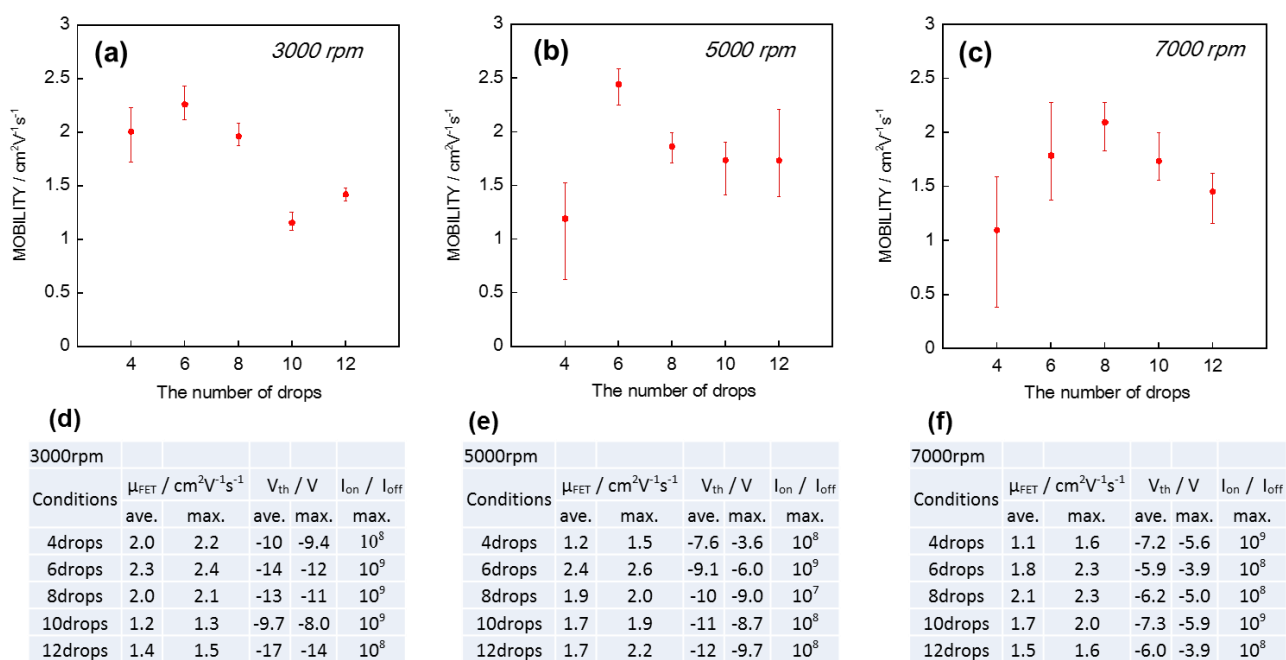


**Figure 9.** Mobilities of 2-EO-DNTT-based TFTs depending on the solution amount and spinning rate during deposition (a–c). Summarized TFT characteristics (d–f).

### 3-2-2 Investigation of device stability

2-EO-DNTT itself is a chemically stable compound, similar to parent DNTT (Figure 10). On the other hand, the 2,9-didecyl-DNTT (C<sub>10</sub>-DNTT)-based TFTs were reported to be not thermally stable, owing to its complicated thermal behaviors observed in DSC.<sup>10, 11</sup> In contrast, 2-EO-DNTT did not show any thermally induced phase transition other than the melting point in DSC (Figure 10c). It is thus interesting to elucidate thermal stability of the 2-EO-DNTT-TFTs for further utilization in various device applications.

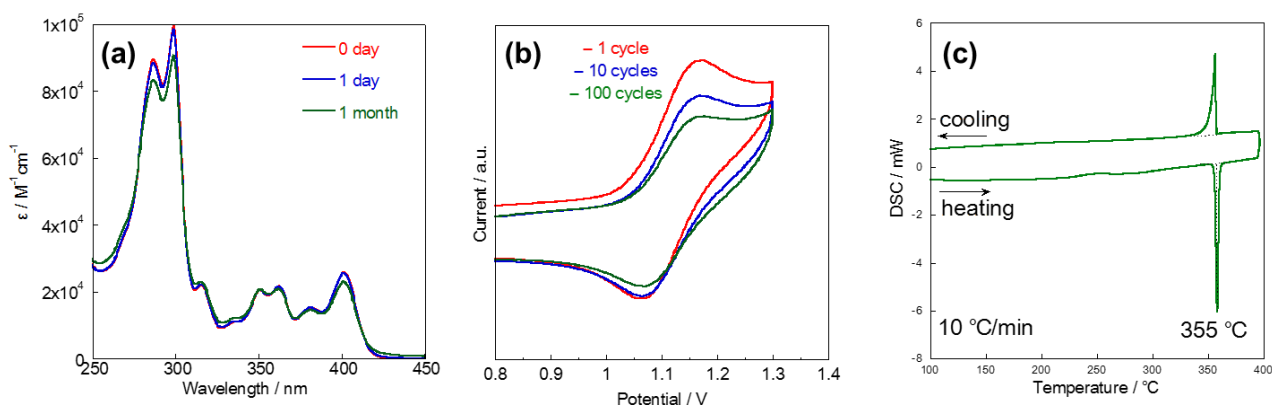


**Figure 10.** UV-vis spectra of 2-EO-DNTT in air-saturated chloroform solution (a). Multi-scan cyclic voltammograms of 2-EO-DNTT (V vs Ag/AgCl). Pt as working and counter electrodes, PhCN as solvent, Bu<sub>4</sub>NPF<sub>6</sub> (0.1 M) as supporting electrolyte, scan rate = 1 V s<sup>-1</sup> (b). Differential scanning calorimetry (DSC) profile of 2-EO-DNTT (c).

I first carried out the shelf life time test under ambient conditions (Figure 11a): although a slight decrease of on-current and a small shift of threshold voltage ( $V_{th}$ ) were observed after six months storage, the overall transfer characteristics were still maintained, and therefore I concluded that environmental stability of the device is mostly the same with that of the DNTT-based devices.<sup>2</sup> For the cycle test, in which on- and off- state were continuously switched, also showed no significant degradation after 3000 cycles (Figure 11b).

On the other hand, thermal treatment of the device at 250 °C for 30 minutes in air induced obvious degradation of the device characteristics; the on-current ( $V_g = -60$  V) and consequently the mobility were decreased by more than one order of magnitude, whereas thermal treatment up to 200 °C for 30 minutes caused a slight and gradual decrease in on-current and mobility (Figure 11c, d). This is sharply contrasted to the parent DNTT-based devices, which can retain the excellent device characteristic up to 100 °C, but thermal treatment at 160 °C or higher brought significant degradation of the device performances.<sup>12</sup> It has been also reported that the C<sub>10</sub>-DNTT-based devices degrade at much lower temperature (~110 °C), owing to the thermal transitions as mentioned above. For DNTT, on the other hand, although no thermal transitions up to 400 °C was detected in DSC,<sup>2</sup> subtle changes in the

molecular orientation on the substrate was observed at 160 °C or higher temperature in the in-plane XRD, which was explained to be the cause for the thermal degradation of the DNNTT-based TFTs.<sup>12</sup>

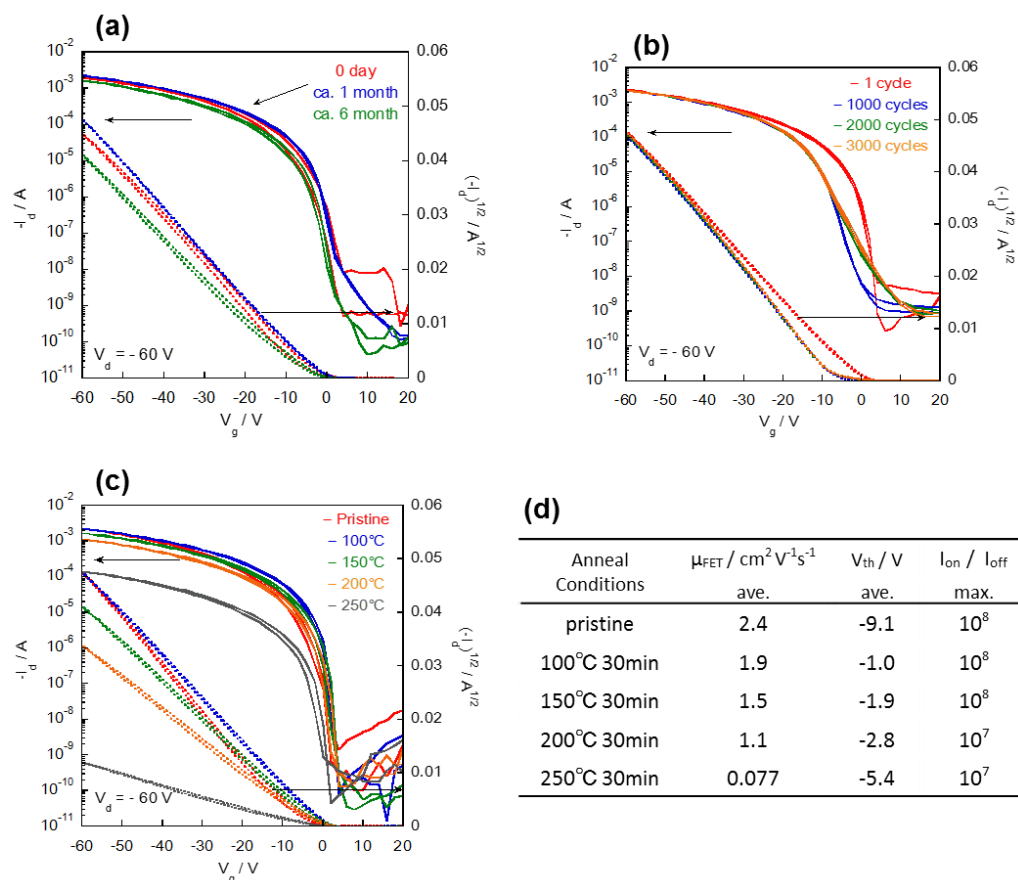


**Figure 11.** Transfer characteristics of 2-EO-DNNTT-based TFTs with different aging time (a), on-off cycles (b), and thermal treatments at different temperatures (c). Summarized TFT characteristics upon thermal treatments (d).

Compared to the not so good thermal stability of the DNNTT- and C<sub>10</sub>-DNNTT-based devices, the 2-EO-DNNTT-based ones are said to be stable, almost comparable to 2,9-diphenyl-DNNTT (DPh-DNNTT)-based ones,<sup>11,13</sup> which is one of the most thermally stable OTFTs at high temperatures.<sup>14,15</sup> The good thermal stability of DPh-DNNTT-based devices was explained by the stiffness of the packing structure of the material in the thin-film state. Although the exact packing structure of 2-EO-DNNTT was not elucidated yet, it was suggested that the molecule has the anti-parallel or staggered orientation in the thin-film state based on the thin-film XRD analysis, indicating<sup>16</sup> that such “inter-locked” structure can resist the

thermal agitation, resulting in stabilization of the molecular packing in the thin-film state. In fact, both the out-of-plane and in-plane XRD patterns were not changed up to 200 °C. However, the thermal treatment at 250 °C abruptly diminished the all the peaks in both the out-of-plane and in-plane XRDs (Figure 12), which is consistent with the degradation of TFT characteristics by the thermal treatment at 250 °C. To further investigate the cause for the degradation, I checked the thermal behaviors of 2-EO-DNTT both in the form of the thin film and powder sample; it turned out that even under the ambient pressure, 2-EO-DNTT in the thin-film form slowly sublime at 250 °C. Furthermore, I noticed gradual thermal degradation of the powder sample of 2-EO-DNTT in air (Figure 13); bright yellow powder of pristine 2-EO-DNTT turned into brown in color at around 200 °C, and by further heating to the melting temperature (ca. 355 °C), the sample became a black solid. These thermal behaviors of 2-EO-DNTT in air are qualitatively consistent with the degradation of TFT characteristics by thermal annealing. I thus conclude that gradual thermal decomposition in air and sublimation of 2-EO-DNTT at the ambient pressure are the cause for the degradation of its TFT devices.

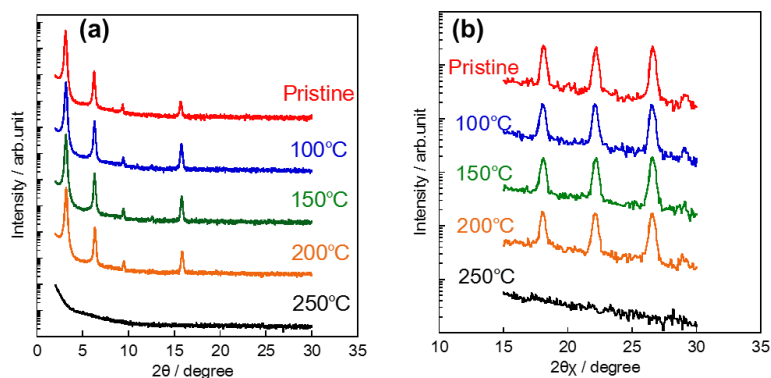


**Figure 12.** Out-of-plane (a) and in-plane (b) XRDs with thermal treatments at different temperatures.

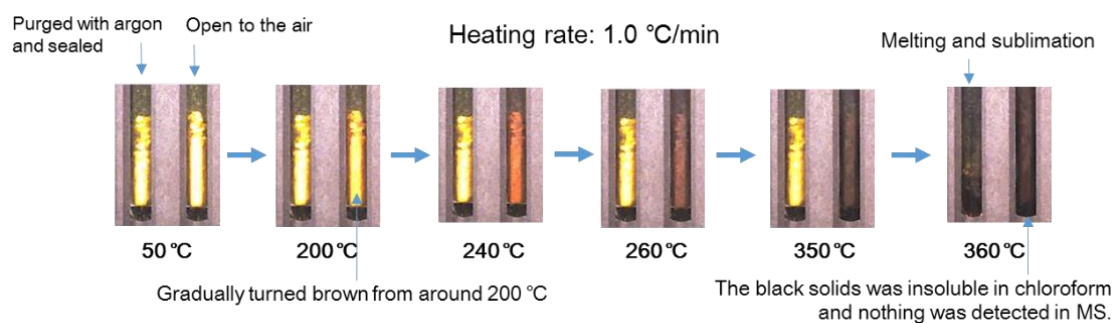


**Figure 13.** Thermal behavior of powder sample of 2-EO-DNTT.

### 3-2-3 Low voltage operation of OTFTs

As mentioned in the introductory part, the state-of-the-art applications of the DNNT-TFTs rely on the low-voltage-operable TFTs fabricated on the  $\text{AlO}_x$ /phosphonic acid-SAM-based gate dielectric. For further application of the present solution-processed 2-EO-DNNT-TFTs, it is important to elucidate its amenability to the  $\text{AlO}_x$ /phosphonic acid-SAM gate dielectric for low-voltage operation.<sup>12,17-22</sup> I thus first prepared the Al/ $\text{AlO}_x$  gate electrode/dielectric on the glass substrates by anodization of vapor-deposited aluminum electrodes,<sup>23</sup> and then the electrode surface was modified with octadecylphosphonic acid (ODPA) and 1*H*,1*H*,2*H*,2*H*-heptadecafluorodecyl phosphonic acid (FDPA) by immersing the substrate with the electrode/gate dielectric in their solution (see Experimental section for detail). The measured capacitance per area of the dielectric was reasonably large, 276 and 310  $\text{nF cm}^{-2}$  for ODPA- and FDPA-SAM, respectively (Figure 14). I then fabricated the thin films on these gate dielectrics by the aforementioned procedure with the 2-EO-DNNT solution in 1,1,2-trichloroethane.

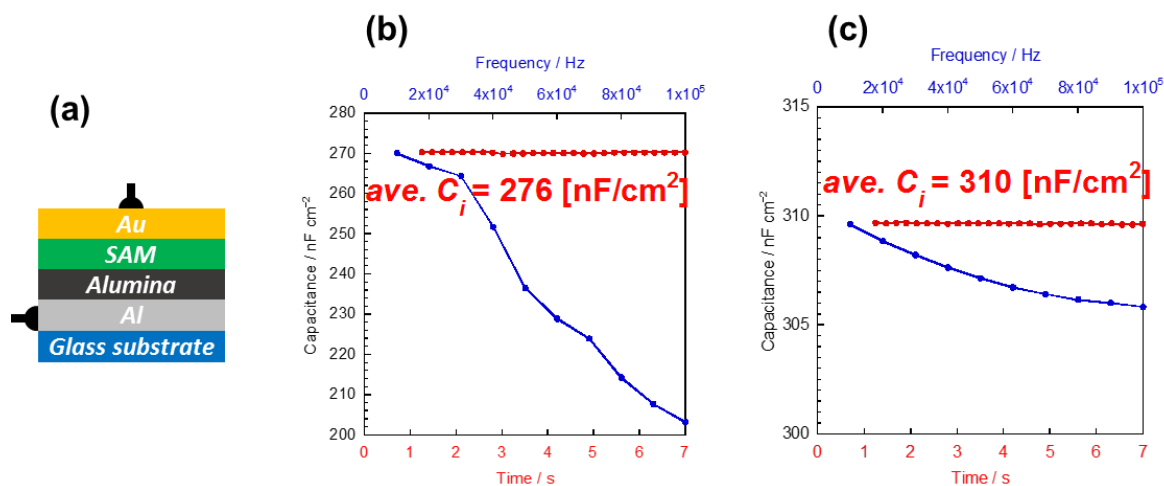


**Figure 14.** Cross-sectional illustration of the capacitor of the gate insulator (a). Capacitance measurements of the gate insulators with ODPA-SAM (b) and FDPA-SAM (c).

Delightedly, the devices showed typical TFT characteristics at low-voltage ( $-3$  V), and the mobilities extracted from the saturation regime were higher than  $1.0 \text{ cm}^2 \text{ V}^{-1} \text{ s}^{-1}$  for the devices with both  $\text{AlO}_x/\text{ODPA}$ - and  $\text{FDPA}$ -SAM gate insulators (Figure 15). Notably, on the  $\text{AlO}_x/\text{FDPA}$ -SAM gate insulator, typical TFT characteristics, almost negligible hysteresis, small  $V_{\text{th}}$  close to 0 V, and linear onset in the output curves at the low drain voltage ( $V_d$ ) region, were confirmed, which is likely ascribed to low carrier-trap density at the interface between the substrate surface modified with the SAM and the organic semiconductor.<sup>24-26</sup> On the other hand, the on-off current ratios were relatively small compared to those obtained from the TFTs on the  $\text{Si}/\text{SiO}_2$  substrate; this is likely due to leakage current between the gate and drain electrode owing to the device configuration with relatively large overlap of the source/drain and gate electrodes (red dotted lines in Figure 15c, e), which will be improved by minimizing the overlap.

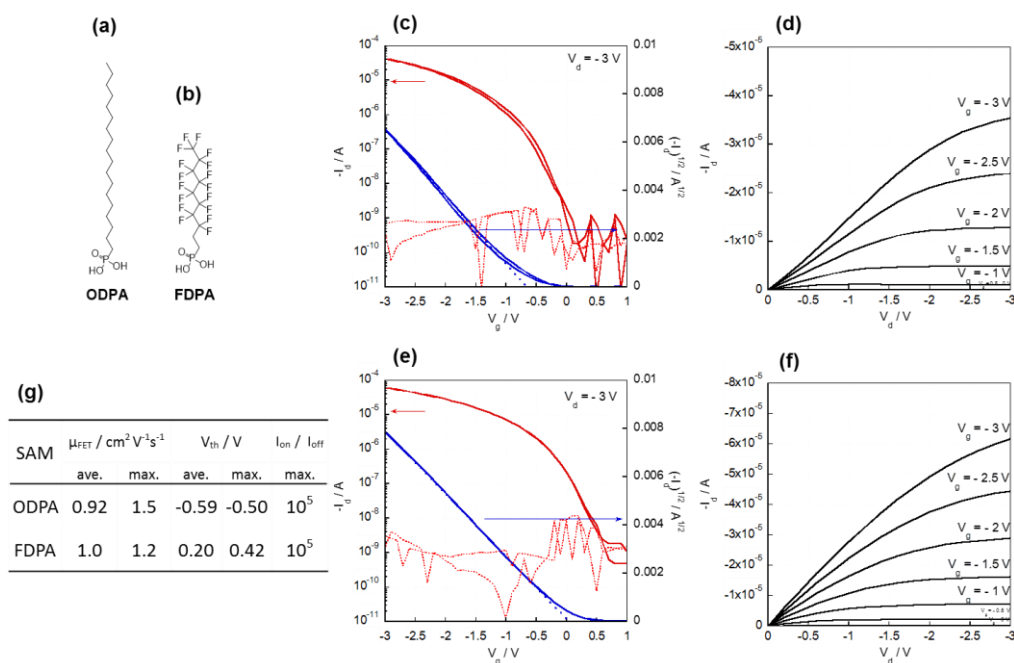


**Figure 15.** Molecular structures of ODPA (a) and FDPA (b). Transfer (c) and output (d) characteristics of 2-EO-DNTT-based TFTs fabricated on the  $\text{AlO}_x/\text{ODPA}$ -SAM gate insulator. Transfer (e) and output (f) characteristics of 2-EO-DNTT-based transistors fabricated on the  $\text{AlO}_x/\text{FDPA}$ -SAM gate insulator. Red dotted lines in (c) and (e) are the gate leak current. Summarized TFT characteristics of 2-EO-DNTT-based TFTs fabricated on the  $\text{AlO}_x/\text{SAM}$  (g).

The excellent device characteristics on the  $\text{AlO}_x$ /phosphonic acid SAM were also rationalized by the molecular orientation and packing structure in the thin-films state elucidated by the thin-film XRD measurements. As shown in Figure 16, there is no virtual difference in the XRDs both for the out-of-plane and in-plane measurements between the thin films on the  $\text{AlO}_x$ /phosphonic acid SAMs and  $\text{Si/SiO}_2$  modified with OTS. This indicates that 2-EO-DNTT affords the identical molecular ordering structure on both substrate that is favorable for effective carrier transport. It should be also noted that solution-processed OTFTs that can operate at lower driving voltage than  $\pm 5$  V have been still limited,<sup>27-29</sup> and therefore the present methods for fabricating 2-EO-DNTT-based TFTs are likely promising as a practical technology, which enables the fabrication of solution-processed TFTs with high mobility, environmental and thermal stability, and low-voltage operation under ambient conditions.

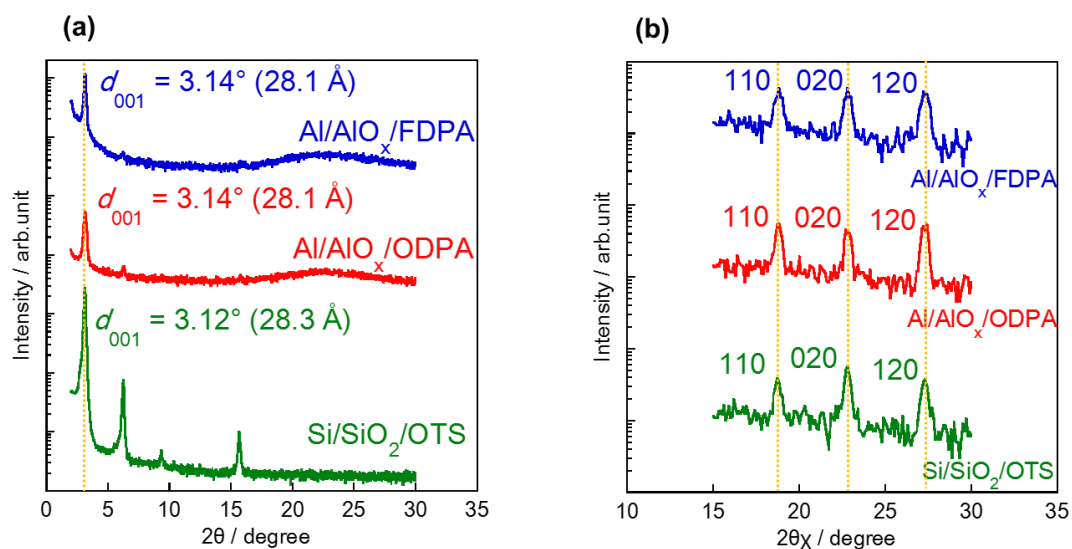


**Figure 16.** Out-of-plane (a) and in-plane (b) XRDs of 2-EO-DNTT spin-coated thin films on  $\text{Si/SiO}_2$ /OTS,  $\text{Al/AlO}_x$ /ODPA and  $\text{Al/AlO}_x$ /FDPA substrates.

### 3-3 Conclusion of chapter 3

By optimizing the deposition conditions of thin films of a soluble DNNT derivative, 2-EO-DNNT with one 4-ethyloctyl group as a solubilizing substituent, the performances of its solution processed OTFTs were greatly improved with the mobility of up to  $2.6 \text{ cm}^2 \text{ V}^{-1} \text{ s}^{-1}$ , which is almost comparable to the ones reported for the vapor-processed DNNT-based TFTs. Moreover, almost the same environmental, operational, and thermal stabilities for the solution-processed 2-EO-DNNT-TFTs as those for the DNNT-based TFTs were achieved. In addition to the comparable performances, I also confirmed that the solution-processed 2-EO-DNNT-TFTs can be fabricated on the  $\text{AlO}_x/\text{SAM}$  gate dielectrics that enables low-voltage operation as low as 3 V with keeping the TFT performances. These results indicate that the importance of deposition conditions in the solution process; control of nucleation and crystal growth are a key to forming the continuous semiconducting channel, in which the desirable molecular orientation and packing structure of the 2-EO-DNNT molecules are realized. Through all these optimizations of deposition conditions and subsequent device applications and evaluations, I can conclude that 2-EO-DNNT is a solution-processable alternative for the vapor-processed parent DNNT.

### 3-4 Experimental section, supporting data and references

#### Fabrication and characterization of OTFTs.

2-EO-DNTT was synthesized according to the reported procedure. OTFT devices based on 2-EO-DNTT were fabricated in a top-contact-bottom-gate (TCBG) configuration on a heavily doped n<sup>+</sup>-Si (100) wafer with a 200 nm thermally grown SiO<sub>2</sub> ( $C_i = 17.3 \text{ nF cm}^{-2}$ ) or a glass substrate with the Al gate-electrode and gate-insulator consisting of AlO<sub>x</sub> with phosphonic acid SAM. The surface of the SiO<sub>2</sub> substrates were modified with OTS-SAM as previously reported.<sup>30</sup> Thin films of 2-EO-DNTT as the active layer were deposited by spin-coating (0.2 wt% solution in chloroform or 1,1,2-trichloroethane) under ambient conditions. On top of the thin films, gold films (80 nm thick) as the drain and source electrodes were vapor-deposited through a shadow mask, and then the OTFTs were annealed at 100 °C for 10 min in air. For a typical device, the drain-source channel length ( $L$ ) and width ( $W$ ) are 40 and 1500 μm, respectively.

Characteristics of the OTFT devices were measured at room temperature under ambient conditions with a Keithley 4200 semiconducting parameter analyzer. Field-effect mobility ( $\mu_{\text{FET}}$ ) was extracted from the characteristics in the saturation regime (TFTs on the SiO<sub>2</sub> substrate:  $V_d = -60 \text{ V}$ , TFTs on the AlO<sub>x</sub>/phosphonic acid SAM:  $V_d = -3 \text{ V}$ ;  $V_d$ : drain voltages) with the following equation;

$$I_d = C_i \mu_{\text{FET}} \frac{W}{2L} (V_g - V_{\text{th}})^2$$

where  $C_i$  is the capacitance per unit area of the SiO<sub>2</sub> or AlO<sub>x</sub> dielectric layer, and  $V_g$  and  $V_{\text{th}}$  are the gate and threshold voltages, respectively. The current on/off ratio ( $I_{\text{on}}/I_{\text{off}}$ ) was determined from the  $I_d$  at the maximum ( $I_{\text{on}}$ ) and minimum ( $I_{\text{off}}$ ) values. The  $\mu_{\text{FETs}}$  reported in this paper were typical values from more than 6 identical devices.

### Stability tests of the OTFT devices

The shelf lifetime tests were carried out as follows: The fabricated OTFT devices were stored in a polystyrene box under ambient conditions, and the OTFT characteristics were measured at ca. 1 and 6 months after fabrication of the devices. For evaluation of operational stability of the devices, the  $V_g$  was repeatedly applied from +20 to -60 V at the  $V_d = -60$  V up to 3000 cycles. For evaluation of thermal stability, the devices were heated on a hotplate at temperatures of 100, 150, 200 and 250 °C for 30 min and then allowed to cool to room temperature. The device characteristics were evaluated at room temperature. All the thermal process and measurements were carried out under ambient conditions.

### Preparation of the $AlO_x$ /phosphonic acid SAM gate insulator

Schematic representation of the fabrication of  $AlO_x$ /phosphonic acid SAM gate dielectrics is shown in [Figure S1](#). The Al gate electrodes (1.8 mm wide, ca. 40 nm thick) were deposited by thermal evaporation through a shadow mask at a pressure of  $10^{-3}$  Pa and a deposition rate of  $3 \text{ nm s}^{-1}$  on glass substrates (Corning EAGLE XG glass), which was cleaned with  $O_2$ -plasma (30 min at 18 W, 700 mTorr) prior to the deposition. The  $AlO_x$  layer was then formed by potentiostatic anodization in a 10 mM citric acid solution, which was prepared with ultrapure water ( $18 \text{ M}\Omega \text{ cm}$ ). The Al gate electrodes on the glass substrate as the working electrode (anode) and a Pt rod as the counter electrode were immersed in the solution. Between the electrodes, anodization voltage of 14.5 V was applied until the current was dropped to ca. 30  $\mu\text{A}$ . It took ca. 3 min. in our experimental settings. After surface activation with  $O_2$ -plasma (30 min at 18 W, 700 mTorr), the substrates were dipped into a 2 mM solution of octadecylphosphonic acid (ODPA) or 1*H*,1*H*,2*H*,2*H*-heptadecafluorodecyl phosphonic acid (FDPA) in isopropyl alcohol for more than 12 h to form the SAMs. Typical capacities of gate dielectric layers were ca. 276 and 310  $\text{nF cm}^{-2}$  for the  $AlO_x$ /ODPA and  $AlO_x$ /FDPA SAM, respectively.

Procedure and configuration of the alumina and phosphonic acid SAM insulating film

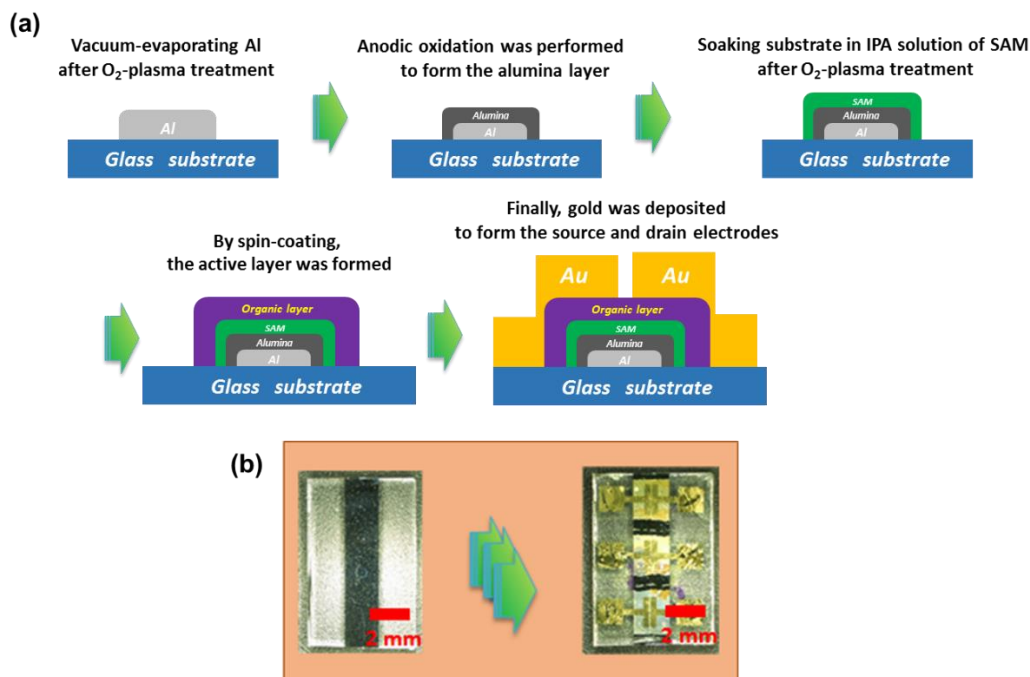


**Figure S1.** Procedure for the fabrication of AlO<sub>x</sub>/phosphonic acid SAM gate dielectric (a) and photographs of the substrate with the gate electrode/gate dielectric and OTFTs (b).

OTFT characteristics using bare substrate

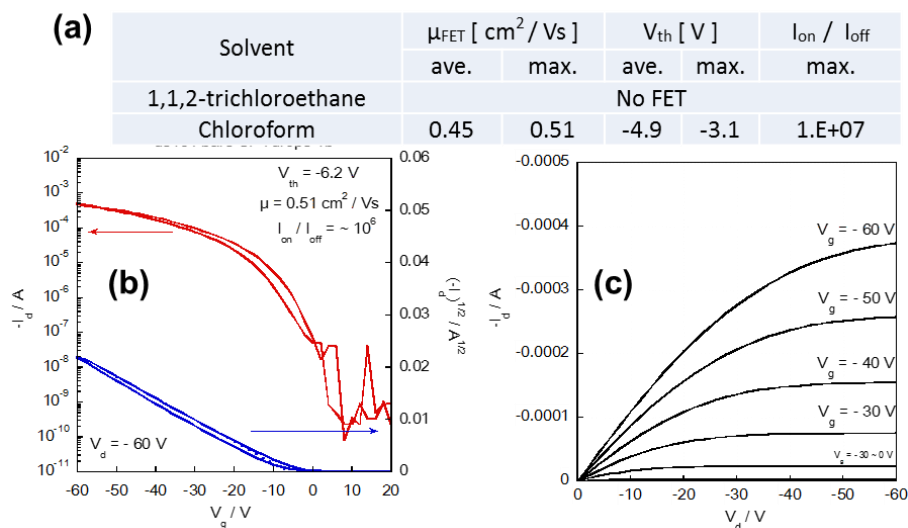


**Figure S2.** Summarized OTFT characteristics on bare substrate (a). Transfer (b) and Output (c) characteristics.

Bias stress test of the TFT on SiO<sub>2</sub> substrate

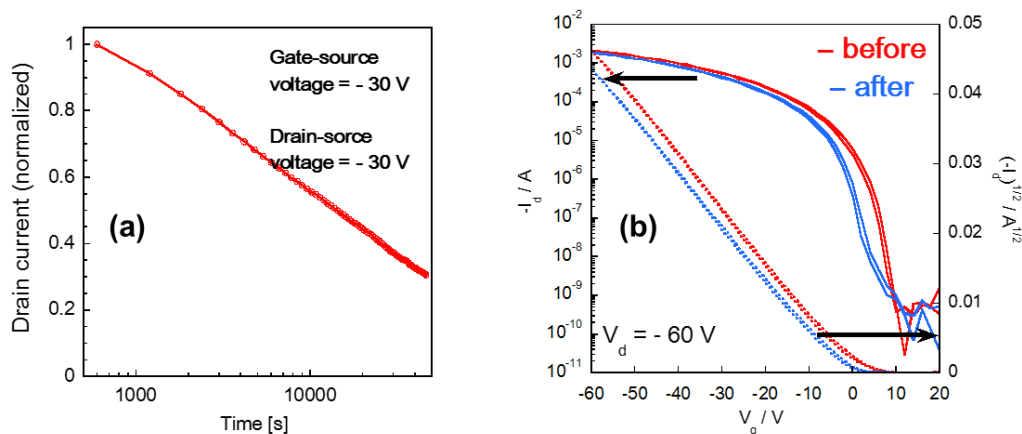


**Figure S3.** Drain current of the TFT as a function of time during bias stress (a). Transfer characteristics of the TFT measured before and after bias stress (b).

Stability tests of 2-EO-DNTT-based OTFTs on AlO<sub>x</sub>/phosphonic acid SAM gate dielectrics

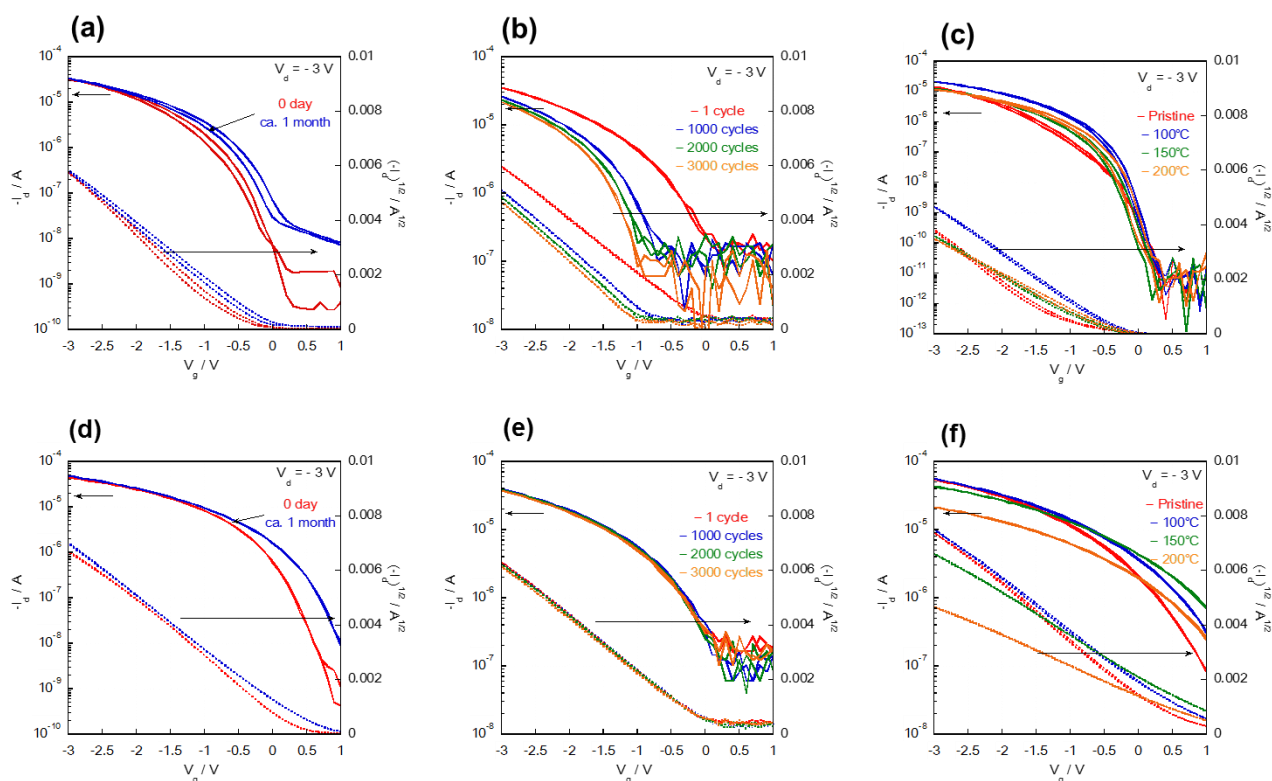


**Figure S4.** TFT characteristics of 2-EO-DNTT-TFTs on AlO<sub>x</sub>/phosphonic acid SAMs: ODPA- (a-c) and FDPA-SAM (d-f). Shelf life time test (a,d), on-off cycle test (b,e), and thermal stability test (c,f).

## References

1. Sawamoto, M.; Kang, M. J.; Miyazaki, E.; Sugino, H.; Osaka, I.; Takimiya, K., Soluble Dinaphtho[2,3-b:2',3'-f]thieno[3,2-b]thiophene Derivatives for Solution-Processed Organic Field-Effect Transistors. *ACS Applied Materials & Interfaces* **2016**, 8 (6), 3810-3824.
2. Yamamoto, T.; Takimiya, K., Dinaphtho[2,3-b:2',3'-f]chalcogenopheno[3,2-b]chalcogenophenes, and Their Application to Field-Effect Transistors. *J. Am. Chem. Soc.* **2007**, 129, 2224.
3. Diao, Y.; Shaw, L.; Bao, Z. A.; Mannsfeld, S. C. B., Morphology control strategies for solution-processed organic semiconductor thin films. *Energy & Environmental Science* **2014**, 7 (7), 2145-2159.
4. Li, Y.; Sun, H. B.; Shi, Y.; Tsukagoshi, K., Patterning technology for solution-processed organic crystal field-effect transistors. *Science and Technology of Advanced Materials* **2014**, 15 (2), 25.
5. Klauk, H., Organic thin-film transistors. *Chemical Society Reviews* **2010**, 39 (7), 2643-2666.
6. Zhang, F. J.; Di, C. A.; Berdunov, N.; Hu, Y. Y.; Hu, Y. B.; Gao, X. K.; Meng, Q.; Sirringhaus, H.; Zhu, D. B., Ultrathin Film Organic Transistors: Precise Control of Semiconductor Thickness via Spin-Coating. *Advanced Materials* **2013**, 25 (10), 1401-1407.
7. Lim, J. A.; Lee, W. H.; Kwak, D.; Cho, K., Evaporation-Induced Self-Organization of Inkjet-Printed Organic Semiconductors on Surface-Modified Dielectrics for High-Performance Organic Transistors. *Langmuir* **2009**, 25 (9), 5404-5410.
8. Dickey, K. C.; Anthony, J. E.; Loo, Y. L., Improving organic thin-film transistor performance through solvent-vapor annealing of solution-processable triethylsilylethynyl anthradithiophene. *Advanced Materials* **2006**, 18 (13), 1721-+.
9. Lee, S. S.; Kim, C. S.; Gomez, E. D.; Purushothaman, B.; Toney, M. F.; Wang, C.; Hexemer, A.; Anthony, J. E.; Loo, Y. L., Controlling Nucleation and Crystallization in Solution-Processed Organic Semiconductors for Thin-Film Transistors. *Advanced Materials* **2009**, 21 (35), 3605-+.
10. Kang, M. J.; Doi, I.; Mori, H.; Miyazaki, E.; Takimiya, K.; Ikeda, M.; Kuwabara, H., Alkylated Dinaphtho[2,3-b:2',3'-f]Thieno[3,2-b]Thiophenes (Cn-DNTTs): Organic Semiconductors for High-Performance Thin-Film Transistors. *Adv. Mater.* **2011**, 23, 1222.
11. Kang, M. J.; Miyazaki, E.; Osaka, I.; Takimiya, K.; Nakao, A., Diphenyl Derivatives of Dinaphtho 2,3-b:2',3'-f thieno 3,2-b thiophene: Organic Semiconductors for Thermally Stable Thin-Film Transistors. *Acs Applied Materials & Interfaces* **2013**, 5 (7), 2331-2336.
12. Kuribara, K.; Wang, H.; Uchiyama, N.; Fukuda, K.; Yokota, T.; Zschieschang, U.; Jaye, C.; Fischer, D.; Klauk, H.; Yamamoto, T.; Takimiya, K.; Ikeda, M.; Kuwabara, H.; Sekitani, T.; Loo, Y. L.; Someya, T., Organic transistors with high thermal stability for medical applications. *Nature Communications* **2012**, 3, 7.
13. Yokota, T.; Kuribara, K.; Tokuhara, T.; Zschieschang, U.; Klauk, H.; Takimiya, K.; Sadamitsu, Y.; Hamada, M.; Sekitani, T.; Someya, T., Flexible Low-Voltage Organic Transistors with High Thermal Stability at 250 degrees C. *Advanced Materials* **2013**, 25 (27), 3639-3644.
14. Abe, M.; Mori, T.; Osaka, I.; Sugimoto, K.; Takimiya, K., Thermally, Operationally, and Environmentally Stable Organic Thin-Film Transistors Based on Bis[1]benzothieno[2,3-d:2',3'-d']naphtho[2,3-b:6,7-b']dithiophene Derivatives: Effective Synthesis, Electronic Structures, and Structure-

Property Relationship. *Chem. Mater.* **2015**, *27*, 5049.

15. Mitsui, C.; Okamoto, T.; Yamagishi, M.; Tsurumi, J.; Yoshimoto, K.; Nakahara, K.; Soeda, J.; Hirose, Y.; Sato, H.; Yamano, A.; Uemura, T.; Takeya, J., High-Performance Solution-Processable N-Shaped Organic Semiconducting Materials with Stabilized Crystal Phase. *Advanced Materials* **2014**, *26* (26), 4546-+.
16. Sawamoto, M.; Kang, M. J.; Miyazaki, E.; Sugino, H.; Osaka, I.; Takimiya, K., Soluble Dinaphtho 2,3-b:2',3'-f thieno 3,2-b thiophene Derivatives for Solution-Processed Organic Field-Effect Transistors. *Acs Applied Materials & Interfaces* **2016**, *8* (6), 3810-3824.
17. Klauk, H.; Zschieschang, U.; Pflaum, J.; Halik, M., Ultralow-power organic complementary circuits. *Nature* **2007**, *445* (7129), 745-748.
18. Zschieschang, U.; Ante, F.; Yamamoto, T.; Takimiya, K.; Kuwabara, H.; Ikeda, M.; Sekitani, T.; Someya, T.; Kern, K.; Klauk, H., Flexible Low-Voltage Organic Transistors and Circuits Based on a High-Mobility Organic Semiconductor with Good Air Stability. *Advanced Materials* **2010**, *22* (9), 982-+.
19. Zschieschang, U.; Yamamoto, T.; Takimiya, K.; Kuwabara, H.; Ikeda, M.; Sekitani, T.; Someya, T.; Klauk, H., Organic Electronics on Banknotes. *Advanced Materials* **2011**, *23* (5), 654-+.
20. Gupta, S.; Hannah, S.; Watson, C. P.; Sutta, P.; Pedersen, R. H.; Gadegaard, N.; Gleskova, H., Ozone oxidation methods for aluminum oxide formation: Application to low-voltage organic transistors. *Organic Electronics* **2015**, *21*, 132-137.
21. Hannah, S.; Cardona, J.; Lamprou, D. A.; Sutta, P.; Baran, P.; Al Ruzaiqi, A.; Johnston, K.; Gleskova, H., Interplay between Vacuum-Grown Monolayers of Alkylphosphonic Acids and the Performance of Organic Transistors Based on Dinaphtho 2,3-b:2',3'-f thieno 3,2-b thiophene. *Acs Applied Materials & Interfaces* **2016**, *8* (38), 25405-25414.
22. Liyanage, L. S.; Lee, H.; Patil, N.; Park, S.; Mitra, S.; Bao, Z. N.; Wong, H. S. P., Wafer-Scale Fabrication and Characterization of Thin-Film Transistors with Polythiophene-Sorted Semiconducting Carbon Nanotube Networks. *Acs Nano* **2012**, *6* (1), 451-458.
23. Kaltenbrunner, M.; Stadler, P.; Schwodiauer, R.; Hassel, A. W.; Sariciftci, N. S.; Bauer, S., Anodized Aluminum Oxide Thin Films for Room-Temperature-Processed, Flexible, Low-Voltage Organic Non-Volatile Memory Elements with Excellent Charge Retention. *Advanced Materials* **2011**, *23* (42), 4892-4896.
24. Zschieschang, U.; Kang, M. J.; Takimiya, K.; Sekitani, T.; Someya, T.; Canzler, T. W.; Werner, A.; Blochwitz-Nimoth, J.; Klauk, H., Flexible low-voltage organic thin-film transistors and circuits based on C-10-DNTT. *Journal of Materials Chemistry* **2012**, *22* (10), 4273-4277.
25. Kobayashi, S.; Nishikawa, T.; Takenobu, T.; Mori, S.; Shimoda, T.; Mitani, T.; Shimotani, H.; Yoshimoto, N.; Ogawa, S.; Iwasa, Y., Control of carrier density by self-assembled monolayers in organic field-effect transistors. *Nature Materials* **2004**, *3* (5), 317-322.
26. Kraft, U.; Sejfic, M.; Kang, M. J.; Takimiya, K.; Zaki, T.; Letzkus, F.; Burghartz, J. N.; Weber, E.; Klauk, H., Flexible Low-Voltage Organic Complementary Circuits: Finding the Optimum Combination of Semiconductors and Monolayer Gate Dielectrics. *Advanced Materials* **2015**, *27* (2), 207-214.
27. Ma, H.; Acton, O.; Hutchins, D. O.; Cernetic, N.; Jen, A. K. Y., Multifunctional phosphonic acid self-assembled monolayers on metal oxides as dielectrics, interface modification layers and semiconductors

for low-voltage high-performance organic field-effect transistors. *Physical Chemistry Chemical Physics* **2012**, *14* (41), 14110-14126.

28. Liu, D. Q.; He, Z. K.; Su, Y. R.; Diao, Y.; Mannsfeld, S. C. B.; Bao, Z. A.; Xu, J. B.; Miao, Q., Self-Assembled Monolayers of Cyclohexyl-Terminated Phosphonic Acids as a General Dielectric Surface for High-Performance Organic Thin-Film Transistors. *Advanced Materials* **2014**, *26* (42), 7190-7196.

29. Nakayama, K.; Uno, M.; Uemura, T.; Namba, N.; Kanaoka, Y.; Kato, T.; Katayama, M.; Mitsui, C.; Okamoto, T.; Takeya, J., High-Mobility Organic Transistors with Wet-Etch-Patterned Top Electrodes: A Novel Patterning Method for Fine-Pitch Integration of Organic Devices. *Advanced Materials Interfaces* **2014**, *1* (5), 6.

30. Takimiya, K.; Ebata, H.; Sakamoto, K.; Izawa, T.; Otsubo, T.; Kunugi, Y., 2,7-Diphenyl 1 benzothieno 3,2-b benzothiophene, a new organic semiconductor for air-stable organic field-effect transistors with mobilities up to  $2.0 \text{ cm}^2 \text{ V}^{-1} \text{ s}^{-1}$ . *Journal of the American Chemical Society* **2006**, *128* (39), 12604-12605.

## Chapter 4

### Di-substituted branched-alkyl DNTT as p-type semiconductor for OPV

#### 4-1 Introduction

Similar to OTFT devices, organic photovoltaic cells (OPV) are also the device expected to be manufactured on a large area and at low cost by wet process.<sup>1</sup> Recently, the power conversion efficiency (PCE) has exceeded 10%.<sup>2-6</sup> The most studied and successful OPV system is composed of conjugated polymers as the electron donor and fullerene derivatives as the acceptor, which is known as polymer–fullerene bulk heterojunction (BHJ) solar cells.<sup>7-10</sup>

Small molecules with favorable optical and electronic properties have also been reported for use in the BHJ devices.<sup>5,6,11-15</sup> Especially, the n-type non-fullerene small molecules which can absorb long-wavelength light are actively studied because fullerene derivatives have lots of drawbacks such as the limited light absorption, instability in air, and typically higher production costs.<sup>11,16</sup> On the other hand, p-type polymers have some problems related to the reproducibility of their synthesis, purification, and typically higher production costs than small molecules.<sup>11,17</sup> Considering the practical use of OPV devices, the material system that makes use of the advantages of non-fullerene and small molecule would be an important topic.

For these reasons, I came up with an idea of applying soluble DNTT derivatives to p-type semiconductor for OPVs, because DNTT core has excellent hole transporting capability and stability (Figure 1).

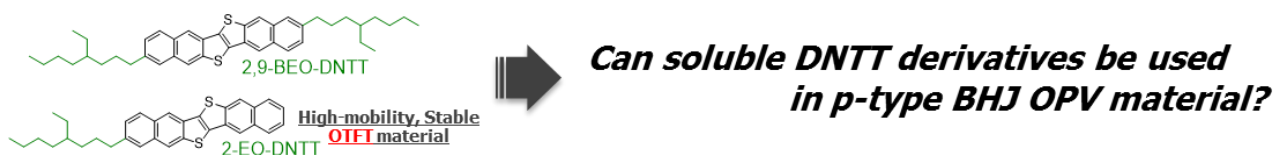


**Figure 1.** Schematic illustration of the concept of chapter 4.

The OPV components and their arrangement depend on the device architecture. In the case of inverted type (Figure 2a) used in this chapter, it consists of transparent substrate (glass), ITO electrode, electron transporting layer ( $ZnO_x$ ), active layer (p/n-BHJ), hole transporting layer ( $MoO_x$ ) and Ag electrode. The simple operating principle is described below (Figure 2b).<sup>18</sup>

- (1) Sunlight is absorbed by the p/n-BHJ layer and exciton is generated. (**Light absorption**)
- (2) The exciton diffuses and reaches the p/n interface. (**Exciton diffusion**)
- (3) The exciton is separated into hole and electron. (**Charge separation**)
- (4) The hole and electron reaches each electrode by drift or diffusion. (**Charge transport**)
- (5) The hole is trapped in the electrode with large work function and electron is trapped in the electrode with small work function. (**Charge collection**)

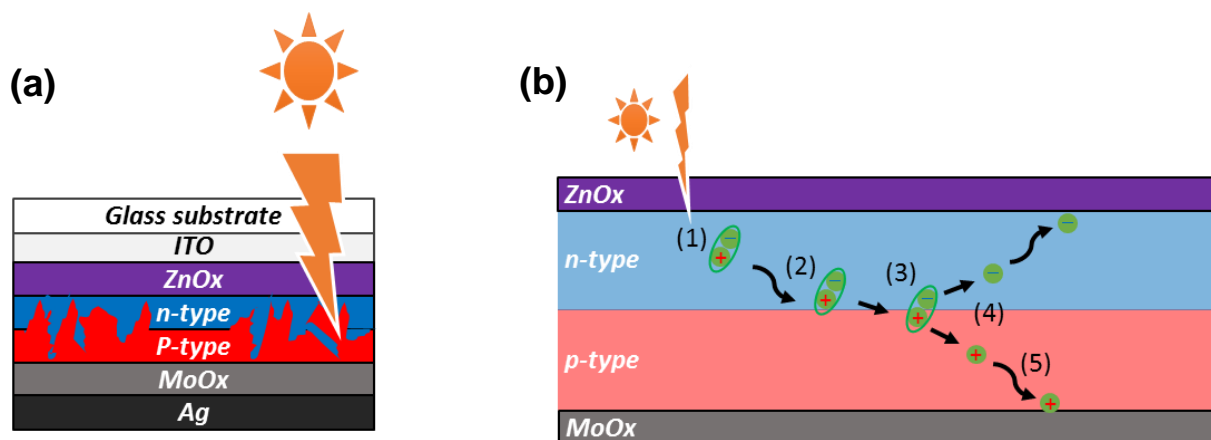
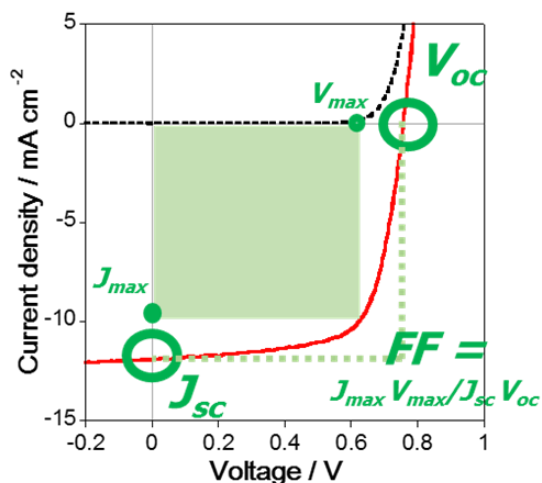


**Figure 2.** Schematic illustration of OPV architecture based on inverted type (a) and photovoltaic conversion mechanism (b).

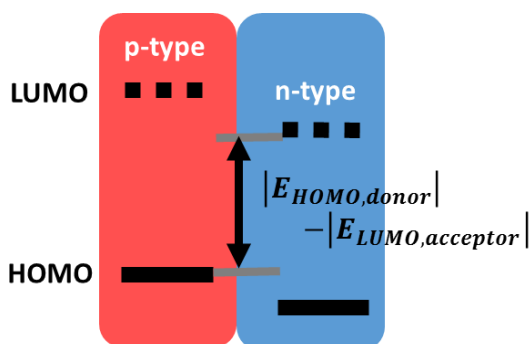
For the evaluation of OPV, the current value is measured as a function of the bias voltage under irradiation with simulated sunlight ( $100 \text{ mW/cm}^2$ ). From the current density-voltage curve as shown in Figure 3, open-circuit voltage ( $V_{oc}$ ), short-circuit current density ( $J_{sc}$ ), and fill factor (FF) are estimated and also energy conversion efficiency (PCE) is calculated using eq. 1.



$$PCE = V_{oc} \times J_{sc} \times FF \quad \text{eq. 1}$$

Figure 3. Typical J-V characteristics of OPV.

According to eq. 1, it is necessary to simultaneously improve three factors to achieve high PCE values.  $V_{oc}$ , as empirically expressed eq. 2, correlates with the energy gap between HOMO level of p-type material and LUMO of n-type (Figure 4).<sup>19,20</sup> Therefore, it is effective to develop material having low-lying HOMO level for p-type or high-lying LUMO for n-type for achieving high  $V_{oc}$  ( $> 1 \text{ V}$ ).



$$V_{oc} = \frac{1}{e} (|E_{HOMO,donor}| - |E_{LUMO,acceptor}|) - 0.3 \quad \text{eq. 2}$$

Figure 4. Energy diagram of p-/n-type material interface.

$J_{sc}$  is expressed by eq. 3,<sup>21,22</sup> where  $\lambda$ ,  $e$ ,  $h$ ,  $c$ , EQE and  $S$  represent the wavelength of the irradiation light, elementary charge, Planck's constant, light velocity, external quantum efficiency and irradiation light intensity, respectively.

$$J_{sc} = \int \left\{ \frac{\lambda e}{hc} \times EQE(\lambda) \times S(\lambda) \right\} d\lambda \quad \text{eq. 3}$$

In order to improve  $J_{sc}$ , it is necessary to raise the EQE which is the product of the efficiency for each elemental process shown in Figure 2a, as expressed by following eq. 4.

$$EQE(\lambda) = \eta_A \eta_{ED} \eta_{CS} \eta_{CT} \eta_{CC} \quad \text{eq. 4}$$

Here,  $\eta_A$ ,  $\eta_{ED}$ ,  $\eta_{CS}$ ,  $\eta_{CT}$  and  $\eta_{CC}$  represent light absorption efficiency, exciton diffusion efficiency, charge separation efficiency, charge transport efficiency and charge collection efficiency, respectively. Therefore, it is effective to expand the absorption region, increase the mobility and optimize the morphology.

Although FF is related to the resistance value of the device, carrier mobility, film morphology, etc., these factors interact with each other complicatedly.<sup>23,24</sup> Therefore, a reliable strategy for improving FF has not been established yet.

Considering the above factors, I have planned to develop small molecular p-type materials with optimum HOMO level to achieve high  $V_{oc}$ ; with this approach, the parameter to tune is the HOMO energy level, not related to film morphology that is difficult to control from the molecular design. Then,  $J_{sc}$  and FF should be improved by further optimization of the molecular design.

In this chapter, I fabricated BHJ-OPV using soluble DNTT derivatives which are expected to show high  $V_{oc}$  because of their deep HOMO levels. Actually, unsubstituted DNTT worked as the p-type material in hetero-junction (HJ) solar cells with  $C_{60}$  fabricated by vapor-deposition, and the solar cell was reported to give high  $V_{oc}$  than the corresponding solar cell consisting of pentacene with much high-lying HOMO level.<sup>25</sup> My trial in this chapter is a kind feasibility study to confirm whether it is possible or not to achieve high  $V_{oc}$  with the DNTT-based donor materials and to get insights into further molecular design strategy for novel small-molecule donor material.

## 4-2 Results and discussion

First of all, I fabricated BHJ OPV using 2-EO-DNTT and PC<sub>61</sub>BM to confirm whether it worked as a solar cell. For the device architecture, inverted type was applied, and the active layer was formed by spin-coating from a hot chloroform solution with p:n = 1:1 and concentration of 3 g / L. As a result, the OPV of 2-EO-DNTT and PC<sub>61</sub>BM did not work as a solar cell (Figure 5). The reasons for this unsuccessful results can be explained by the fact that 2-EO-DNTT has high crystallinity and low solubility, which makes the films non-uniform, resulting in the short-circuiting between the anode and cathode electrodes.

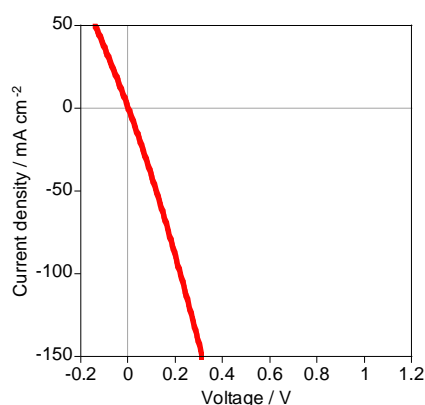


**Figure 5.** J-V characteristics of 2-EO-DNTT/PC<sub>61</sub>BM mixed film.

Then, I employed 2,9-BEO-DNTT, the disubstituted DNTT derivative reported in Chapter 2. Because 2,9-BEO-DNTT has good solubility, the thin film with low crystallinity can be obtained and has deep IP value of 5.5 eV, although the mobility is not so high (ca.  $10^{-5}$  cm<sup>2</sup>/Vs).<sup>26</sup> When the OPVs were fabricated by spin-coating from a hot chloroform solution with p:n = 1:1 and the concentrations of 3, 6, 9, 12 or 15 g / L, they worked as a solar cell under the condition with 9 g / L or higher (Table 1). As expected, the V<sub>oc</sub> was higher than 1 V and also the FF was relatively good as 0.58 at the maximum. J<sub>sc</sub> was, however, very low as 1.65 mA cm<sup>-2</sup> at the maximum, and hence the PCE was 0.91% at the maximum (Figure 6a).

**Table 1. Characteristics of OPV based on 2,9-BEO-DNTT and PC<sub>61</sub>BM.**

Concentration / g L <sup>-1</sup>	V <sub>oc</sub> / V	J <sub>sc</sub> / mA cm <sup>-2</sup>	FF	PCE / %	Ave. film thickness / nm
3		No OPV characteristics			Difficult to measure
6	0.54	0.76	0.39	0.16	60
9	0.90	1.01	0.44	0.40	104
12	1.01	1.40	0.58	0.82	221
15	1.01	1.65	0.55	0.91	226

The results in the table were extracted from several OPV devices.

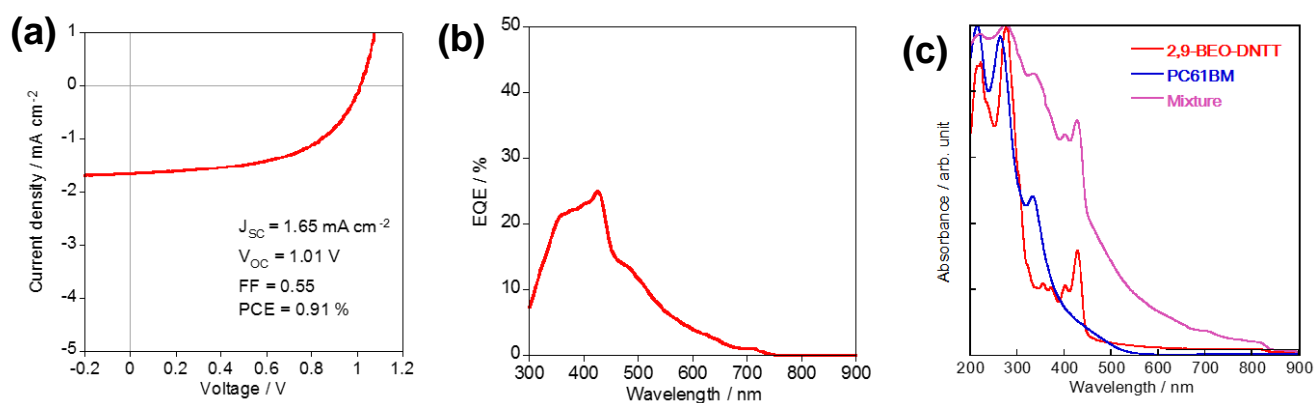


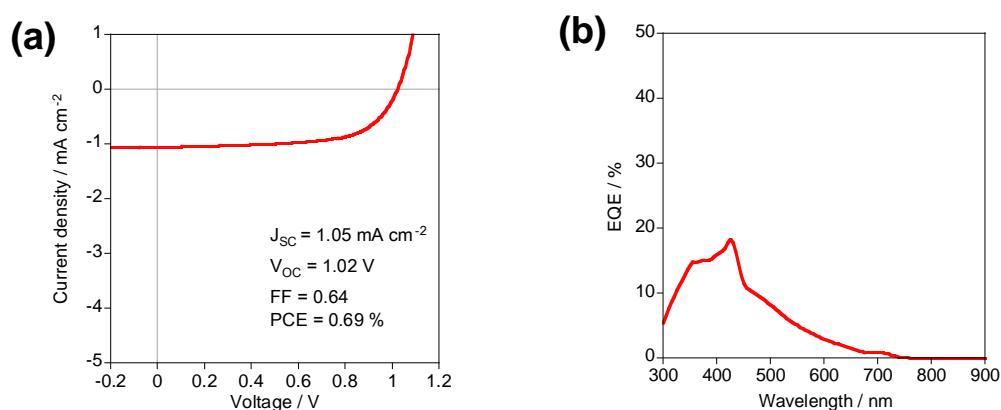
**Figure 6.** J-V curve (a) and EQE spectra (b) of 2,9-BEO-DNTT/PC<sub>61</sub>BM OPV. UV-vis absorption spectra of 2,9-BEO-DNTT, PC<sub>61</sub>BM and mixed thin film (c).

As one reason for low J<sub>sc</sub>, the absorption spectra of 2,9-BEO-DNTT and PC<sub>61</sub>BM are limited in relatively short wavelength region (~ 500 nm) and not complementary, and thus they cannot absorb sunlight sufficiently (Figure 6b, c). Furthermore, even in the absorbing region, the EQE is about 20% at the maximum, which is considered that there are some problems in exciton diffusion or charge transport (Figure 6b). In order to improve the EQE, optimization of the p/n ratio was attempted, but it was not so effective (Table 2, Figure 7).

**Table 2. Characteristics of OPV based on 2,9-BEO-DNTT and PC<sub>61</sub>BM with different p/n ratio.**

p/n ratio	V <sub>oc</sub> / V	J <sub>sc</sub> / mA cm <sup>-2</sup>	FF	PCE / %	Ave. film thickness / nm
2 : 1	1.03	1.05	0.45	0.48	256
1.5 : 1	1.00	1.66	0.48	0.81	188
1 : 1	1.00	1.44	0.55	0.79	217
1 : 1.5	1.02	1.05	0.64	0.69	166
1 : 2	1.01	0.83	0.61	0.51	170

The results in the table were extracted from several OPV devices.

**Figure 7. J-V curve (a) and EQE spectra (b) of 2,9-BEO-DNTT/PC<sub>61</sub>BM OPV with p/n ratio of 1:1.5.**

Since the V<sub>oc</sub> as high as 1V is quite appealing, I then tried to improve J<sub>sc</sub> by changing the n-type materials to realize complementary light absorption in the whole visible region. So, I searched for suitable n-type material having optical absorption spectrum and molecular energy level suitable to 2,9-BEO-DNTT, which are two key factors for realizing the efficient light harvesting and generation of free charges. As shown in Figure 8, PNDTI-BTz is considered to be suitable for both light absorption and molecular energy level.<sup>27</sup>

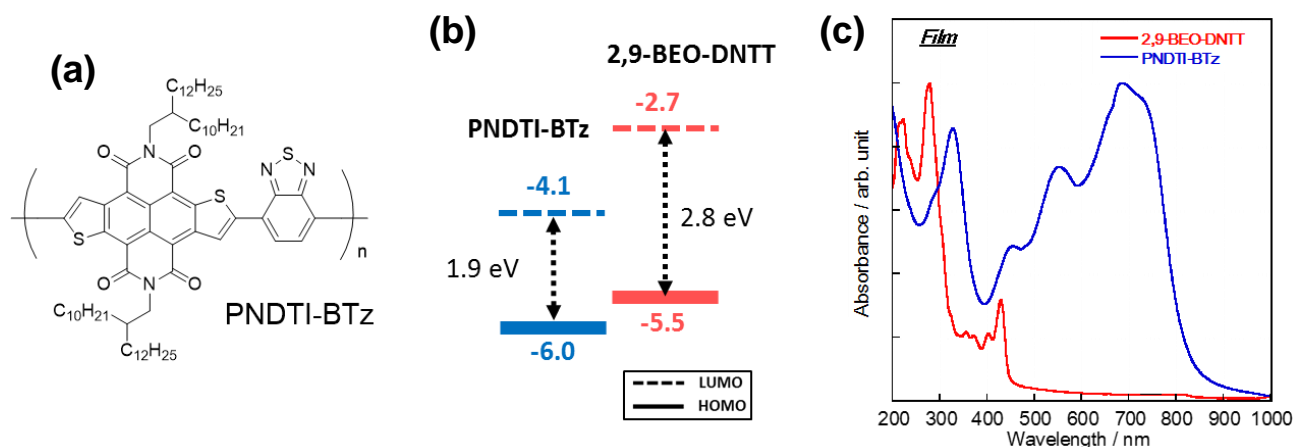


**Figure 8.** Chemical structure of PNDTI-BTz (a), molecular energy diagrams of PNDTI-BTz and 2,9-BEO-DNTT (b), UV-vis absorption spectra of PNDTI-BTz and 2,9-BEO-DNTT thin film (c).

As a result,  $V_{oc}$  was 0.88 V at maximum, which was a reasonable value expected from the molecular energy levels. However,  $J_{sc}$  was quiet low, ca. 0.3 mA/cm<sup>2</sup>, and EQE was also very low, ca. 3% at the maximum (Table 3, Figure 9). Judging from the onset and shape of EQE spectrum, it can be seen that both 2,9-BEO-DNTT and PNDTI-BTz contribute to photocurrent generation, but very low EQE implies that the system has problems in exciton diffusion or charge transport, similar to the 2,9-BEO-DNTT/PC<sub>61</sub>BM system.

**Table 3. Characteristics of OPV based on 2,9-BEO-DNTT with PNDTI-BTz.**

Rotation speed / rpm	$V_{oc}$ / V	$J_{sc}$ / mA cm <sup>-2</sup>	FF	PCE / %	Ave. film thickness / nm
500	0.67	0.32	0.39	0.08	119
1000	0.39	0.30	0.43	0.05	145
1500	0.88	0.29	0.43	0.11	128
2000	0.87	0.25	0.42	0.09	106

The results in the table were extracted from several OPV devices.

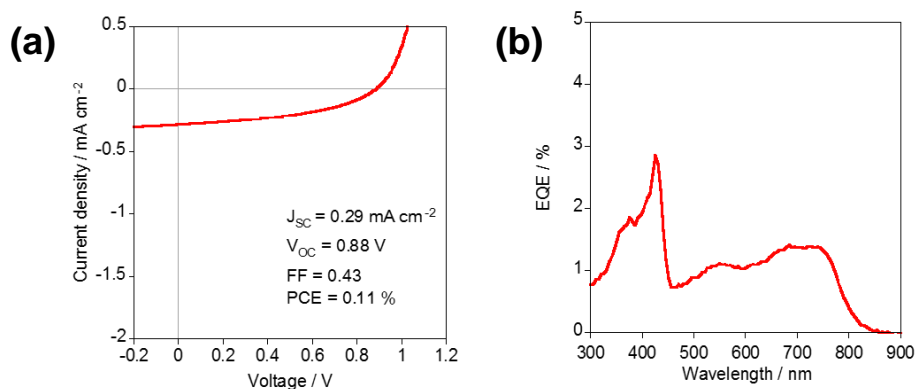


**Figure 9.** J-V curve (a) and EQE spectra (b) of 2,9-BEO-DNTT/PNDTI-BTz BHJ OPV.

As one of the reasons for this poor nature of the DNTT-based p-type materials for OPV devices, I should point out that DNTT derivatives have a planar molecular core optimized for OTFT,<sup>28</sup> which is not suitable for transporting carriers in the vertical direction. In fact, Rajaram et al. reported solar cells with n-type materials based on perylene diimide (PDI), which is one of most widely studied n-type semiconductors for OFET applications. When the planar PDI derivatives with high crystallinity was used,  $J_{sc}$  was very low, whereas twisted PDI dimer with low crystallinity gave higher  $J_{sc}$ .<sup>29</sup> This approach, i.e., deformation of the planar structure of DNTT and related materials is expected to improve the transport properties in the vertical direction in OPV devices, which will be an interesting strategy for novel small molecular p-type OPV materials.

With this molecular design guideline, I invented a molecule as shown in [Figure 10a](#). By using 9,9'-spirobi[9H-fluorene] (SF) core, the planarity of the molecule as a whole can be easily destroyed.<sup>30</sup> The reasons for choosing [1]benzothieno[3,2-b][1]benzothiophene (BTBT) instead of DNTT were following; BTBT is easily accessible and is mono-brominated,<sup>31</sup> and has higher solubility and deeper HOMO level.<sup>32</sup> In fact, the target molecule called SF-BTBT<sub>4</sub> has HOMO and LUMO levels of ca. -5.2 and -1.6 eV, respectively, according to the DFT calculations ([Figure 10b, c](#)).

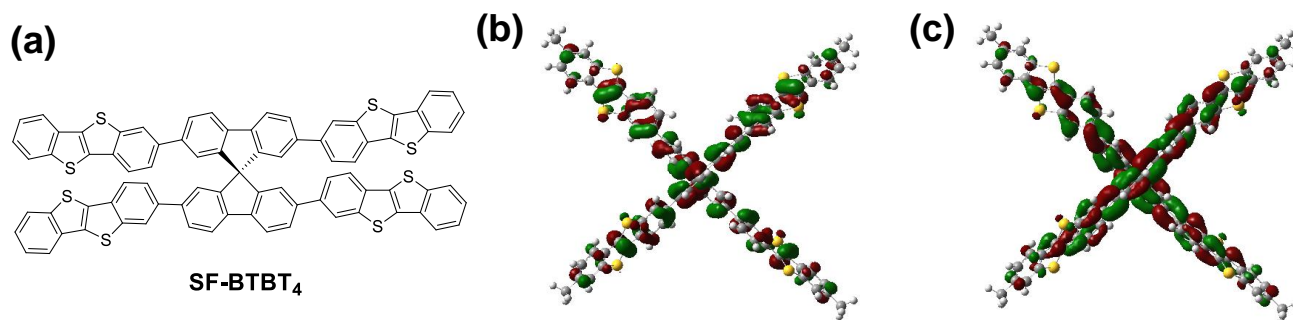
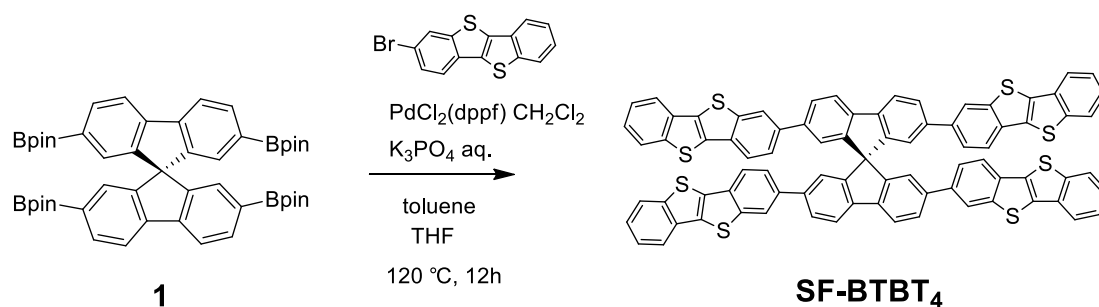


**Figure 10.** Chemical structure of invented molecule (a) and optimized structure and HOMO (b) and LUMO (c) orbital by DFT calculation. DFT calculation is carried out using the B3LYP functional and 6-31G\*\* basis set.

As trial experiments, I synthesized SF-BTBT<sub>4</sub> from 2,2',7,7'-tetrakis(4,4,5,5-tetramethyl-1,3,2-dioxaborolan-2-yl)-9,9'-spirobi[fluorene] (**1**) using palladium-catalyzed Suzuki-Miyaura cross coupling reaction as shown in [Scheme 1](#). Unexpectedly, SF-BTBT<sub>4</sub> was found to be soluble in chloroform, even though any alkyl group is not introduced.<sup>33</sup> SF-BTBT<sub>4</sub> is expected to be an interesting archetypical material as small-molecule p-type material for OPV by wet process.



**Scheme 1.** Synthesis of SF-BTBT<sub>4</sub> by Suzuki-Miyaura cross coupling reaction.

### 4-3 Conclusion of chapter 4

The feasibility study was conducted by using soluble DNTTs to fabricate BHJ OPV by spin-coating, expecting high  $V_{oc}$  ( $> 1$  V). As a result, 2-EO-DNTT which is mono-substituted DNTT derivative, was unable to form a homogeneous film due to its low solubility and high crystallinity, and the thin films did not work as the active layer in the solar cells. On the other hand, 2,9-BEO-DNTT, di-substituted DNTT derivative, was able to form a homogeneous film and work as the active layer affording OPVs with high  $V_{oc}$  (ca. 1 V), when PC<sub>61</sub>BM was used as n-type semiconductor. FF was also higher than 0.6, which is moderate value for OPVs reported so far. However,  $J_{sc}$  was very low, 1.65 mA/cm<sup>2</sup> at the maximum, so the PCE was as low as 0.91% at the maximum. In the case of the cells with PNDTI-BTz, a narrow-bandgap n-type polymer that affords complementary light-absorption,  $J_{sc}$  was not improved. Although 2,9-BEO-DNTT afforded high  $V_{oc}$  in the solar cells, this molecule may have problems of exciton diffusion or charge transport. For future molecular design guidelines for novel small molecular p-type OPV materials, to break the planarity of molecules would be the key, and based on this idea, a synthetic demonstration was made; SF-BTBT<sub>4</sub> with non-planar molecular structure with four BTBT electron donor units was synthesized. Because of the limitation of time, I cannot fabricate SF-BTBT<sub>4</sub>-based OPV devices. However, its relatively high solubility, which was an unexpected outcome from actual synthetic trials, should be the positive implication for the future success of this kind of molecules for OPV applications.

#### 4-4 Experimental section, supporting data and references

##### Fabrication and characterization of OPVs.

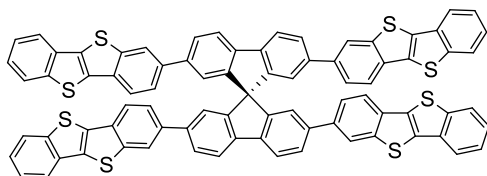
ITO substrates were pre-cleaned sequentially by sonicating in a detergent bath, de-ionized water, acetone, and IPA at rt, and in a boiled IPA bath, each for 10 min. Then, the substrates were subjected to UV/ozone treatment at rt for 20 min. The pre-cleaned ITO substrates (masked at the electrical contacts by Kapton tape) were coated with ZnO precursor by spin-coating (5000 rpm, 30 s, 80  $\mu$ L) a precursor solution prepared by zinc acetate dihydrate (275 mg) and ethanolamine (0.078 mL) in 2.5 mL of 2-methoxyethanol stirring for 3 h. They were then baked in air at 170 °C for 30 min, then sonicating in acetone and IPA, and in a boiled IPA bath, each for 10 min.

The active layer was deposited in a glove box by spin-coating hot chloroform solution containing 2,9-BEO-DNTT and PC<sub>61</sub>BM or PNDTI-BTz for 30 s. The thin films were transferred into a vacuum evaporator connected to the glove box, and MoO<sub>x</sub> (7.5 nm) and Ag (100 nm) were deposited sequentially through a shadow mask by thermal evaporation under  $\sim 10^{-5}$  Pa, where the active area of the cells was 0.16 cm<sup>2</sup>.

J-V characteristics of the cells were measured with a Keithley 2400 source measure unit in nitrogen atmosphere under 1 Sun (AM1.5G) conditions using a solar simulator (SAN-EI Electric, XES-40S1, 1000 W m<sup>-2</sup>). The light intensity for the J-V measurements was calibrated with a reference PV cell (Konica Minolta AK-100 certified by the National Institute of Advanced Industrial Science and Technology, Japan). EQE spectra were measured with a Spectral Response Measuring System (Soma Optics, Ltd., S-9241). The thickness of the active layer was measured with an AlphaStep® D-100 surface profiler (KLA Tencor).

## Synthesis

### 2,2',7,7'-tetrakis(benzo[b]benzo[4,5]thieno[2,3-d]thiophen-2-yl)-9,9'-spirobi[fluorene] (*SF-BTBT*<sub>4</sub>)



Chemical Formula: C<sub>81</sub>H<sub>40</sub>S<sub>8</sub>  
Molecular Weight: 1269.7043  
m/z: 1268.0896 (100.0%), 1269.0929 (87.6%),  
1270.0963 (37.9%), 1270.0854 (36.2%),  
1271.0887 (31.7%),

2-bromo BTBT (31 mg, 0.096 mmol), PdCl<sub>2</sub>(dppf) CH<sub>2</sub>Cl<sub>2</sub> (1.0 mg, 0.0012 mmol) and 1M K<sub>3</sub>PO<sub>4</sub> aq. (0.14 mL, 0.14 mmol) were added to toluene (2.5 mL) and THF (1.5 mL) mixed solution of **1** (10 mg, 0.12 mmol). After Ar bubbling for 3 min, the mixture was stirred for 12 h at 120 °C under the Ar. Then, the mixture was cooled to r.t. and added to a large amount of methanol. The resulting precipitate was collected by filtration and was washed with water, methanol and ethyl acetate to give crude *SF-BTBT*<sub>4</sub> (5 mg, 33%) as powder.

FD-MS m/z = 1268 [M<sup>+</sup>]; HR-MS (FD) Calcd for C<sub>81</sub>H<sub>40</sub>S<sub>8</sub> [M<sup>+</sup>]: 1268.0896, found: 1268.0836.

## References

1. Dou, L.; You, J.; Hong, Z.; Xu, Z.; Li, G.; Street, R. A.; Yang, Y., 25th Anniversary Article: A Decade of Organic/Polymeric Photovoltaic Research. *Advanced Materials* **2013**, *25* (46), 6642-6671.
2. Vohra, V.; Kawashima, K.; Kakara, T.; Koganezawa, T.; Osaka, I.; Takimiya, K.; Murata, H., Efficient inverted polymer solar cells employing favourable molecular orientation. *Nature Photonics* **2015**, *9* (6), 403-+.
3. Liu, Y. H.; Zhao, J. B.; Li, Z. K.; Mu, C.; Ma, W.; Hu, H. W.; Jiang, K.; Lin, H. R.; Ade, H.; Yan, H., Aggregation and morphology control enables multiple cases of high-efficiency polymer solar cells. *Nature Communications* **2014**, *5*, 8.
4. Kawashima, K.; Fukuhara, T.; Suda, Y.; Suzuki, Y.; Koganezawa, T.; Yoshida, H.; Ohkita, H.; Osaka, I.; Takimiya, K., Implication of Fluorine Atom on Electronic Properties, Ordering Structures, and Photovoltaic Performance in NaphthobisthiadiazoleBased Semiconducting Polymers. *Journal of the American Chemical Society* **2016**, *138* (32), 10265-10275.
5. Kan, B.; Li, M. M.; Zhang, Q.; Liu, F.; Wan, X. J.; Wang, Y. C.; Ni, W.; Long, G. K.; Yang, X.; Feng, H. R.; Zuo, Y.; Zhang, M. T.; Huang, F.; Cao, Y.; Russell, T. P.; Chen, Y. S., A Series of Simple Oligomer-like Small Molecules Based on Oligothiophenes for Solution-Processed Solar Cells with High Efficiency. *Journal of the American Chemical Society* **2015**, *137* (11), 3886-3893.
6. Zhao, W. C.; Qian, D. P.; Zhang, S. Q.; Li, S. S.; Inganas, O.; Gao, F.; Hou, J. H., Fullerene-Free Polymer Solar Cells with over 11% Efficiency and Excellent Thermal Stability. *Advanced Materials* **2016**, *28* (23), 4734-4739.
7. Cheng, Y. J.; Yang, S. H.; Hsu, C. S., Synthesis of Conjugated Polymers for Organic Solar Cell Applications. *Chemical Reviews* **2009**, *109* (11), 5868-5923.
8. Facchetti, A., Polymer donor-polymer acceptor (all-polymer) solar cells. *Materials Today* **2013**, *16* (4), 123-132.
9. Osaka, I.; Takimiya, K., Backbone orientation in semiconducting polymers. *Polymer* **2015**, *59*, A1-A15.
10. Yao, H. F.; Ye, L.; Zhang, H.; Li, S. S.; Zhang, S. Q.; Hou, J. H., Molecular Design of Benzodithiophene-Based Organic Photovoltaic Materials. *Chemical Reviews* **2016**, *116* (12), 7397-7457.
11. Eftaiha, A. F.; Sun, J. P.; Hill, I. G.; Welch, G. C., Recent advances of non-fullerene, small molecular acceptors for solution processed bulk heterojunction solar cells. *Journal of Materials Chemistry A* **2014**, *2* (5), 1201-1213.
12. Sun, Y. M.; Welch, G. C.; Leong, W. L.; Takacs, C. J.; Bazan, G. C.; Heeger, A. J., Solution-processed small-molecule solar cells with 6.7% efficiency. *Nature Materials* **2012**, *11* (1), 44-48.
13. Chen, Y. S.; Wan, X. J.; Long, G. K., High Performance Photovoltaic Applications Using Solution-Processed Small Molecules. *Accounts of Chemical Research* **2013**, *46* (11), 2645-2655.
14. Lin, Y. Z.; Li, Y. F.; Zhan, X. W., Small molecule semiconductors for high-efficiency organic photovoltaics. *Chemical Society Reviews* **2012**, *41* (11), 4245-4272.
15. Mishra, A.; Bauerle, P., Small Molecule Organic Semiconductors on the Move: Promises for Future Solar Energy Technology. *Angewandte Chemie-International Edition* **2012**, *51* (9), 2020-2067.

16. Sauve, G.; Fernando, R., Beyond Fullerenes: Designing Alternative Molecular Electron Acceptors for Solution-Processable Bulk Heterojunction Organic Photovoltaics. *Journal of Physical Chemistry Letters* **2015**, *6* (18), 3770-3780.
17. Yang, L.; Zhang, S.; He, C.; Zhang, J.; Yao, H.; Yang, Y.; Zhang, Y.; Zhao, W.; Hou, J., New Wide Band Gap Donor for Efficient Fullerene-Free All-Small-Molecule Organic Solar Cells. *Journal of the American Chemical Society* **2017**, *139* (5), 1958-1966.
18. 安達千波矢, *有機半導体のデバイス物性*. 講談社: **2012**.
19. Scharber, M. C.; Wuhlbacher, D.; Koppe, M.; Denk, P.; Waldauf, C.; Heeger, A. J.; Brabec, C. L., Design rules for donors in bulk-heterojunction solar cells - Towards 10 % energy-conversion efficiency. *Advanced Materials* **2006**, *18* (6), 789-+.
20. Elumalai, N. K.; Uddin, A., Open circuit voltage of organic solar cells: an in-depth review. *Energy & Environmental Science* **2016**, *9* (2), 391-410.
21. Clarke, T. M.; Durrant, J. R., Charge Photogeneration in Organic Solar Cells. *Chemical Reviews* **2010**, *110* (11), 6736-6767.
22. Stoltzfus, D. M.; Donaghey, J. E.; Armin, A.; Shaw, P. E.; Burn, P. L.; Meredith, P., Charge Generation Pathways in Organic Solar Cells: Assessing the Contribution from the Electron Acceptor. *Chemical Reviews* **2016**, *116* (21), 12920-12955.
23. Guo, X. G.; Zhou, N. J.; Lou, S. J.; Smith, J.; Tice, D. B.; Hennek, J. W.; Ortiz, R. P.; Navarrete, J. T. L.; Li, S. Y.; Strzalka, J.; Chen, L. X.; Chang, R. P. H.; Facchetti, A.; Marks, T. J., Polymer solar cells with enhanced fill factors. *Nature Photonics* **2013**, *7* (10), 825-833.
24. Qi, B. Y.; Wang, J. Z., Fill factor in organic solar cells. *Physical Chemistry Chemical Physics* **2013**, *15* (23), 8972-8982.
25. Mori, H.; Takimiya, K., Efficient Photocurrent Generation at Dinaphtho 2,3-b:2',3'-f thieno 3,2-b thiophene/C-60 Bilayer Interface. *Applied Physics Express* **2011**, *4* (6), 3.
26. Sawamoto, M.; Kang, M. J.; Miyazaki, E.; Sugino, H.; Osaka, I.; Takimiya, K., Soluble Dinaphtho 2,3-b:2',3'-f thieno 3,2-b thiophene Derivatives for Solution-Processed Organic Field-Effect Transistors. *Acs Applied Materials & Interfaces* **2016**, *8* (6), 3810-3824.
27. Nakano, M.; Osaka, I.; Takimiya, K., Naphthodithiophene Diimide (NDTI)-Based Semiconducting Copolymers: From Ambipolar to Unipolar n-Type Polymers. *Macromolecules* **2015**, *48* (3), 576-584.
28. Yamamoto, T.; Takimiya, K., Dinaphtho[2,3-b:2',3'-f]chalcogenopheno[3,2-b]chalcogenophenes, and Their Application to Field-Effect Transistors. *J. Am. Chem. Soc.* **2007**, *129*, 2224.
29. Rajaram, S.; Shivanna, R.; Kandappa, S. K.; Narayan, K. S., Nonplanar Perylene Diimides as Potential Alternatives to Fullerenes in Organic Solar Cells. *Journal of Physical Chemistry Letters* **2012**, *3* (17), 2405-2408.
30. Saragi, T. P. I.; Spehr, T.; Siebert, A.; Fuhrmann-Lieker, T.; Salbeck, J., Spiro compounds for organic optoelectronics. *Chemical Reviews* **2007**, *107* (4), 1011-1065.
31. Inoue, S.; Minemawari, H.; Tsutsumi, J.; Chikamatsu, M.; Yamada, T.; Horiuchi, S.; Tanaka, M.; Kumai, R.; Yoneya, M.; Hasegawa, T., Effects of Substituted Alkyl Chain Length on Solution-Processable

Layered Organic Semiconductor Crystals. *Chemistry of Materials* **2015**, *27* (11), 3809-3812.

32. Takimiya, K.; Osaka, I.; Mori, T.; Nakano, M., Organic Semiconductors Based on 1 Benzothieno 3,2-b 1 benzothiophene Substructure. *Accounts of Chemical Research* **2014**, *47* (5), 1493-1502.

33. Geng, Y. H.; Katsis, D.; Culligan, S. W.; Ou, J. J.; Chen, S. H.; Rothberg, L. J., Fully spiro-configured terfluorenes as novel amorphous materials emitting blue light. *Chemistry of Materials* **2002**, *14* (1), 463-470.

## *Chapter 5*

### **Concluding remarks**

This doctoral thesis entitled “Development of Soluble DNTT Derivatives and Application to Organic Devices” describes the development of soluble OTFT and OPV materials using DNTT core by organic synthesis, device fabrication and evaluation in series. As mentioned in Chapter 1, the performances required for materials in the wet processed OTFTs are; (1) High mobility, (2) Good coating suitability, (3) Good stability, (4) Low-voltage drivability, and (5) Good circuit design suitability. All these requirements must be achieved simultaneously to produce commercial devices by wet process.

In Chapter 2, I tried to solubilize DNTT by introducing branched alkyl groups. Then I confirmed that di-substituted branched alkyl DNTT derivatives only showed poor OTFT characteristics because of their poor crystalline order in the thin films, although they have high solubility. On the other hand, mono-substituted branched alkyl DNTT derivatives did not lower solubility considerably and yielded good OTFT characteristics with the mobilities of up to  $0.5 \text{ cm}^2 \text{ V}^{-1} \text{ s}^{-1}$  by spin-coating thanks to their high crystalline order in the thin films. I also studied the correlation between different branching positions in the branched alkyl group and the OTFT characteristics. As a result, the different branching positions gave slight differences in solubility and melting point due to odd-even effect, but do not significantly affect the OTFT characteristics. From these results, I can conclude that this simple design strategy as the introduction of one branched alkyl group on a largely  $\pi$ -extended thienoacene core is a promising strategy for the development of wet-processable organic semiconductors. In addition, I selected 2-EO-DNTT as the most promising DNTT derivative for a wet-processable material.

In Chapter 3, with 2-EO-DNTT selected in Chapter 2, optimization of spin-coating conditions to achieve better device performances were discussed. In addition, I tested device stabilities (environmental, electrical, and thermal stabilities), and low-voltage operations. As a result, 2-EO-DNTT-based devices can show the mobility of up to  $2.6 \text{ cm}^2 \text{ V}^{-1} \text{ s}^{-1}$  by optimizing the spin-coating manners and solvents. In addition, OTFT of 2-EO-DNTT had similar environmental, electrical and thermal stability to those of OTFTs based on parent DNTT. Furthermore, OTFT of 2-EO-DNTT fabricated on the  $\text{AlO}_x$  and phosphonic acid SAM insulating film can be operated at low-voltage ( $\ll -3 \text{ V}$ ) and showed mobilities higher than  $1 \text{ cm}^2 \text{ V}^{-1} \text{ s}^{-1}$  at  $-3 \text{ V}$ . From these results, I can say that 2-EO-DNTT is a wet-processable material that is comparable to the vacuum-processable parent DNTT in terms of high mobility, good stability and low-voltage drivability.

In Chapter 4, as a feasibility study, I attempted to apply soluble DNTT derivatives into p-type OPV semiconductor. To demonstrate the possibilities and issues of small molecular p-type OPV semiconductor, I focused on a deep HOMO level of DNRR derivatives, which can realize high  $V_{oc}$  in OPV devices. The best result was obtained from 2,9-BEO-DNTT, which is di-substituted branched alkyl DNTT derivative as shown in Chapter 2; OPVs combined with  $\text{PC}_{61}\text{BM}$  showed high  $V_{oc}$  (ca. 1 V), though the  $J_{sc}$  ( $1.65 \text{ mA/cm}^2$  at the maximum) and PCE were very low (0.91%) at the maximum. The poor characteristics in  $J_{sc}$  and PCE can be ascribed to problems associated with exciton diffusion and/or charge transport. To solve this problems, it is necessary to change the molecular design for improving vertical carrier transport. For future developments, I designed and synthesized one candidate molecule.

As mentioned in the general introduction of Chapter 1, organic electronics is an interdisciplinary area that incorporates chemistry (material), physics (device), engineering (process), etc., and there are various obstacles to achieve practical use. In order to accelerate the research on organic electronics, it is important to simultaneously study materials, devices and processes as much as possible. Furthermore, it is also important to find a universal concept such as effective synthesis method, molecular design guideline and physical principle, etc.

In this doctor thesis, I presented molecular design guideline of introducing one branched alkyl group to solubilize DNTT and high mobilities in wet process by deepening my comprehension of spin-coating. Additionally, by applying soluble DNTT derivatives to OPV devices, it was found that high  $V_{oc}$  was achieved, which would be a useful knowledge for future development of small molecular p-type OPV materials. Further improvements of the device characteristics are required for industrialization, so we have to progress material design, synthesis, device fabrication and evaluation. I hope this thesis will contribute to industrialization of organic electronics in the near future.

## List of publications

### Contributed papers

(1) Sawamoto, M.; Kang, M. J.; Miyazaki, E.; Sugino, H.; Osaka, I.; Takimiya, K., Soluble Dinaphtho[2,3-*b*:2',3'-*f*]thieno[3,2-*b*]thiophene Derivatives for Solution-Processed Organic Field-Effect Transistors.

*ACS. Appl. Mater. Interfaces.*, **2016**, 8, 3810.

(2) Sawamoto, M.; Sugino, H.; Nakano, M.; Takimiya, K.,

Submitted.

### Other works

(1) Nakano, M.; Sawamoto, M.; Yuki, M.; Takimiya, K., N,N'-Unsubstituted Naphthodithiophene Diimide: Synthesis and Derivatization via N-Alkylation and -Arylation.

*Org. Lett.*, **2016**, 18, 3770.

(2) Kawabata, K.; Osaka, I.; Sawamoto, M.; Zafra, J. L.; Burrezo, P. M.; Casado, J.; Takimiya, K., Dithienyl Acenedithiophenediones as New  $\pi$ -Extended Quinoidal Cores: Synthesis and Properties.

*Chem. Eur. J.*, **2017**, 23, 1.

## Acknowledgements

本研究は理化学研究所 創発物性科学研究センター(CEMS) 創発分子機能研究グループにおいて、2014年から2016年にかけて行われました。恵まれた研究環境と大学院リサーチ・アソシエイト (JRA) として採用していただき、金銭的にも支援していただいた理化学研究所に深く感謝申し上げます。

また、この博士論文を作成するにあたり、多くの方々にご支援ご協力を賜りました。本研究を遂行し学位論文をまとめるにあたり、修士2年から博士3年までの4年間、有機合成・デバイス・物性評価に関して、また口頭発表の仕方や論文の書き方について、厳しくも非常に専門的で的確な御指導、御意見を賜りました瀧宮和男グループディレクターに深く感謝申し上げます。

また、論文の主査・副査を快諾頂き、貴重なご指導とご助言を頂いた埼玉大学 大学院理工学研究科の白井肇教授、鎌田憲彦教授、上野啓司准教授にも感謝申し上げます。特に、白井先生には、埼玉大学の所属研究室の先生としてご指導頂いてお世話になりました。

実験の実施に際しては瀧宮グループの皆様の協力を頂きました。尾坂格上級研究員、中野正浩博士、川畑公輔博士、阿部正宏博士、斎藤慎彦博士、川島和彰博士、杉野寛佳博士、Wang Chengyan 博士、テクニカルスタッフの竹村典子さん、鈴木康仁さん、結城瑞恵さん、また修士2年時、共に切磋琢磨した森崇充修士、加々良剛志修士、宝珍善伸修士の皆様には有機合成・デバイス作製・物性評価において、装置の使い方から研究に関する議論まで様々なことでお世話になりました。そして日々の研究生活において、アシスタントの橋本恵子さんには、いつも笑顔で助けて励まして下さいました。瀧宮グループの皆様に深く感謝いたします。

最後に、12年間に及ぶ大学・大学院での生活を支えていただき、金銭面でも助けていただいた両親に深く感謝いたします。

今後は博士課程での良い経験を活かして有機エレクトロニクスの発展に取り組んでいきたいと思っています。

2017年 3月  
澤本 尚典